Surface and Near-Surface Motion of Oil in the Sea

by
S. Leibovich
Environmental Sciences of Ithaca
FINAL REPORT
Contract 14–35–0001–30612
Submitted to Minerals Management Service
Department of the Interior

April 1, 1997

Executive Summary

This is the Final Report for Minerals Management Service Contract 14–35–0001–30612.

The Minerals Management Service is responsible for assessing environmental risks associated with shipping and offshore production of oil. A basic tool in the risk assessment procedure is a computer model that simulates the motion of oil on the sea surface. The research carried out under this contract treats near-surface physical behavior not included in existing oil tracking procedures, but which has the potential to significantly affect oil trajectories.

Existing oil spill models do not account for energetic wind-driven convective motions, known as Langmuir circulation, that can affect surface transport. Nearly thirty years of observations of oil spill events at sea clearly shows that this phenomenon alters the surface distribution of oil.

Langmuir circulation is the three-dimensional current system driven by the wind. The surface drift current created by Langmuir circulation has downwind and crosswind components. The crosswind component sweeps floating surface material into bands parallel to the wind. Field observations of this banded structure appear in all detailed reports of oil spills at sea. Crosswind sweeping affects downwind transport rates because of the crosswind variability of the downwind surface drift velocity in the Langmuir

circulation system. In particular, the downwind surface speeds are larger in the surface convergence zones, where flotsam collects, than elsewhere on the surface. The vertical motions in Langmuir circulation systems are comparable to the surface sweeping component. As a consequence, in addition to the surface organization of oil, Langmuir circulation promotes the suspension of oil into the water column. To the extent that this subsurface suspension is significant, it should affect the fate of spilled oil, as well as prospects and strategies for oil-spill cleanup.

All of these consequences of Langmuir circulation are considered here.

This report is divided into two parts. In Part I, the physics of the interaction of floating oil with the wind driven Langmuir current system is reviewed and extended as needed to provide reasonable estimates of the effects on oil transport. In Part II, this information is assembled in a computer code for the surface and subsurface transport of oil. Part II can be read independently and used to experiment with the effects Langmuir circulation may have on oil spill transport.

The models introduced in Part I are aimed at estimating transport from commonly available environmental data. The bulk of Part I was written over the five year span of the contract. During the course of the effort, some of the initial strategies tried were abandoned in favor of others, and the written accounts of these preliminary avenues of investigation submitted earlier to the MMS are omitted from Part I. For example, hindcasts of the Pacific Ocean field experiments known as MILDEX were carried out using direct numerical simulation of the nonlinear partial differential equations thought to govern Langmuir circulation. These were reported to MMS in extensive detail in 1992 and 1993, but are excluded from Part I.

Those portions which are retained contribute to the final transport model proposed. For the most part, the report carries over portions originally submitted to MMS as preliminary reports. As a consequence, references to research on Langmuir circulation published in the interim have not been systematically incorporated. Some of the elements included describe efforts that are important to oil spill transport and fate, but are not implemented in the final transport model because it is believed that further research is advisable. For example, the chapter devoted to modelling the breakup of floating oil into fragments that can be drawn into suspension in the water column requires data and hypotheses concerning turbulence right at the ocean surface. The results of the model indicate that the assumptions concerning turbulent intensities in this region may need further examination.

Part II of the report is intended to bring the physical models for near surface oil transport developed in Part I into concrete form by construction of

a computer code for oil spill trajectory simulation embodying these models. This has been implemented in MATLAB[1] in a code dubbed OILTRACK.

Environmental data of only a limited nature is available, and gaps in available data make it necessary to adopt or develop mathematical models for characteristics of the ocean environment needed to determine near surface motions and oil transport. The development of such models has been an important part of this research program.

Input data to OILTRACK consists of wind speed and direction at a prescribed sampling rate; background surface current (not locally wind generated), provided from an external program, historical data, or observation; mixed layer depth as determined from on-scene measurements, or historical data at the given time of year at nearby locations (if no data on mixed layer depth is available, an Ekman layer depth is substituted, requiring the latitude to be provided); water temperature and salinity; oil density and its interfacial tension against seawater (this may include an algorithm to account for changes in properties with weathering).

From this input data, the computational model produces the sea state, which is required for the existing theory of Langmuir circulation, and a set of oil transport "attributes" that extend or improve the information provided by past oil spill prediction technology. These attributes include Lagrangian oil surface transport velocity, accounting for surface velocity structure; collection rates of oil into windrows, or "oil lanes"; oil lane separation; the fraction of open surface water and oil lanes. In addition to these attributes, the modelling of Part I permits additional attributes – the percentage of subsurface oil; percentage of oil in oil lanes; oil resurfacing time; and the depth of subsurface oil concentrations – to be calculated. The models for these attributes depend directly on the breakup of floating oil, and their implementation in OILTRACK has consequently been deferred.

[1]MATLAB is a trademark of The MathWorks, Inc..

Surface and Near-Surface Motion of Oil in the Sea Part I: Physical Modelling

by
S. Leibovich
Environmental Sciences of Ithaca
FINAL REPORT
Contract 14–35–0001–30612
Submitted to Minerals Management Service
Department of the Interior

March 29, 1997

Contents

1 Introduction to Langmuir Circulation and its effects on Surface Drift 4

1.1 Introduction 4

1.2 Occurences and Implications of Langmuir Circulations 6

1.2.1 General Description of Langmuir Circulation 6

1.2.2 Data from FLIP 9

1.2.3 Implications of Langmuir Circulations: Physics of the Mixed Layer 10

1.2.4 Implications of Langmuir Circulations: Oil Spills . . . 11

1.3 Thermal convection: Mechanism and scales 13

1.4 Elements of Vorticity Dynamics 17

1.4.1 Navier–Stokes equations 18

1.4.2 Vortex lines and tubes, and circulation 19

1.4.3 Kelvin's theorem: "Permanence" of vortex lines 21

1.4.4 Vorticity intensification by vortex line stretching . . . 24

1.5 Water Waves and Stokes Drift 25

1.5.1 Stokes drift of plane monochromatic gravity waves . . 26

1.5.2 Stokes drift arising from a continuous spectrum 29

1.6 Derivation of Langmuir Circulation Theory 30

1.6.1 Mean vorticity 30

1.6.2 Derivation by the Generalized Lagrangian Mean . . . 33

1.6.3 The Coriolis Acceleration and Stratification 38

1.7 Langmuir Circulation: Scales 41

1.8 Reduction of Complexity 43

1.8.1 Structureless equilibria 43

1.8.2 Weak instability, amplitude equations, and patterns . 44

1.8.3 Strong instability and patterns 45

1.8.4 Applications to Langmuir circulations 46

2 Specification of the Sea State and Boundary Conditions 47
2.1 Representation of the sea state 47
2.1.1 Stokes drift for a random wave field 50
2.1.2 Specification of the wave spectrum and its development in space and time 53
2.1.3 Stokes drift specification 58
2.2 Exchange processes at the mixed layer boundaries 60
2.2.1 a. Boundary conditions 61
2.2.2 b. Structureless equilibrium 64
2.2.3 c. Typical parameter magnitudes 66

3 Estimates for Turbulent Exchange Coefficients 68
3.1 Classical estimates 68
3.1.1 Ekman layer fit 69
3.1.2 Wave associated turbulence 69
3.1.3 Estimates from shear flow turbulence 70
3.2 Estimates from numerical experiments 72

4 Collection of Surface Oil into Windrows 74
4.1 Introduction 74
4.2 Thin films on water 75
4.3 Estimates of surface water velocity 78
4.4 Oil in windrows and its surface transport 80
4.4.1 Sweeping of oil into windrows 80
4.4.2 Collection effects on downwind transport 84

5 Oil Suspended in the Water Column 87
5.1 Introduction 87
5.2 Oil breakup 89
5.3 Subsurface Trapping of Oil 90
5.3.1 Stommel's model problem 90
5.3.2 Transport across the retention zone boundary 92

6 Disintegration of Coherent Oil into Droplets 95
6.1 A statistical model for droplet size 97
6.1.1 Conditional probability density 97
6.1.2 Allowing for energy supply rate variability 99
6.1.3 Simulation of stochastic breakup 100
6.2 Dissipation rate near the sea surface 102

6.3 Terminal velocity by oil product type 106

7 Model for Three-Dimensional Current Structure 111
7.1 Introduction 111
7.2 Simulation problem 112

References 124

Chapter 1

Introduction to Langmuir Circulation and its effects on Surface Drift

1.1 Introduction

Irving Langmuir carried out the first scientific investigation of the phenomenon now called Langmuir circulations, and reported the results in 1938 ([44]). This physical phenomenon became known to him as a consequence of the spatial aggregation of biological material that it caused, and which he observed as rows of *Sargassum* on the ocean surface during a cross-Atlantic voyage by ship. Had the patchiness in the *Sargassum* distribution been less apparent, it is very likely that the discovery of the physical phenomenon would have taken a much longer time.

The rows were essentially parallel to the direction of the surface wind, and are called windrows. Earlier published references to rows aligned with the wind on natural bodies of water can be found (see the review in [52]), but the underlying causes had not been considered. Langmuir, in the subsequent series of experiments on Lake George in New York State reported in his 1938 paper, showed that the collection of surface material into rows was due to convective motions, and inferred that the phenomenon owed its existence to the action of the wind through some unknown mechanism.

The potential biological significance of Langmuir circulations was quickly appreciated, being first pointed out by Woodcock [92] in 1944. The relevance to marine biology is now commonly recognized (see, for example, the reviews

by Fasham [20] and by Denman & Powell [19]). In an important short paper, Stommel [82] recognized that Langmuir circulations, as well as other convective motions, can lead to a suspension of particulate matter well removed from the surface at which, by virtue of their weight, they would normally be imagined to congregate. This observation enlarges the scope of spatial aggregation from a surface phenomenon situated at locations of surface water convergence to a three–dimensional question. The vertical transport in convective motion apparently is of greater biological import than the horizontal sweeping that creates the most readily observed patterns. This conclusion is likely to apply with equal force to the motion of oil spills.

Patterning of the sea surface by convective processes clearly has a potential impact in creating patterns, both in the horizontal and in the vertical, of any buoyant material introduced into the ocean, whether living or not. Here the interest is in the distribution of oil spilled at sea. In this context, the known features of Langmuir circulations suggest that the interaction of spilled oil with this physical phenomenon should affect the net rate of movement of the oil, as well as its distribution both on and below the sea surface. These known features will be surveyed in the next section. It can be stated with confidence, however, that Langmuir circulations do affect the distribution of spilled oil, since there are a number of observations confirming this effect (see, for example [5], [30]).

Convective processes such as Langmuir circulation are not the only physical phenomena leading to the formation of patterned arrangements in the upper layers of the ocean. These arrangements commonly appear in the form of rows, and reports of such patterns may be traced back hundreds of years [6], although mostly without recognition that the material making the patterns visible was living. In [70], zooplankton *Oikopleura longicauda* were observed collected into rows by thermal convecttion, which occurs when there is cooling of the water at the air-sea interface). Other mechanisms such as thermohaline convection, which is due to very disparate rates of the molecular diffusivities of salt and heat, internal wave activity, and fronts separating water masses with different properties, and a number of other possible causes, may lead to patterning.

§1.2 discusses the occurences of Langmuir circulations and the implications the phenomenon has on physical oceanography and on pollution questions. In order to introduce the central theme of convective instability in the simplest terms, the physical mechanisms responsible for thermal convection, the prototypical convective activity, will be discussed in a nonmathematical fashion in §1.3. The relevant scales for these processes are

extracted heuristically, with the aim of developing an understanding of the prospects for interaction with floating material, such as oil, in the ocean.

The discussion of Craik–Leibovich (CL) theory of Langmuir circulations starts in §1.4 with a review of the basic fluid mechanical concept of vorticity, which comprises the first element needed for Langmuir circulations to exist. The second element needed, according to the CL theory, is propagating surface waves. Propagating fluctuations create a slow mass drift, known as Stokes drift, and §1.5 discusses this Lagrangian drift current. The formal derivation of the CL theory follows in §1.6. In §1.7, a heuristic and nonmathematical discussion is presented arriving at the relevant scales for the convective motion in Langmuir circulations. The approach here follows the method used for thermal convection. To calculate many Langmuir circulation fields from the full CL theory is a formidable task, and a method of reduction of the complexity is outlined in §1.8. This will be explained in some detail in subsequent chapters.

1.2 Occurences and Implications of Langmuir Circulations

A survey of observations of Langmuir circulations prior to 1982 may be found in the review [52]. In this chapter, a distillation of the features reported in these observations will be given, together with a synopsis of the more recent field observations. The early observations are often confined to the visual appearance of surface patterns. Even when subsurface measurements were also included, the data on water motions was fragmentary, and reports of surface wind speeds and sea state were not given concurrently. As attempts at theoretical description suggested the need, and as improvements in measurement technology became available, field experiments have become more comprehensive and complete. In a subsequent section, the important data recorded by Weller and Price [88] will be analyzed.

1.2.1 General Description of Langmuir Circulation

Langmuir circulations are generally agreed to be generated by the wind, as Langmuir himself originally concluded [44], and to take the form of a series of counterrotating vortices with axes closely parallel to the wind direction. The vortices lie in the upper layers, extending from the surface to some depth that cannot be considered to be definitively established. An

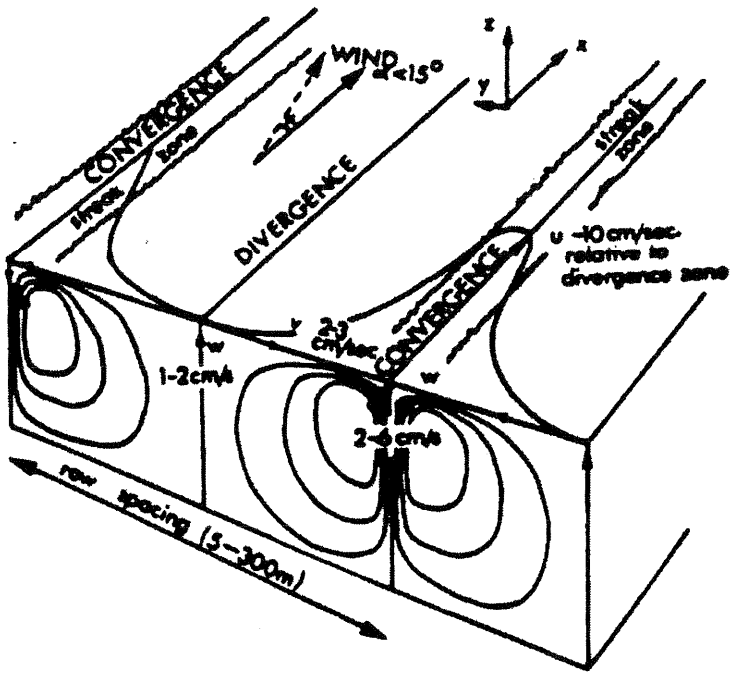

Figure 1.1: Sketch of the general features of Langmuir circulations, taken from Pollard.

immediate consequence of the vortices is the production of lines of surface convergence, which, though coexisting with a wind–generated surface wave field that produces substantially larger water particle speeds, nevertheless is persistent, and sweeps floating material into rows, known as "windrows". Figure 1.2.1 illustrates the general features of Langmuir circulations (which will often be abbreviated in these reports as LC). The particular values cited on the sketch, which is taken from Pollard [73], may be regarded as more or less "typical". The values for the windward and vertical velocities, for example, must scale with the surface wind speed. Furthermore, the more detailed "modern" measurements suggest that the intensity of the circulations is greater than that suggested in the sketch.

The surface streaks are readily visible when the wind speed exceeds 3m/s, provided surface tracer material, such as seaweed, foam, or other flotsam is abundant. Even in the absence of flotsam, naturally occuring organic film is swept into the windrows, and, because capillary waves are damped by

the presence of the film, windrows may be visible as slicks where the water surface is relatively smooth. The surface streaks are often quite regularly spaced; at other times, they are somewhat less regular, but they are always aligned close to the wind.

This direct association of the vortical structures with the wind may be taken to define Langmuir waves to interact with a current, and still produce surface rows. As a consequence, surface rows may, at least in theory, result from swell originating at some distant source of wind forcing, provided the current structure is suitable. Thus local wind forcing may not be necessary to the existence of wave–current generated set of surface rows. With this in mind, it is reasonable to assume that the primary role of the wind in Langmuir circulations is to generate both surface waves and current which have the relationships appropriate to each other to result in the characteristic vortical structures.

Although many of the reports of Langmuir circulations suggest a minimum wind speed of 3m s^{-1}, this condition is not required. Because the circulations have been observed for lower wind speeds, it appears that the minimum wind speed, assuming that one exists, does not have a universal threshhold value, but instead depends on the situation in a potentially complicated way.

Windrows form within a few minutes of the onset of a sufficiently strong wind. Since windrows lie above convergence zones, the spaceing between two neighboring rows describes the horizontal width of a pair of counter-rotating cells. The rapidity of formation suggests that the circulations are initially shallow and of small scale. Observational evidence indicates that the convective cells produced by the Langmuir vortices may extend to the base of the mixed layer, typically several tens of meters. This indicates that the cells, though initially affecting only a shallow layer, grow in scale and penetrate deeper with time. The spacing of windrow ranges from lengths on the order of a meter to hundreds of meters. A hierarchy of scales is often reported, suggesting that the small scales are continuously produced, and cascade to larger scales with the largest scales limited by the depth of the existing mixed layer.

The downwelling flow, under the lines of surface convergence, and the upwelling flow, under lines of surface divergence, are not symmetrical. Indeed, the downwelling takes place in a relatively concentrated "jet" occupying only a minor fraction of the spacing between rows, and therefore the downwelling is substantially more intense than the upwelling, which is spatially more diffuse, and presumably occupies the balance of the space outside of the jet.

The windward surface currents are also stronger in surface convergences than they are outside of the downwelling jets. This surface current anomaly is almost always reported, usually without concurrent reporting of the wind speed or further details of the current structure.

1.2.2 Data from FLIP

While visual observations of LC in the ocean are numerous, detailed measurements are extremely difficult. The measurements reported in Weller et al. [89], and in particular in Weller & Price [88] and Smith et al. [80] are unique and extremely valuable. These papers describe data taken during a series of three cruises (the third as part of the MILDEX – Mixed Layer Dynamics Experiment), in 1982 and 1983. The measurements were made from the Research Platform FLIP of the Scripps Institute of Oceanography as it drifted from 200 to 850 km off the coast of California. The experiments are unique, because they provide accurate three–dimensional velocity and temperature data from the surface to the thermocline, together with simultaneous records of wind speed and direction, sea surface temperature, surface visualizations of windrows which could be correlated with velocity features, and finally, a rough indication of sea state.

This experiment confirmed the following characteristics of LC, which had previously emerged as a composite picture of many earlier and more fragmentary studies.

- LC cause convergences, or windrows, approximately parallel to the surface wind direction.
- The penetration depth is a significant fraction of the mixed layer depth, which during their experiments was on the order of 50 m. They found strong effects of LC down to about half (20–35 m) the mixed layer depth. Reports from other studies indicate penetration throughout the mixed layer.
- Convergences were found in a hierarchy of spacings, ranging from several meters up to 100 m.
- Vertical downwelling speeds below surface convergences in excess of 25 cm/s were measured, amounting to as much as 2% of the wind speed. Downwelling zones are narrow compared to a broad and diffuse upwelling that occurs between convergences. This narrow "jet" has been reported by virtually all observers.

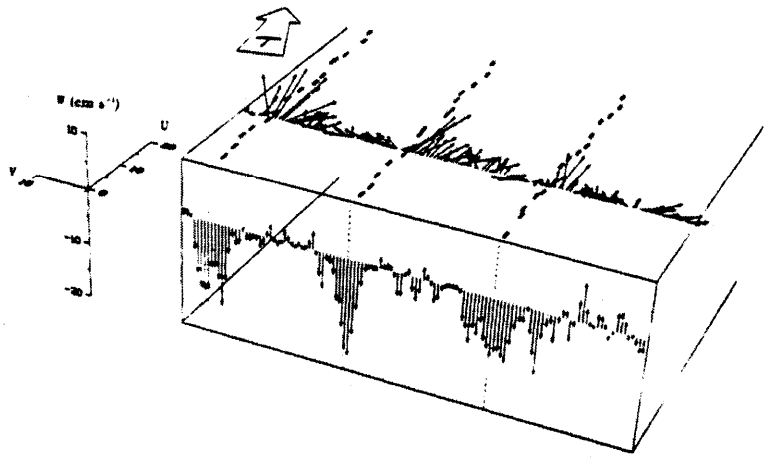

Figure 1.2: Measured data in Langmuir circulations, from Weller & Price.

- Associated with the downwelling jet is an increase of speed in the downwind direction of a comparable amount. Thus, the jet is oriented roughly 45° to the horizontal. Furthermore, this downwind speed anomaly is greatest a few meters *below* the surface. That this might happen was predicted ten years earlier in calculations from the CL theory (see [50], [54]).

Figure 1.2.2 is from the Weller & Price paper. This figure graphically presents their data and concisely captures the general structure of Langmuir circulations.

A number of ambitious field experiments have been carried out since the MILDEX project discussed above, but the features outlined have not been altered. A large body of recent data is discussed by Plueddemann et al. (1993).

1.2.3 Implications of Langmuir Circulations: Physics of the Mixed Layer

The mixed layer connects the atmosphere to the ocean. Most of the solar radiation is absorbed in the waters of the mixed layer, and the heat stored here is later redistributed. The momentum transferred from air to sea, like

the heat transfers, are communicated through the mixed layer.

The distribution of heat, buoyancy, and gas exchanges modulated by the mixed layer are important to the general circulation of the ocean, to climate modelling, to an understanding of the CO_2 budget, to marine biology, and to naval operations.

Langmuir circulation constitute one of the mechanisms that maintains the mixed layer in its mixed condition. The stirring needed to keep the properties of temperature, salt, momentum, and passive additives like dissolved gases nearly uniform in the mixed layer is accomplished by small scale turbulence generated by shear instabilities and by breaking waves, and convective motions arising from thermal instability and from Langmuir circulations. The latter do not require surface cooling needed for thermal instability, and are commonly present when there is at least a modest wind. Furthermore, in a modest wind, the Langmuir circulation mechanism is more powerful than thermal instabilities arising from typical surface cooling. In contrast to incoherent turbulence, Langmuir circulations are large scale, and penetrate most of the water in the mixed layer. In this way, the large scale stirring actively ties together the entire mixed layer, and thereby serves as efficient means of homogenizing the bulk properties of the mixed layer.

It is worth noting that, when both thermal instability and Langmuir circulations are simultaneously possible, the resulting motion appears like Langmuir circulations, but with added vigor. When there is surface heating, thermal effects are stabilizing. Nevertheless, Langmuir circulations are still possible and continue to be effective in mixing the upper layers, although the stabilizing thermal effects may weaken the mixing effect. Both the enhancement effect of thermal instability and the restraining effect of thermal stability on Langmuir circulations have been documented (see the survey [52] for references). More recently, Li and Garrett [60] have used the CL theory to assess the relative importance of thermal instability and Langmuir circulation, and conclude that under reasonable values of surface cooling, Langmuir circulation dominates even under relatively low wind conditions.

where Pr_T is a turbulent Prandtl number. Assuming prescribed stress and waves, they determine the value of the H They conclude that under typical conditions of surface heat flux and wind generated waves

1.2.4 Implications of Langmuir Circulations: Oil Spills

The role of Langmuir circulations (LC) in the formation of surface oil into bands has been discussed (see, for example, [30], [5]) in reports of the phys-

ical surveys of oil spill occurences at sea.

A common rule of thumb used to estimate the surface drift of floating material under wind action is to assume that it moves at a speed proportional to the wind speed. The constant of proportionality is often fixed at 3% to 4% of the wind speed.

It has been known, at least since the Santa Barbara Channel blow–out in 1969, that oil tends to collect in bands on the sea surface. This is the origin of the formation of bands of oil that subsequently form "ropes" of "chocolate mousse" as the oil incorporates water in a water–in–oil emulsion. In fact, the organization of floating material into streaks aligned within a few degrees of the wind direction has been known for much longer, the first scientific documentation of windrows being due to Langmuir in 1938 [44], and rapidly being documented to be of ecological importance by marine biologists. Among the documentations of banded structure in the context of oil spill events may be found in the accounts given in [5] concerning the IXTOC I oil spill in June, 1979. Color photographs included in that report and in an earlier NOAA report on the AMOCO CADIZ accident ([30]) show banded oil structures similar in all main respects to bands of marine organisms.

It is known that water in windrows moves faster than water between windrows. A survey of the main characteristics of Langmuir circulations (LC), the general origin of windrows, will be given in §8. For the purposes of this section, it suffices to say that it is known that surface convergences marked by windrows contain narrow "jets" of fluid moving at speeds that can be more than twice the speeds between convergences. Furthermore, these jets have a vertical component, and carry water down, as well as downwind, at an angle of roughly 45° to the horizontal (see measurements made from R.P. *Flip* by Weller and Price [88]), and the maximum in the downwind velocity occurs below the water surface. Data indicates that the downwind velocity anomoly is comparable to the vertical velocity anomaly in LC. Weller & Price, for example, found maximum vertical velocities in their LC data that exceeded 2% of the wind velocity.

Since floating material is gathered in convergence zones, it is affected more by the underlying water motion in these regions than it is by the average water motion. The implications for oil movement prediction are obvious and significant. For example, if the wind is steady in direction and speed at 10m/s, and if all of the oil were concentrated in windrows and moved with the underlying water, then in a 24 hour period the oil would move 17.3 km further than would the horizontally averaged surface water.

This is likely to exaggerate the effect of windrows, but also illustrates their potential relevance to surface transport. Another way to look at the effect is this: if the "rule" adopted is to estimate the wind induced current at 3.5% of the windspeed, then oil concentrated in windrows can move at up to 5.5% of the windspeed. This may well be an important contributor to the notorious variability of the parameterization of drift with wind speed.

1.3 Thermal convection: Mechanism and scales

Convective processes are mainly up-down water motion set up by vertical gradients. They tend to equalize the vertical property variations in the water column responsible for the convection. This means that they are inherently self–limiting, since they act to erase the agency that gives rise to them. The prototype of convective processes is thermal convection, and we start by looking at this phenomenon in an entirely heuristic and physical way.

The standard idealized model for thermal convection, upon which more realistic problems are based, contemplates a horizontal layer of fluid (liquid or gas) of finite depth, say d. Its top surface (coinciding with the plane $z = d$) is maintained at one fixed temperature, T_{top}, and the bottom surface (at the plane $z = 0$) is held at a another fixed temperature, $T_{bottom} > T_{top}$. Under most circumstances, fluids expand when heated and thereby become less dense, or lighter per unit volume, and contract and become more dense, hence heavier per unit volume, when cooled. Heavier fluid lying above lighter fluid will, as common sense would tell us, tend to sink. "Tend" is the operative word, because if the fluid temperature and hence its density were stratified in perfectly horizontal layers, the temperature and density varying only in the vertical direction, z, it would be in equilibrium and could maintain this (unnatural) state of affairs forever if left unperturbed. The equilibrium is one with no motion, and a temperature variation

$$T = T_{bottom} - \Delta T \frac{z}{d}, \qquad \Delta T \equiv T_{bottom} - T_{top}.$$

It is impossible to prevent very small disturbances to this (Platonic) situation, however, and so one must suppose that any equilibrium will be disturbed so that there are (at least very small) variations of the density in the horizontal as well as the vertical direction, and the equilibrium force balance will be disrupted, causing motion. Still, the motion that results could either further disrupt the equilibrium, leading to an increase in the

disturbance or it could decrease, returning the system to its original condition. The first possibility is the hallmark of an *unstable* equilibrium, and the second of a stable one.

It is an empirical fact that disturbances do tend to damp out, implying a stable situation, when the temperature difference across the layer is smaller than some clearly defined amount that depends on the depth of the layer, say d, and the properties of the fluid involved. Why doesn't the heavy fluid always continue to sink and the light fluid always rise, even when the temperature difference is small? The answer is that the cold fluid gains heat from the warmer surroundings it falls through, and the rising hot fluid cools down as it loses heat to the colder surroundings it traverses during its rise. If the temperature anomaly of a falling or rising blob starts out being too small, it can be dissipated before the blob has had a chance to move any significant distance. This can be seen from the following simplified analysis.

Suppose our static equilibrium state is slightly disturbed so as to produce a small blob of fluid hotter than the surrounding fluid, with a temperature excess δT. Suppose the blob has volume V, so its characteristic length scale is $a = V^{1/3}$. Because the blob is hotter, it is lighter than the surroundings, with a density difference $\delta\rho = -\rho\beta(\delta T)$, where β is the coefficient of thermal expansion of the fluid. Since it is lighter, the blob experiences an Archimedian buoyancy force, $\mathcal{B} = -g\delta\rho V$, where g is the acceleration due to gravity. The buoyancy force causes the blob to rise (slowly, because $|\delta\rho|$ is small). If the upward speed of rise is U, the frictional drag, $\mathcal{F}$, with which the surrounding fluid resists the motion of the blob is proportional to U, to the coefficient of viscosity, μ, and to the length scale of the blob, a, or

$$\mathcal{F} = C_1 a \mu U,$$

where C_1 is a dimensionless number that depends only on the shape of the blob. For example, if blob were a rigid sphere of radius R, $\mathcal{F} = 6\pi R\mu U$, so in this case $C_1 = 2(9\pi/2)^{2/3}$.

The blob loses heat to the colder surroundings. If this were not the case, the higher the blob would rise, the greater its temperature excess relative to the fluid it encountered, causing the buoyancy force to become larger, and its upward speed larger, and so on. The heat transfer between the blob and its surroundings takes place on a time scale τ proportional to the surface area, a^2, and inversely proportional to the thermal diffusivity, κ, of the fluid, so

$$\tau = C_2 a^2/\kappa,$$

for some dimensionless constant C_2. In the absence of heat transfer, a fluid blob displaced vertically upward a distance ℓ will keep the temperature of the background fluid at the location from which it started. Its temperature excess relative to its new location is therefore $(\Delta T/d)\ell$. But heat transfer does occur, and the temperature tends to equalize in a time interval of order τ. For the purpose of estimating a *sustainable* temperature excess of a blob moving vertically upward, we therefore may suppose that ℓ is of order of the distance the blob may move in a time of order τ. This estimate indicates a temperature excess of

$$\delta T = \frac{\Delta T}{d} U\tau,$$

and a corresponding buoyancy force of

$$\mathcal{B} = \frac{\beta g \Delta T}{\kappa d} \rho V U C_2 a^2.$$

Newton's second law applied to the vertical direction gives

$$\begin{aligned} \rho V \frac{dU}{dt} &= \mathcal{B} - \mathcal{F} \\ &= \rho V U \{C_2 \frac{\beta g \Delta T a^2}{\kappa d} - C_1 a^{-2}\}. \end{aligned}$$

The blob will accelerate upwards when the term in $\{\} > 0$, causing the departure from equilibrium to be accentuated, or the system to be unstable. If this quantity is negative, then the force on the blob is a restoring force, so the system is stable. Now the term in $\{\}$ is greatest when a is as large as it possibly can be, or $a = C_3 d$ (where C_3 is a number no larger than $1/2$, which would correspond to a spherical blob), and this will be connected with the smallest ΔT for which the bracket is positive, so instability can occur. This

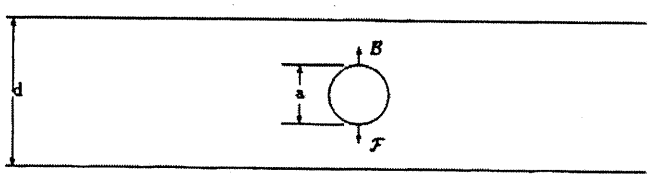

Figure 1.3: Sketch of forces on a blob of light fluid surrounded by heavy fluid.

smallest ΔT for which the bracket is positive, so instability can occur. This smallest ΔT may be found from the relation

$$\frac{\beta g \Delta T d^3}{\kappa \nu} > \frac{C_1}{C_2 C_3^4},$$

where $\nu \equiv \mu/\rho$ is the so-called kinematic viscosity. The left hand side of this expression is a dimensionless quantity, called the "Rayleigh number," Ra, and the right hand side is the "critical value" of the Rayleigh number, denoted Ra_c. Our estimate of Ra_c depends on the constants of proportionality that appeared in our parameterization of the fundamental physical processes that are involved. In a more complete mathematical treatment, Ra_c is found to depend on the boundary conditions imposed on thermal and mechanical processes. For example, if the top and bottom boundaries support no shear stresses and are held at constant temperature (i.e., isothermal boundaries), $Ra_c = 657.5$. The important point to make here is that stability depends on the parameter

$$Ra = \frac{\text{Archimedean buoyancy force}}{\text{Diffusive "resistances"}}$$

exceeding a threshold value, Ra_c.

When instability sets in, it does so in the form of cells having a characteristic horizontal length scale. The only geometrical length scale involved in the setting up of this stability issue is the depth of the layer, d. It is not surprising then, that according to linear stability theory, the preferred horizontal length scale is proportional to d. The constant of proportionality depends on the boundary conditions. When the boundaries are isothermal, for example, the cells are nearly square, with roughly equal horizontal and vertical extents, the cell shape depending only weakly on the mechanical boundary conditions. With this in mind, the natural choice for the prevailing horizontal length scale is d.

To find the expected velocity scale for the vertical motions that take place in an unstable layer, we note that the driving force for convection is buoyancy, and so the maximum work per unit mass of fluid that can be obtained is the maximum buoyancy force times the maximum distance over which the buoyancy force can act, or $\beta g \Delta T \times d$. The kinetic energy/mass must be smaller than this maximum work, so the greatest possible kinetic energy/mass derivable from the temperature difference across the layer is $\beta g d \Delta T$, implying the maximum possible speed of the convecting fluid layer

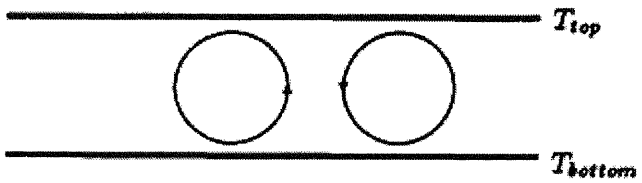

Figure 1.4: Sketch of a counter-rotating pair of convection cells with isothermal boundaries.

is $U_{max} = \sqrt{2\beta g d \Delta T}$, or

$$U_{max} = \frac{\kappa}{d}\sqrt{\sigma Ra}, \text{ where } \sigma \equiv \frac{\nu}{\kappa} \text{ is the "Prandtl number".}$$

This is a suitable scale for the convection, and in fact is an upper bound. It ignores dissipation entirely. For example, we know that for $Ra < Ra_c$, there is no motion induced by instability. With this in mind, an improved estimate would be

$$U_{max} \sim \frac{\kappa}{d}\sqrt{\sigma(Ra - Ra_c)}.$$

1.4 Elements of Vorticity Dynamics

The principal physical mechanism underlying Langmuir circulations is an inertial one. The diffusive effects of viscosity, although important, serve to set the scene rather than to play the lead role in it.

One time–honored way to arrive at an understanding of fluid phenomena dominated by inertial effects is to focus attention on the *vorticity* of the flow. Vorticity is a vector, denoted by the symbol $\boldsymbol{\omega}$, defined to be the curl of the velocity vector. It has a direct and fundamental physical meaning: the vorticity vector is exactly twice the instantaneous angular velocity of a fluid particle. Thus, if one were to (conceptually only, of course) isolate a small fluid mass and instantaneously freeze it without otherwise changing the state of its motion, it would be a rigid body translating and rotating through space, and its angular velocity would be half the vorticity.

There is a sizeable body of knowledge about the behavior of vorticity that is often referred to as "vorticity dynamics". We need a few key results only, and these are derived here.

1.4.1 Navier–Stokes equations

The motion of a Newtonian fluid is determined by the Navier–Stokes equations, which express conservation of momentum. Written in an inertial coordinate system, these are,

$$\rho\frac{D\mathbf{u}}{Dt} = -\nabla p + \nabla\cdot\mathbf{T}_\mu + \rho\mathbf{f}, \tag{1.1}$$

where ρ is the fluid density, p the pressure, $\mathbf{f}$ the body force per unit mass, $\mathbf{T}_\mu$ is the part of the stress tensor that is proportional to the fluid viscosity, μ, and

$$\frac{D}{Dt} = \frac{\partial}{\partial t} + \mathbf{u}\cdot\nabla\mathbf{u}$$

is the "material derivative". The latter expresses the rates of change as measured by an observer moving with a fluid particle. An important special case is the material derivative of the velocity vector, which is the acceleration of a fluid point.

These equations must be supplemented by a specification of the body force, the thermodynamic equation of state and thermodynamic constitutive equations giving coefficients of expansion, specific heats and related thermodynamic properties, and the equations for conservation of energy and mass. The latter equation, the equation of continuity, is

$$\frac{D\rho}{Dt} + \rho\nabla\cdot\mathbf{u} = 0. \tag{1.2}$$

In (1.1), the viscous part of the stress tensor

$$\mathbf{T}_\mu = \mu\{[\nabla\mathbf{u} + (\nabla\mathbf{u})^T] - \frac{2}{3}(\nabla\cdot\mathbf{u})\,\mathbf{I} \tag{1.3}$$

when the bulk viscosity is neglected (which is always permissible for liquids and nearly always so for gases). In this equation, $(\nabla\mathbf{u})^T$ is the transpose of the velocity gradient tensor, and $\mathbf{I}$ is the identity tensor.

When a fluid motion may be regarded as incompressible, which by definition means that $\nabla\cdot\mathbf{u} = 0$, then the equations simplify. This is an approximation appropriate to oceanographic flows. Furthermore, if the flow is dominated by inertial effects, we can ignore the viscous part of the stress. We will always assume incompressibility, and in this section, we shall assume inertially dominated motion.

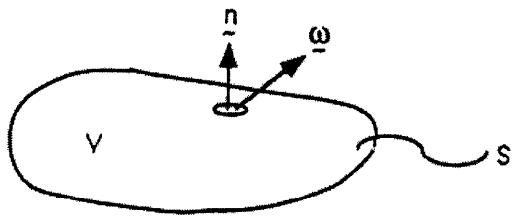

Figure 1.5: The net flux of vorticity out of any closed volume vanishes identically.

1.4.2 Vortex lines and tubes, and circulation

Since

$$\boldsymbol{\omega} = \nabla \times \mathbf{u},$$

where $\mathbf{u}(\boldsymbol{x},t)$ is the velocity vector defined everywhere in some prescribed volume in space,

$$\nabla \cdot \boldsymbol{\omega} = 0. \tag{1.4}$$

Here the position vector, $\boldsymbol{x} = (x, y, z)$ describes the position of each point occupied by fluid, and t is the time. Since its definition leads to its divergence–free character, the divergence theorem guarantees that the surface integral over the bounding surface, S, of any subvolume, V, containing only fluid, of the normal component of the vorticity vector must vanish, or

$$\int_S \mathbf{n} \cdot \boldsymbol{\omega} dS = 0, \tag{1.5}$$

where $\mathbf{n}$ is the unit outward normal to S (see sketch).

A "vortex line" is defined to be a line everywhere tangent to the vorticity vector. It is analogous to a fluid streamline, which is defined to be a line everywhere parallel to the velocity vector. A "vortex tube" is a bundle of vortex lines, generated by the set of vortex lines passing through the points on a closed curve, as shown in Figure 1.4.2.

Choose a volume V coinciding with a segment of a vortex tube between cross–sectional areas A_1 and A_2, and apply (1.5). The integral over the part of S made up of vortex lines automatically vanishes, since $\mathbf{n} \cdot \boldsymbol{\omega} \equiv 0$ there.

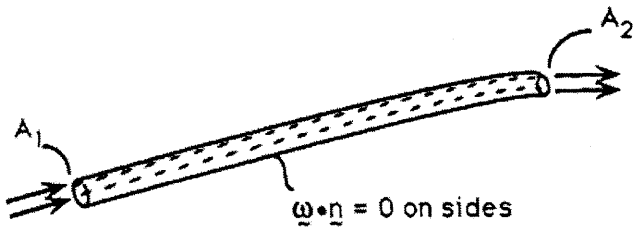

Figure 1.6: A vortex tube is a bundle of vortex lines. Here a section of finite length between cross–sectional areas A_1 and A_2 is shown.

This leaves the contributions over the part of S made up of A_1 and A_2 over which there is a nonzero component of $\mathbf{n}\cdot\boldsymbol{\omega}$. Over these two areas, the unit normal is nearly parallel or antiparallel to the vorticity vector. Suppose at area 2, the normal is approximately aligned with the vorticity direction, then at area 1 it will be essentially antiparallel to the vorticity. Let the normal over area 2 be $\mathbf{n}_2 = \boldsymbol{\nu}_2$ and that over area 1 be $\mathbf{n}_1 = -\boldsymbol{\nu}_1$. Then

$$\int_{A_1} \boldsymbol{\nu}_1\cdot\boldsymbol{\omega} dS = \int_{A_2} \boldsymbol{\nu}_2\cdot\boldsymbol{\omega} dS, \tag{1.6}$$

which says that the amount of vorticity "flowing" into the tube across area A_1 leaves the tube across area A_2.

By passing to the limit in which the cross–sectional area of the tube shrinks to zero, the result above is interpreted as proving that vortex lines do not "begin" or "end" in the interior of the fluid. Thus, vortex lines are either closed curves (including the possibility of closing at infinity if the region of space is infinite), or that vortex lines begin and end on the physical *boundaries* of the fluid.

The "circulation" is defined for any closed path, say C, that can be drawn in the fluid. Usually denoted by the symbol gamma, the circulation is

$$\Gamma_C \equiv \oint_C \mathbf{u}\cdot d\mathbf{s}, \tag{1.7}$$

where $\mathbf{u}$ is the fluid velocity and $d\mathbf{s}$ is the differential of the directed arclength

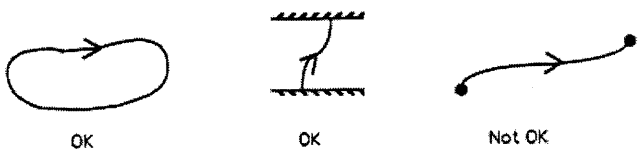

Figure 1.7: Possible and impossible arrangements for vortex lines.

on the curve. The circulation measures the average degree by which the fluid rotates about a point located inside the defining curve.

By Stokes theorem, the circulation can be written in an alternative way,

$$\Gamma_{\mathcal{C}} = \int_{\mathcal{S}} \mathbf{n}\cdot\boldsymbol{\omega} dS, \tag{1.8}$$

where $\mathcal{S}$ is any open surface having $\mathcal{C}$ as its edge, and $\mathbf{n}$ is the unit normal vector on $\mathcal{S}$ defined so that it is oriented via the right–hand rule by the orientation of the path about $\mathcal{S}$.

Now consider a closed path $\mathcal{C}_1$ drawn around a vortex tube, as in Figure 1.4.2, and a second path $\mathcal{C}_2$ drawn about the same tube. Then (1.8) and (1.6) together show that $\Gamma_{\mathcal{C}_1} = \Gamma_{\mathcal{C}_2}$. Since the two paths are arbitrarily chosen and have only the common feature that they both link the same vortex tube, this shows that the circulation around all paths linking a given vortex tube have the same value.

1.4.3 Kelvin's theorem: "Permanence" of vortex lines

Consider a closed path marked in the fluid at some instant of time, and then follow this collection of fluid particles as time proceeds. This collection of fluid particles will always mark a closed curve in space, so we may designate this *material curve* for all time by $\mathcal{C}(t)$. At each instant, the circulation about the material curve can be calculated, and the result is a scalar function of time. Kelvin's theorem says that this function is in fact a constant provided the body force is conservative, and provided the motion is barotropic, which means that the density is a function of the pressure alone. Both assumptions are often good ones.

To derive this result, it is easiest to write the line integral in (1.7) as an ordinary integral by describing the curve $\mathcal{C}(t)$ in parametric form. Consider one fluid point on the curve, and suppose that it was located at $\mathbf{X}$ at the initial time. Then at all subsequent times, its position vector will occupy positions on the trajectory of the fluid point, $\mathbf{x}(\mathbf{X}, t)$. The argument t of course indicates time, and the argument $\mathbf{X}$ identifies which fluid particle is under consideration and is called the Lagrangian label, or Lagrangian coordinate.

A parametric representation of the initial closed curve will be a description of the form $\mathbf{X} = \mathbf{X}(\sigma)$, where σ is the parameter selected, and can always be chosen to vary from zero to one as the closed curve is traversed. Thus $\sigma = 0$ and $\sigma = 1$ correspond to the same point in space. With this representation, we can say that each fluid point on the closed curve is given by

$$\mathbf{x} = \hat{\mathbf{x}}(\sigma, t)$$

for some specific value of σ less than one, and as σ varies, the tip of the vector $\hat{\mathbf{x}}(\sigma, t)$ traces out the curve $\mathcal{C}(t)$ at the corresponding time. Furthermore,

$$\Gamma_{\mathcal{C}(t)} = \int_0^1 \mathbf{u}(\hat{\mathbf{x}}(\sigma, t), t) \cdot \frac{d\hat{\mathbf{x}}(\sigma, t)}{d\sigma} d\sigma. \tag{1.9}$$

The time rate of change of (1.9) is

$$\frac{d\Gamma_{\mathcal{C}(t)}}{dt} = \int_0^1 \frac{D\mathbf{u}}{Dt} \cdot \frac{d\hat{\mathbf{x}}(\sigma, t)}{d\sigma} + \int_0^1 \mathbf{u} \cdot \frac{d\mathbf{u}}{d\sigma} d\sigma, \tag{1.10}$$

since the time rate of change of $\mathbf{u}(\hat{\mathbf{x}}(\sigma, t), t)$ holding σ constant is just the material derivative. The quantity appearing under the second integral sign is a perfect differential of half the square of the speed, $|\mathbf{u}|^2$, and so can be intergrated to give half the difference in the square speed at $\sigma = 0$ and $\sigma = 1$. Since this is the same fluid point the difference is zero. Furthermore, the remaining integral can be rewritten as a line integral, so that

$$\frac{d\Gamma_{\mathcal{C}(t)}}{dt} = \oint_{\mathcal{C}(t)} \frac{D\mathbf{u}}{Dt} \cdot d\mathbf{s}. \tag{1.11}$$

This is the integral of the fluid *acceleration* around the closed path.

The acceleration can be replaced by the forces, using the momentum equation. If viscosity is ignored the Navier–Stokes equations (1.1) reduce to the Euler equations

$$\frac{D\mathbf{u}}{Dt} = -\frac{1}{\rho} \nabla p + \mathbf{f} \tag{1.12}$$

on dividing by density.

Substituting for the acceleration in (1.11),

$$\frac{d\Gamma_{C(t)}}{dt} = \oint_{C(t)} \{-\frac{1}{\rho}\nabla p + \mathbf{f}\}\cdot d\mathbf{s}.$$

The contribution from the body force vanishes when it is conservative, because the line integral around a closed path of any gradient dotted with the directed arclength is identically zero. Assuming a conservative body force, only the integral involving the pressure remains, and using Stokes theorem to write the contour integral as a surface integral,

$$\frac{d\Gamma_{C(t)}}{dt} = -\oint_{S} \mathbf{n}\cdot[\nabla\left(\frac{1}{\rho}\right) \times \nabla p]dS. \tag{1.13}$$

This shows that circulation can be generated when the surfaces of constant density and those constant pressure do not coincide, and the result is known as Bjerknes theorem.

If the motion is barotropic, then the surfaces of constant pressure coincide with surfaces of constant pressure, and the integrand in (1.13) is identically zero. In this case, Kelvin's theorem

$$\frac{d\Gamma_{C(t)}}{dt} = 0 \tag{1.14}$$

results.

Now consider a "vortex surface" defined to be a surface comprised of vortex lines. Such a surface passes through every point of space. If the conditions of Kelvin's theorem hold, the theorem can be used to show that vortex surfaces are material surfaces; that is, if a vortex surface is identified at some initial time, and the fluid particles lying on the surface are followed as they move, at a later time the same particles form a surface that continues to be a vortex surface. To see this, consider a closed contour drawn in a vortex surface, as illustrated in Figure 1.4.3. Since the normal component of vorticity vanishes on the vortex surface by definition, (1.8) shows that the circulation around the contour vanishes. Following the progress of this material circuit as time progresses, its circulation continues to be zero, by virtue of Kelvin's theorem. This is true for all contours that one can draw in the original vortex surface. Therefore the material surface that coincided with the original vortex surface has zero normal component of vorticity at all points, and therefore this material surface is also a vortex surface.

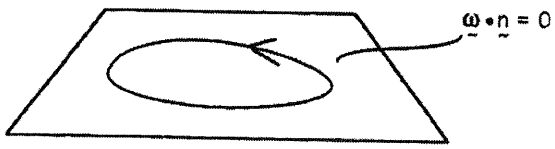

Figure 1.8: Vortex surface.

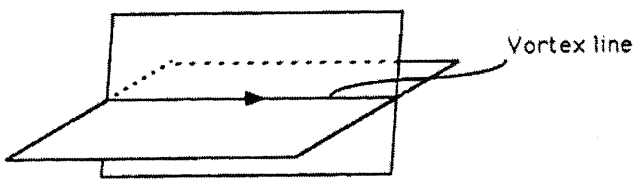

Figure 1.9: Vortex surfaces intersect in a vortex line, which moves with the fluid.

If two vortex surfaces intersect, they do so in a line which must be parallel to the vorticity vector, and therefore is a vortex line. Since each of two intersecting vortex surfaces are material surfaces a vortex line must be a material line. Therefore each individual vortex line coincides with a material line. It is this that is meant by the phrase "vortex lines move with the fluid".

1.4.4 Vorticity intensification by vortex line stretching

The area averaged vorticity in a vortex tube at a cross–section with area Σ is

$$\overline{|\omega|} \equiv \frac{1}{\Sigma}\int_{\Sigma} \mathbf{n}\cdot\boldsymbol{\omega}\, dS = \frac{\Gamma}{\Sigma}, \tag{1.15}$$

where Γ is the circulation for the vortex tube. Since the circulation is an invariant for the tube, the average vorticity is inversely proportional to the tube cross–sectional area.

But a vortex tube is a material tube. Consider a segment of a vortex tube of initially small cross–sectional area, Σ_0, and initially small length, ℓ_0. If the two cross–sections marking the boundaries of the tube segment are taken to move with the fluid (i.e., be material surfaces themselves), then the mass within the tube segment is a constant, and the tube segment is a material volume. Since mass is constant, at later time t, when the tube segment has length ℓ and cross–sectional area Σ, the mass will be $\rho\ell\Sigma$ and will be the same as the initial mass, $\rho_0\ell_0\Sigma_0$. This, together with (1.15) shows that

$$\overline{|\boldsymbol{\omega}|} = \overline{|\boldsymbol{\omega}_0|}\frac{\rho}{\rho_0}\frac{\ell}{\ell_0}, \tag{1.16}$$

where $\overline{|\boldsymbol{\omega}_0|}$ is the initial magnitude of the vorticity in the tube.

The result (1.16) shows that if a tube stretches its length, its vorticity intensifies, as a skater's angular speed increases when she stretches. When the fluid density is constant, or very nearly so, as in the ocean, then the density ratio in (1.16) is unity, and the only factor changing the level of vorticity is then the stretching (or contraction) of vortex lines. While this is limited in validity to the circumstances in which Kelvin's theorem holds (conservative body force, barotropic motion, negligible viscous force), it is a simple, powerful, and highly geometric way to understand the vorticity in the flow. Its magnitude is given by (1.16) and its direction coincides with the material line initially coinciding with its initial vortex line.

1.5 Water Waves and Stokes Drift

Many wave motions, including waves on the surface of natural bodies of water have small amplitudes in the sense that the particle speeds induced by the wave are small compared to the speed of propagation of the waveform. Furthermore, in these cases, the particle motion associated with the wave is oscillatory in time if measured at a fixed point in space, and the time average of any velocity component will vanish if there is no other agency causing the motion. An average at a fixed point in space is called an *Eulerian* mean.

An average following a fluid particle is called a *Lagrangian* mean. Even when the Eulerian mean velocity is precisely zero, the Lagrangian mean velocity may be, and usually is, nonzero. Thus, there generally is a persistent

net drift of mass connected with progressive water waves, and this drift, first explained by Stokes [81], is called the Stokes drift.

This can be most easily explained for progressive plane waves having a single frequency (monochromatic), and this will be done in the next subsection. Fortunately, since the assumption of small amplitude waves is often suitably accurate, an arbitrary (small amplitude) wave field may be constructed, by Fourier synthesis, from a collection of plane waves, and the resulting drift calculated. The drift arising from such a continuous spectrum of plane waves will be described in the second subsection.

1.5.1 Stokes drift of plane monochromatic gravity waves

Water waves are irrotational to a good approximation, and the velocity vector of the water at any point $\mathbf{x} = (x, y, z)$ is

$$\mathbf{u}_w = \text{Real}\{ac[F\mathbf{k} - ikF'(kz)\mathbf{e}_3]\exp(i\Theta)\} \tag{1.17}$$

$$\mathbf{k} = k_1\mathbf{e}_1 + k_2\mathbf{e}_2 \tag{1.18}$$

$$k = \sqrt{k_1^2 + k_2^2}, \tag{1.19}$$

where 'Real' indicates the real part of the complex quantity, a prime represents differentiation with respect to the argument, k is the wavenumber, or $2\pi/\lambda$, with λ being the length of the the wave, $\mathbf{k}$ is the wave number vector with $\mathbf{e}_{1,2,3}$ being the unit vectors in the x, y, and z directions respectively. Furthermore, the phase function Θ and the phase speed, c, are defined by

$$\Theta \equiv k_1 x + k_2 y - \sigma t, \quad c \equiv \frac{\sigma}{k}. \tag{1.20}$$

Here we have taken the mean–free surface to be located at the plane $z = 0$, the water in $z < 0$, and c is the phase speed of the wave. The vertical position of the instantaneous free–surface above the mean–free surface is

$$\zeta(x, y, t) = \text{Real}\{ae^{i\Theta}\}. \tag{1.21}$$

Assuming the undisturbed water depth is constant, so the bottom is located at $z = -d$, the amplitude function F and the frequency σ are

$$F(kz) = \frac{\cosh\, k(z+d)}{\sinh\, kd}, \quad \sigma = \sqrt{gk\tanh\, kd}, \tag{1.22}$$

and the function F' in (1.17) is the derivative of F with respect to its argument (not z alone). When kd is large, the water is said to be deep, and

(1.22) is accurately replaced by

$$F(kz) = e^{kz}, \quad \sigma = \sqrt{gk}. \tag{1.23}$$

Mathematically, (1.23) is the limiting form of (1.22) when $d/\lambda \to \infty$. In fact, the water depth does not have to be large compared to the wavelength in order for the deep water forms to be good approximations to the finite depth forms (1.22). In fact, the frequency is given to an accuracy of better than one percent when $d > \frac{1}{4}\lambda$, and the velocity field is accurate to about four percent.

The small amplitude assumption which leads to the description above requires that the parameter

$$\varepsilon = ka,$$

a measure of the maximum slope of the wave, be small.

The Lagrangian motion is that experienced by a fluid particle. Suppose, as in §1.4, we assign a Lagrangian label $\mathbf{X}$ to each fluid particle. Then the trajectory of a fluid particle is described by

$$\mathbf{x} = \boldsymbol{\chi}(\mathbf{X}, t). \tag{1.24}$$

Specifying the motion completely in terms of $\mathbf{X}$ and t rather than in terms of $\mathbf{x}$ and t is an option. The first method is called a Lagrangian description, and $\mathbf{X}$ the Lagrangian coordinates, and the second approach, where the interest is focussed not on a fixed fluid particle ($\mathbf{X}$) but on a fixed position in space ($\mathbf{x}$), is called an Eulerian description with $\mathbf{x}$ being the Eulerian coordinates. Given one description, we can in principle move to the other. For example, given (1.24), we can invert the vector function $\boldsymbol{\chi}$ holding t fixed to give

$$\mathbf{X} = \boldsymbol{\chi}^{-1}(\mathbf{x}, t) \tag{1.25}$$

The velocity on the trajectory is defined in terms of the Eulerian velocity field, $\mathbf{u}(\mathbf{x}, t)$ by

$$\dot{\boldsymbol{\chi}} = \mathbf{u}(\boldsymbol{\chi}(\mathbf{X}, t), t). \tag{1.26}$$

The Lagrangian displacement, $\boldsymbol{\xi}(\mathbf{X}, t)$ is the vector displacement of the particle at time t from its original position, $\mathbf{X}$, or

$$\boldsymbol{\xi}(\mathbf{X}, t) \equiv \boldsymbol{\chi}(\mathbf{X}, t) - \mathbf{X}. \tag{1.27}$$

Let $\mathbf{u}^L(\mathbf{X}, t)$ be defined to be $\dot{\boldsymbol{\chi}}$, then this is the velocity history as measured by the particle having Lagrangian label $\mathbf{X}$, and so we can call this the

Lagrangian velocity. The current particle position is then

$$\chi = \mathbf{X} + \boldsymbol{\xi}(\mathbf{X}, t) = \mathbf{X} + \int_0^t \mathbf{u}^L(\mathbf{X}, t)\, dt = \mathbf{X} + \int_0^t \mathbf{u}(\mathbf{X} + \boldsymbol{\xi}(\mathbf{X}, t), t)\, dt. \quad (1.28)$$

If $\mathbf{u}$ is small, so is $\mathbf{u}^L$, and therefore $\boldsymbol{\xi}$ will be small at least for a long time interval. This is the case for water waves, so to a good approximation

$$\mathbf{u}^L(\mathbf{X}, t) = \mathbf{u}(\mathbf{X}, t) + \boldsymbol{\xi}(\mathbf{X}, t) \cdot \nabla \mathbf{u} = \mathbf{u}(\mathbf{X}, t) + \left(\int_0^t \mathbf{u}(\mathbf{X}, t)\, dt \right) \cdot \nabla \mathbf{u}. \quad (1.29)$$

Wherever $\mathbf{X}$ appears, it can be replaced using (1.25), returning the relevant quantity to Eulerian coordinates. Supposing this is done in (1.29), and the result averaged in some suitable way. If averaging is done over time or phase (for example), the *mean* Lagrangian velocity is given by

$$\bar{\mathbf{u}}^L = \overline{\mathbf{u} + \int_0^t \mathbf{u}(\mathbf{x}, t)\, dt \cdot \nabla \mathbf{u}(\mathbf{x}, t)} = \overline{\mathbf{u}} + \mathbf{u_s}. \quad (1.30)$$

This shows that the mean Lagrangian velocity is equal to the mean Eulerian velocity plus an additional velocity vector, $\mathbf{u_s}$, which may be called the Stokes drift velocity. In the ocean, the largest component of the instantaneous velocity field near the surface is that due to the orbital velocity, $\mathbf{u}_w$, in the surface gravity waves. This means that

$$\mathbf{u_s} = \overline{\int_0^t \mathbf{u}_w(\mathbf{x}, t)\, dt \cdot \nabla \mathbf{u}_w(\mathbf{x}, t)}. \quad (1.31)$$

The small amplitude water wave velocity field in Eulerian coodinates, $\mathbf{u}_w(\mathbf{x}, t)$, quoted above has a zero time average. There will be, in general, a small nonzero Eulerian mean velocity, but this will typically be comparable to the Stokes drift, which is of second order with respect to the wave slope.

If (1.17,1.22) are substituted into (1.30),

$$\mathbf{u_s} = a^2 \sigma \frac{\cosh 2k(z+d)}{2 \sinh^2 kd} \mathbf{k} \quad (1.32)$$

$$(1.33)$$

In elementary textbooks, it is shown that particle orbits in deep water waves are circles to lowest order, with radii decreasing exponentially with the depth. However, if one allows for the very small variation of velocity with depth encountered by a given fluid particle as it executes its orbit, it

is seen that the particle moves slightly faster over the top part of its orbit than it does over the bottom part. This leads to a slight breaking of the circle, and to a very small advance in the direction of wave propagation over each period of the the wave motion. A similar net drift is also experienced by particles moving under the influence of extremely shallow water waves, where there is no detectable difference in speeds from the "top" to the "bottom" of the orbit. This drift can easily be explained as due to the fact that, in a progressive wave, the particle moves in the direction of wave propagation for a longer fraction of the period than it moves in the opposite direction. Therefore, even though the "forward" and "backward" speeds may be identical, the particle manages a net move forward over each cycle here too. In point of fact, one can show that the drift in deep water waves is due to both effects, the difference in speed from top to bottom, and the difference in time moving with the wave on the forward and back portions of the cycle, with each contributing in equal measure.

1.5.2 Stokes drift arising from a continuous spectrum

The surface wave field is not monochromatic. If it can be supposed to be the linear superposition of a finite number of waves with distinct amplitudes, a_j, $j = 1, 2, \ldots$, and wavenumber vectors, $\mathbf{k}_j, j = 1, 2, \ldots$, (with corresponding frequencies), then we can write the small amplitude approximation to the velocity and surface displacement field by a sum over of terms of the form given by (1.17, 1.21).

It is easy then to show that the Stokes drift for this collection of waves is

$$\mathbf{u_s} = \sum_j \sigma(k_j) a_j^2 \exp(2\, k_j z)\, \mathbf{k}_j \tag{1.34}$$

for deep water.

When the wavefield is random (but horizontally homogeneous and stationary in time) and contains a continuum of wavenumbers, we still can use the formula (1.32) to calculate the drift. This leads to the result (see, for example [33, 34])

$$\mathbf{u_s} = \int\int 2\,\sigma(k)\mathbf{k}\Psi(\mathbf{k}) \exp(\,2kz)\; dk_1 dk_2, \tag{1.35}$$

where the integral is over all relevant wavenumbers in the spectrum. The function $\Psi(\mathbf{k})$ is the directional wavenumber spectrum, which is the Fourier transform of the spatial covariance of the sea surface displacement (see

Phillips [71], for a full description). The qualifier 'relevant' is included here because it is apparent that very short waves ought not included, since surface tension has been neglected. Furthermore, in dealing with problems requiring computation, scales below the resolution of the calculation ought not to be included.

1.6 Derivation of Langmuir Circulation Theory

The theory of Langmuir circulations that originated with Craik & Leibovich [14] can be derived in more than one way. The original derivation, which is in its most complete form in [50] and [48], is a systematic perturbation approach that centers on the vorticity dynamics. Another derivation begins with the generalized Lagrangian mean formalism of Andrews & McIntyre [3], and may be found in [51].

In this section, we proceed to derive the full theory in stages.

We will first show, in the next subsection, how the main result for an incompressible, inviscid fluid may be found by a new and simple vorticity argument that essentially amounts to a combination of the two methods mentioned. The subsection to follow gives a formal derivation through the generalized Lagrangian mean formalism, allowing for weak effects of viscosity. The final subsection introduces the density stratification by means of the Boussinesq approximation.

1.6.1 Mean vorticity

Suppose we consider the detailed motion of an inviscid, incompressible fluid. The Eulerian velocity field is assumed to consist of an oscillatory part and a mean part

$$\mathbf{u} = \bar{\mathbf{u}} + \mathbf{u}', \tag{1.36}$$

where an overbar indicates an average and a prime a fluctuating quantity with zero mean. We may think of averages such as an average over time, an average over the phase of the oscillation, or more generally as an average over an ensemble of realizations of the fluctuating system.

According to §1.4, the circulation about any closed path is a constant in time. Now consider a particular closed path $\mathcal{C}(t)$ with circulation Γ

$$\Gamma = \oint_{\mathcal{C}} \mathbf{u}(\mathbf{x}, t) \cdot d\mathbf{x}. \tag{1.37}$$

If we take the average of this quantity, then the average is also independent of time. Furthermore the average will be

$$\overline{\frac{d\Gamma}{dt}} = \overline{\oint_C \mathbf{u}\cdot d\,\mathbf{x}} = \oint_{\bar{C}} \bar{\mathbf{u}}\cdot d\,\mathbf{x}, \tag{1.38}$$

where $\bar{C}$ is the mean closed circuit. To justify replacing the integrand by $\bar{\mathbf{u}}$, we may use (1.36) and then argue, for example, that the net contribution to the line integral at any instant made by the fluctuating velocity field vanishes. This is not precisely correct in general, but the replacement is exactly correct for any motion in which the fluctuating velocity is irrotational, since the contribution of the fluctuation then vanishes exactly *before* averaging is done. In the event that the fluctuation is not irrotational, a slightly different result emerges, exactly, and this is described in the next subsection. For fluctuations arising from ocean waves, however, the assumption of irrotationality is defensible and the results to be found here do not require alteration.

We now invoke a general mathematical rule for the time rate of change of a contour integral of an arbitrary differential vector field, say $\mathbf{A}(\mathbf{x}, t)$, on a contour that moves at an arbitrarily prescribed velocity, say $\mathbf{v}(\mathbf{x}, t)$. Suppose

$$I(t) = \oint_{C(t)} \mathbf{A}(\mathbf{x}, t)\cdot d\,\mathbf{x}. \tag{1.39}$$

Then

$$\frac{dI}{dt} = \oint_{C(t)} \left\{ \frac{\partial A}{\partial t} + \mathbf{v}\cdot\nabla\mathbf{A} + (\nabla\mathbf{v})\cdot\mathbf{A} \right\}\cdot d\,\mathbf{x}, \tag{1.40}$$

where the result is written in terms of the second–rank tensor $(\nabla\mathbf{v})$. Rewriting the integrand as

$$\frac{\partial\,\mathbf{A}}{\partial t} - \mathbf{v}\times \operatorname{curl}\mathbf{A} + \nabla(\mathbf{v}\cdot\mathbf{A}),$$

we have

$$\frac{dI}{dt} = \oint_{C(t)} \left\{ \frac{\partial\,\mathbf{A}}{\partial t} - \mathbf{v}\times\operatorname{curl}\mathbf{A} \right\}\cdot d\,\mathbf{x} = \int_{S(t)} \mathbf{n}\cdot \left(\frac{\partial \operatorname{curl}\mathbf{A}}{\partial t} - \operatorname{curl}[\mathbf{v}\times\operatorname{curl}\mathbf{A}] \right) d\,S, \tag{1.41}$$

where we use the fact that the line integral of a gradient over a closed path is identically zero, and then invoke Stokes theorem, where $S(t)$ is the (open) surface with $C(t)$ as boundary. If $dI/dt = 0$ for all such contours, then we must have

$$\frac{\partial \operatorname{curl}\mathbf{A}}{\partial t} - \operatorname{curl}(\mathbf{v}\times\operatorname{curl}\mathbf{A}) = 0. \tag{1.42}$$

Now apply this rule to (1.38), to find that

$$\frac{\partial \bar{\omega}}{\partial t} - \text{curl}(\bar{\mathbf{u}}^L \times \bar{\boldsymbol{\omega}}) = 0. \tag{1.43}$$

Here

$$\bar{\boldsymbol{\omega}} \equiv \text{curl}\bar{\mathbf{u}}, \tag{1.44}$$

is the mean vorticity. The velocity $\bar{\mathbf{u}}^L$ appears here for $\mathbf{v}$ because the circuit $\bar{C}$ moves with the Lagrangian mean velocity (since the instantaneous path moves with the instantaneous fluid velocity).

This establishes an equation for the mean vorticity vector, which we may now express as a single curl operation,

$$\text{curl}\left\{\frac{\partial \bar{\mathbf{u}}}{\partial t} - \bar{\mathbf{u}}^L \times \bar{\boldsymbol{\omega}}\right\} = 0.$$

This can be integrated, to give

$$\frac{\partial \bar{\mathbf{u}}}{\partial t} - \bar{\mathbf{u}}^L \times \bar{\boldsymbol{\omega}} = -\nabla \pi_1,$$

where π_1 is some scalar field. Rewriting this, using (1.30), we have our final result for this section,

$$\frac{\partial \bar{\mathbf{u}}}{\partial t} + \bar{\mathbf{u}} \cdot \nabla \bar{\mathbf{u}} = -\nabla \pi + \mathbf{u_s} \times \bar{\boldsymbol{\omega}} + \mathbf{f}, \tag{1.45}$$

where π is a pressure–like scalar function, and $\mathbf{f}$ is the mean body force per unit mass, assuming that the body force is conservative.

This equation is the appropriate one to describe Langmuir circulations that are either laminar and inviscid or the large scale motion when turbulent but inertially dominated. The important observation is that the equations for the mean momentum derived here are the same as for the instantaneous momentum, except for the appearance of an apparent body force term that we call the "vortex force",

$$\mathbf{F}_v \equiv \mathbf{u_s} \times \bar{\boldsymbol{\omega}}. \tag{1.46}$$

It is the appearance of the vortex force that characterizes the Craik–Leibovich theory of Langmuir circulation.

1.6.2 Derivation by the Generalized Lagrangian Mean

Atmospheric motions are strongly affected by wave activity, and the waves generate a rectified effect leading to mean atmospheric motions. The search for a rational way to separate "waves" from "mean flow", and to define wave–mean flow interaction, was a long one culminating in the generalized Lagrangian mean theory of Andrews and McIntyre [3] (which will be abbreviated here as A & M).

The latter paper gives both the history of the search and a comprehensive exposition of the GLM theory. Here the structure of this theory is reviewed in the context of a constant density fluid and is contrasted to Eulerian–mean, or Reynolds, averaging.

Basic formulation

Assume the Eulerian velocity field $\mathbf{u}(\mathbf{x}, t)$ is known. Then we may construct the trajectory,

$$\begin{aligned} \mathbf{x} &= \boldsymbol{\chi}(\mathbf{X}, t), \quad \text{where} \\ \frac{d\boldsymbol{\chi}}{dt} &= \mathbf{u}(\boldsymbol{\chi}, t) \end{aligned}$$

of a particle which, at some reference time such as $t = 0$ is located at position $\mathbf{x} = \mathbf{X}$. The choice made here for the Lagrangian label, $\mathbf{X}$, is natural but not the only one.

Suppose now we choose to shift to an alternative Lagrangian label in the following way. Consider an observer moving with a different "reference" flow (at the moment, quite arbitrarily), described by the velocity field $\hat{\mathbf{u}}$, then, a particle with Lagrangian coordinate $\mathbf{X}$ follows the trajectory

$$\begin{aligned} \hat{\mathbf{x}} &= \hat{\boldsymbol{\chi}}(\mathbf{X}, t), \quad \text{where} \\ \frac{d\hat{\boldsymbol{\chi}}}{dt} &= \hat{\mathbf{u}}(\hat{\boldsymbol{\chi}}, t). \end{aligned}$$

Both trajectories begin at the same place, $\mathbf{X}$, but the first follows the path of a fluid particle, and the second follows the arbitrarily prescribed reference path.

Now we *choose* to describe the position of the fluid particle from the perspective of the observer following the "hatted" trajectory, and write

$$\mathbf{x} = \boldsymbol{\chi}(\mathbf{X}, t) = \hat{\boldsymbol{\chi}}(\mathbf{X}, t) + \boldsymbol{\xi}(\mathbf{X}, t) \tag{1.47}$$

so ξ is the particle vector displacement measured from the observer's current position. Since $\hat{\mathbf{x}} = \hat{\chi}(\mathbf{X}, t)$, we can invert to get $\mathbf{X} = \hat{\chi}^{-1}(\hat{\mathbf{x}}, t)$, so (1.47) may be reexpressed in terms of $\hat{\mathbf{x}}$ instead of $\mathbf{X}$. This replacement of the particle label then describes the actual particle position in the form

$$\mathbf{x} = \chi(\hat{\mathbf{x}}, t) = \hat{\mathbf{x}} + \xi(\hat{\mathbf{x}}, t) \tag{1.48}$$

which produces the mapping from the observer's position to the particle's position

$$\hat{\mathbf{x}} \mapsto \hat{\mathbf{x}} + \xi(\hat{\mathbf{x}}, t).$$

The meaning of $\xi(\hat{\mathbf{x}}, t)$ is therefore the following: at any position $\hat{\mathbf{x}}$ and time t in the fluid, $\xi(\hat{\mathbf{x}}, t)$ is the position of the fluid particle, relative to $\hat{\mathbf{x}}$, which at $t = 0$ was at the position found by tracing the reference flow trajectory backwards through a time interval t from $\hat{\mathbf{x}}$.

The total derivative of (1.48) yields

$$\frac{\partial \xi}{\partial t} + \hat{\mathbf{u}} \cdot \nabla_{\hat{\mathbf{x}}} \xi = \mathbf{u}(\chi, t) - \hat{\mathbf{u}}(\hat{\chi}, t) \tag{1.49}$$

$$= \mathbf{u}(\hat{\mathbf{x}} + \xi(\hat{\mathbf{x}}, t), t) - \hat{\mathbf{u}}(\hat{\mathbf{x}}, t). \tag{1.50}$$

This gives a *field* description of particle positions, since the $\hat{\mathbf{x}}$ coordinates are just Eulerian in character. If we define

$$\frac{\hat{D}()}{\hat{D}t} \equiv \frac{\partial()}{\partial t} + \hat{\mathbf{u}} \cdot \nabla_{\hat{\mathbf{x}}}(), \tag{1.51}$$

and, for any field $\phi(\mathbf{x})$

$$\phi^{\xi} \equiv \phi(\hat{\mathbf{x}} + \xi(\hat{\mathbf{x}}, t), t), \tag{1.52}$$

then

$$\frac{\hat{D}}{\hat{D}t}\phi^{\xi} = (\frac{\mathrm{D}\phi}{\mathrm{D}t})^{\xi}. \tag{1.53}$$

Here

$$\frac{\mathrm{D}()}{\mathrm{D}t} \equiv \frac{\partial()}{\partial t} + \mathbf{u} \cdot \nabla_{\hat{\mathbf{x}}}()$$

is the usual material derivative as it is expressed in an Eulerian framework. The left–hand side is the rate of change following the reference path of a particle quantity, and the right–hand side is the material rate of change of the fluid particle with displacement ξ.

Up to this point, the reference trajectory is entirely arbitrary. Now invoke any averaging operation that commutes with time or space differentiation (like the customary ones of time, space, or ensemble averages). Let the average be denoted by an overbar, and *require*

$$\bar{\xi} = 0. \tag{1.54}$$

This defines a particular reference trajectory, one for which the average displacement from this reference path of any quantity evaluated at the true Lagrangian position of a fluid particle is zero. This would seem to be a natural definition of "mean Lagrangian" motion, and is the one adopted by A & M. Accordingly, for any quantity, f, related to the fluid motion, set

$$\bar{f}^L \equiv \overline{f^\xi},$$

which defines the (generalized) Lagrangian mean, or "GLM". In particular, in view of (1.50) and (1.54) the Lagrangian mean velocity field is $\overline{\mathbf{u}^\xi} = \bar{\mathbf{u}}^L = \hat{\mathbf{u}}$, and

$$\frac{\hat{D}}{\hat{D}t} = \frac{\partial()}{\partial t} + \bar{\mathbf{u}}^L \cdot \nabla_{\hat{\mathbf{x}}} \equiv \frac{\bar{\mathrm{D}}^L}{\mathrm{D}t},$$

which I shall call the "pseudomaterial derivative". With this definition (1.50) becomes

$$\frac{\bar{\mathrm{D}}^L}{\mathrm{D}t}\xi = \mathbf{u}(\hat{\mathbf{x}} + \xi(\hat{\mathbf{x}}, t), t) - \bar{\mathbf{u}}^L(\hat{\mathbf{x}}, t). \tag{1.55}$$

The equations governing the generalized Lagrangian mean velocity field are found (see A & M) by premultiplying the instantaneous momentum equations by the tensor $\nabla_{\hat{\mathbf{x}}}\boldsymbol{\chi}$ and averaging, and by calculating the pseudomaterial derivative of the Jacobian, J, of the tranformation $\hat{\mathbf{x}} \mapsto \boldsymbol{\chi}(\hat{\mathbf{x}}, t) = \hat{\mathbf{x}} + \xi(\hat{\mathbf{x}}, t)$, so

$$J = \det(\nabla_{\hat{\mathbf{x}}}\boldsymbol{\chi}) = \det(\mathbf{I} + \nabla_{\hat{\mathbf{x}}}\xi) \tag{1.56}$$

(where $\mathbf{I}$ is the identity matrix) followed by enforcement of mass conservation (we will assume here that the fluid is incompressible, but the general theory of A & M is not restricted by this assumption). The first gives GLM momentum equations, and the second expresses GLM mass conservation. These steps yield the GLM momentum equations (and from here on, we drop the hat on $\mathbf{x}$),

$$\frac{\bar{\mathrm{D}}^L(\bar{\mathbf{u}}^L - \mathsf{p})}{\mathrm{D}t} + \nabla\bar{\mathbf{u}}^L \cdot (\bar{\mathbf{u}}^L - \mathsf{p}) = -\nabla\pi + \mathcal{F}, \tag{1.57}$$

where

$$\mathsf{p} \equiv -\overline{(\nabla\xi \cdot \frac{\bar{\mathrm{D}}^L\xi}{\mathrm{D}t})}, \tag{1.58}$$

is called the "pseudomomentum",

$$\mathcal{F} \equiv \nu\overline{\nabla\boldsymbol{\chi} \cdot \nabla^2\mathbf{u}^\xi} \tag{1.59}$$

is the contribution of the viscous force, and

$$\bar{\pi} \equiv \frac{\bar{p}^L}{\rho} + \frac{1}{2}\overline{|\mathbf{u}^\xi|^2},$$

is a modified pressure head. The equation for mass conservation is

$$\frac{\bar{\mathrm{D}}^L \log J}{\mathrm{D}t} + \nabla \cdot \bar{\mathbf{u}}^L = 0. \tag{1.60}$$

A&M show that $\overline{J} = J$, so J, although formed from instantaneous variables, is automatically a mean quantity.

It is also important to relate $\bar{\mathbf{u}}^L$ to the usual Eulerian mean velocity vector, and this is done through the "Stokes drift" velocity, $\bar{\mathbf{u}}^S$, defined to be

$$\bar{\mathbf{u}}^S \equiv \bar{\mathbf{u}}^L - \bar{\mathbf{u}}. \tag{1.61}$$

This definition reduces, for small perterbations of a fluid at rest, to the classical definition of mass drift (1.30) discussed in §1.5.

Equations (1.57) and (1.60), together with the definitions for $\mathcal{F}$, p, and J, govern the generalized Lagrangian mean variables for a constant density fluid, in the form given by A&M. Notice that the generalized Lagrangian–mean velocity, $\bar{\mathbf{u}}^L$, is not solenoidal, so the GLM motion is rather like the flow of a compressible fluid with "density" J determined by the fluctuating field. Furthermore, the equations clearly are not closed. To form the quantities $\mathcal{F}$, p, and J, one needs to know the behavior of fluctuations about the mean, which are given by ξ. As we will show, these very general equations simplify considerably when the fluctuations are due to (nearly) irrotational surface waves.

Now return to (1.57), and let

$$\mathbf{v} \equiv \bar{\mathbf{u}}^L - \mathsf{p}, \tag{1.62}$$

$$\Pi \equiv \bar{\pi} + \mathsf{p} \cdot \mathbf{v}, \tag{1.63}$$

then (1.57), expressed in terms of $\mathbf{v}$, becomes

$$\frac{\partial \mathbf{v}}{\partial t} + \mathbf{v} \cdot \nabla \mathbf{v} = -\nabla \Pi + \mathsf{p} \times \omega + \mathcal{F} \tag{1.64}$$

where

$$\omega = \nabla \times \mathbf{v} \tag{1.65}$$

is like a mean vorticity, which might be called the "pseudovorticity". The GLM equations in the form (1.65) might be called "Langmuir circulation form", because this is precisely the same as the equations derived for the Craik-Leibovich theory of Langmuir circulations (Leibovich, 1977), with p replaced by $\bar{\mathbf{u}}^S$, and $\mathbf{v}$ replaced by the Eulerian–mean velocity, $\bar{\mathbf{u}}$.

When working with the Langmuir circulation form of the GLM equations, the continuity equation is conveniently expressed in terms of $\mathbf{v}$ as

$$\nabla \cdot \mathbf{v} = \Sigma \tag{1.66}$$

$$\Sigma = -(\frac{1}{J})(\frac{\partial J}{\partial t} + \mathbf{v} \cdot \nabla J + \nabla \cdot (\mathsf{p} J)). \tag{1.67}$$

There is an alternative form for Σ, obtained from (1.61) and the fact that $\bar{\mathbf{u}}$ is solenoidal. This is

$$\Sigma = \nabla \cdot (\bar{\mathbf{u}}^S - \mathsf{p}), \tag{1.68}$$

which shows that there is no need to deal with both $\bar{\mathbf{u}}^S$ and with J, and since we must have information about the former, as previously explained, this alternative representation of Σ in (1.67) is preferable.

There also is another form of (1.57), rather similar to (1.65) but written in terms of $\bar{\mathbf{u}}^L$ rather than $\mathbf{v}$. This is

$$\frac{\bar{\mathrm{D}}^L \bar{\mathbf{u}}^L}{\mathrm{D}t} = -\nabla \hat{\Pi} + \bar{\mathbf{u}}^L \times \mathrm{curl}\mathsf{p} + \frac{\partial \mathsf{p}}{\partial t} + \mathcal{F} \tag{1.69}$$

where

$$\hat{\Pi} \equiv \bar{\pi} + \frac{1}{2}\overline{|(\bar{\mathbf{u}}^L)^2|} - \mathsf{p} \cdot \bar{\mathbf{u}}^L, \tag{1.70}$$

but this seems less convenient than (1.65).

Application to Langmuir circulation

In Langmuir circulations, the source of the fluctuations is the motion induced by surface gravity waves, if incoherent turbulence is set aside and parameterized separately. The water wave motion is irrotational to good

accuracy. When the Eulerian flucuations are irrotational, the Stokes drift is identical to the pseudomomentum vector, $\bar{\mathbf{u}}^S = \mathsf{p}$. (See A & M for this, which follows directly from the definitions.) Furthermore, since $\mathbf{v} = \bar{\mathbf{u}}^L - \mathsf{p}$, $\mathbf{v} = \bar{\mathbf{u}}^L - \bar{\mathbf{u}}^S$, which by definition of the Stokes drift is the Eulerian mean velocity. Therefore equation (1.64) is an equation for the Eulerian mean velocity vector, $\bar{\mathbf{u}}$, and the continuity equation is simply

$$\nabla\cdot\bar{\mathbf{u}} = 0. \tag{1.71}$$

To close the equations in the present circumstances, we need to be given the surface wave field, or, more precisely, the Stokes drift they generate, and we must model the viscous or net force due to incoherent turbulence. In [51], it is shown that if a constant eddy viscosity, ν_T, is appropriate in the absence of waves, then it is also appropriate when waves are present, and we may then set

$$\mathcal{F} = \nu_T\nabla^2\bar{\mathbf{u}}, \tag{1.72}$$

and so the completed set of equations, in the absence of nonconservative body forces, can be written as

$$\frac{\partial\bar{\mathbf{u}}}{\partial t} + \bar{\mathbf{u}}\cdot\nabla\bar{\mathbf{u}} = -\nabla\Pi + \mathbf{u_s}\times\bar{\boldsymbol{\omega}} + \nu_T\nabla^2\bar{\mathbf{u}}, \tag{1.73}$$

$$\nabla\cdot\bar{\mathbf{u}} = 0, \tag{1.74}$$

where any conservative body force is absorbed into the "modified mean pressure", Π.

1.6.3 The Coriolis Acceleration and Stratification

The equations of the previous section assume a description in an inertial reference frame, and also assume a fluid of uniform density. These simplifications are relaxed here by incorporating the possibility of a uniformly rotating reference frame, as is convenient in geophysical fluid dynamics, and density stratification.

Acceleration of the reference frame affects only the momentum equation; and balance equations required for all scalar quantities, like fluid temperature, have the same form in inertial and accelerated frames. If the frame is noninertial due only to rotation of the frame with constant angular velocity $\boldsymbol{\Omega}$, then the direct transformation of (1.73) to coordinates fixed in the

rotating frame is

$$\frac{\partial \bar{\mathbf{u}}_r}{\partial t} + \bar{\mathbf{u}}_r \cdot \nabla \bar{\mathbf{u}}_r + 2\boldsymbol{\Omega} \times \bar{\mathbf{u}}_r = -\nabla \left(\Pi - \frac{1}{2} |\boldsymbol{\Omega}|^2 r^2 \right) + \mathbf{u_s} \times (\bar{\omega}_r + 2\boldsymbol{\Omega}) + \nu_T \nabla^2 \bar{\mathbf{u}}, \tag{1.75}$$

where the subscript "r" indicates that the quantity is measured relative to the rotating frame. Thus, $\bar{\omega}_r = \text{curl}\bar{\mathbf{u}}_r$ is the mean vorticity seen in the rotating frame.

We may allow for density stratification arising from either thermal expansion or by solute concentration, or both. The main effects in the near surface layer more often are due to thermal causes, and in any event, the equations that result are of the same form with either of the stratification agencies. Consequently, we focus on thermal expansion only.

The Boussinesq (or Oberbeck–Boussinesq) approximation allows for buoyancy force, which depends on density variations, without the need to deal with the additional nonlinearities and physical complications that arise when the fluid is regarded as compressible. In this approximation, which is usually acceptable in geophysical fluid dynamics, three simplifications are introduced. First, the motion is regarded as incompressible, in fact constant density, with the exception of the body force term due to gravity. Second, the variation of density (or the buoyancy, which is the fractional density decrement times the acceleration of gravity) is specified as a linear function of the temperature anomaly. If salinity variations cause the density to change then the buoyancy is specified as a linear function of the salt concentration anomaly. Third, the thermal energy equation assumes heat transfer by conduction only, and that the rate of dissipation of mechanical energy is small compared to the rate of change of stored heat. These conditions lead to an approximate equation of state relating the density variations from a reference state (denoted by the subscript 'ref') arising from temperature variations from the reference, or

$$\frac{\rho - \rho_{ref}}{\rho_{ref}} = -\beta(T - T_{ref}). \tag{1.76}$$

The density variations impose a buoyancy force per unit volume of fluid of

$$\mathbf{F}_B = \beta g (T - T_{ref}) e_3, \tag{1.77}$$

where β is the coefficient of volume expansion, T is the temperature, and e_3 is the unit normal vector in the vertical direction (opposing gravity). In

the Boussinesq approximation, the density is regarded as constant with the exception of its effect in creating the buoyancy force.

To close the equation set, an equation for temperature (and salinity, if contributions of salt variations to buoyancy are included) is needed. The Boussinesq approximation takes this to be

$$\frac{\partial T}{\partial t} + \mathbf{u}\cdot T = \kappa \nabla^2 T, \tag{1.78}$$

where κ is the thermal diffusivity (thermal conductivity divided by heat capacity of the fluid), and $\mathbf{u}$ is the instantaneous fluid velocity vector (which may be prescribed in either an inertial or accelerating frame). This equation is the differential expression of the conservation law which says that the thermal energy content of a fixed mass of fluid may increase only due to conduction of heat across its boundaries.

We now need to average to remove the fluctuations associated with the surfaces waves. The generalized Lagrangian mean formalism accomplishes this immediately for any conserved scalar, with simple results. The GLM formalism of § 1.6.2 produces the average,

$$\overline{\frac{\partial \phi}{\partial t} + \mathbf{u}\cdot\phi} = \frac{\partial \bar{\phi}^L}{\partial t} + \bar{\mathbf{u}}^L \cdot \nabla \bar{\phi}^L.$$

Consequently, if ϕ is a conserved scalar (so $D\phi/Dt = 0$) then the generalized Lagrangian mean implies that the averaged ϕ, $\bar{\phi}^L$ is conserved following the generalized Lagrangian mean velocity vector, $\bar{\mathbf{u}}^L = \bar{\mathbf{u}} + \mathbf{u_s}$. If we now restore the heat conductivity, and identify ϕ with the temperature, we have

$$\bar{T}t + (\bar{\mathbf{u}} + \mathbf{u_s})\cdot\nabla\bar{T} = \kappa_T \nabla^2 \bar{T}, \tag{1.79}$$

where, κ_T the eddy thermal diffusity accounting for unresolved turbulent motions as well as the molecular diffusity of heat.

As with the momentum equations, the equation for mean temperature can be derived directly by perturbation analysis.[1]

The enlargement of the problem described by (1.73) to include buoyancy under the Boussinesq approximation and rotation of the reference frame can now be summarized in the following equation set.

$$\frac{\partial \bar{\mathbf{u}}}{\partial t} + \bar{\mathbf{u}}\cdot\nabla\bar{\mathbf{u}} + 2\boldsymbol{\Omega}\times(\bar{\mathbf{u}} + \mathbf{u_s}) = -\nabla\pi + \mathbf{u_s}\times\bar{\boldsymbol{\omega}} + \nu_T\nabla^2\bar{\mathbf{u}} + \beta g(\bar{T} - T_{ref})\theta_3 \tag{1.80}$$

[1]This was done in [48], but an error exists in that paper, so that the Stokes drift contribution to the advection velocity was omitted. The correction of the error is straightforward.

$$\bar{T}t + (\bar{\mathbf{u}} + \mathbf{u_s}) \cdot \nabla \bar{T} = \kappa_T \nabla^2 \bar{T} \tag{1.81}$$

$$\nabla \cdot \mathbf{v} = 0, \tag{1.82}$$

where all quantities are referenced with respect to the rotating frame, and π is a modified pressure that includes the centripetal "force potential" of (1.75) in addition to the terms appearing in Π in set (1.73) and the hydrostatic pressure contribution due to ρ_{ref}.

1.7 Langmuir Circulation: Scales

The final result of the derivation given in §1.6 is this: the form of the equations for the mean motion are the same as they would be prior to filtering out the gravity waves, but with an extra force appearing representing their rectified effects. This apparent force has been called the "vortex force", and is given (per unit volume) by

$$\mathbf{F}_v \equiv \rho \, \mathbf{u}_s \times \boldsymbol{\omega}.$$

The classical Stokes drift (Stokes [81]) decays with depth on a length scale comparable to the wavelength (λ) of the most energetic waves. Given the characteristics of the surface waves, then $\mathbf{u}_s$ can be calculated provided the wave slopes are not large. For the monochromatic deep water wave train discussed in §1.5 with a waveheight H (twice the wave amplitude), the Stokes drift speed is

$$|u_s| = \left(\pi \frac{H}{\lambda}\right)^2 \sqrt{\frac{g\lambda}{2\pi}} \exp[4\pi(z/\lambda)].$$

For example, if the wave height were 1.5 m and the wave length were 24 m, this formula would give 24 cm/s for the surface value of the Stokes drift. Typically, $\mathbf{u}_s$ is a decreasing function of depth only, and if the waves are generated by the local wind, it is reasonable to suppose that $\mathbf{u}_s$ is parallel to the wind direction.

It is possible to have "equilibrium flows" with $\mathbf{u}_s$ and $\mathbf{u}$ parallel to each other and to the wind direction. In such cases, the vortex force tends to destabilize this equilibrium, much like a destabilizing temperature distribution. When this tendency is sufficiently large to cause instability, vertical convective motions ensue, disturbing the "structureless" equilibrium.

Since the driving force behind Langmuir circulations is the vortex force (at least according to the CL theory), we can estimate the intensity of convection due to this phenomenon. The maximum possible vortex force occurs when $\mathbf{u}_s$ and $\boldsymbol{\omega}$ are at right angles. Now suppose a layer of depth d

is considered (see sketch) in which Langmuir circulation takes place. Let $\max|\boldsymbol{\omega}| = \Omega_c$ be the maximum of the vorticity vector in the current. Then the work done by the vortex force over a distance equal to the depth of the layer does not exceed

$$\rho\Omega_c \int_{-d}^{0} u_s dz < \rho\Omega_c \int_{-\infty}^{0} u_s dz = \Omega_c |\mathcal{M}|, \tag{1.83}$$

where $|\mathcal{M}|$ is the total momentum carried by the surface waves in the layer, per unit area of the water surface. The maximum convective kinetic energy obtainable by work done by the vortex force is therefore $\Omega_c|\mathcal{M}|$, so an upper bound for the vertical speed in the Langmuir circulation is estimated to be

$$U_{LC} = \sqrt{2\frac{|\mathcal{M}|}{\rho}\Omega_c}. \tag{1.84}$$

Again taking the case of a monochromatic train of deep water waves for illustration, (1.84) leads to the

$$U_{LC} = \sqrt{2\mathcal{U}_s \frac{\lambda}{4\pi}\Omega_c},$$

where $\mathcal{U}_s$ is the surface value of the Stokes drift. If we have a direct means of estimating the current shear, then we can substitute it and $\mathcal{U}_s$ into this expression. In the absence of an observed value for the shear, we can suppose that the vorticity in the current is derived only from the local applied wind stress. In this case, the maximum vorticity tends to occur at the surface. The surface value of $|\boldsymbol{\omega}| = \tau_{wind}/\mu$, where τ_{wind} is the stress applied by the wind to the water surface, and μ is the viscosity (in natural circumstances, the water is more often than not turbulent, in which case μ must be interpreted as an eddy viscosity). This leads to

$$U_{LC} = \sqrt{2\mathcal{U}_s \frac{\lambda}{4\pi}\frac{\tau_{wind}}{\mu}} = u_* \sqrt{2\mathcal{U}_s \frac{\lambda}{4\pi\nu}}. \tag{1.85}$$

The last replacement is a bow to the convention of defining a "friction velocity", u_*, by the relation

$$u_*^2 \equiv \frac{\tau_{wind}}{\rho},$$

where ρ, as before, is the water density.

We can give an estimate of U_{LC}, based, for example, on (1.85). Suppose the wind speed is 10m/s, then we can estimate (very crudely) that $u_* \approx$ 1.5cm/s. The wave characteristics used above to illustrate rough magnitudes for Stokes drift are reasonable for the so-called "significant waves" generated by a wind speed of this level, so we can take $\mathcal{U}_s$ to be 24cm/s and $\lambda \sim 24$ m. The price we pay for using the wind stress as our method of estimating the current shear is the introduction of a semi–empirical eddy viscosity, to which it is difficult to assign a value. From standard ways to guess at an appropriate value for this parameter when the wind speed is 10m/s, the value $\nu \approx 23\text{cm}^2/\text{s}$ is plausible (see [55], pg. 504), which leads to $U_{LC} = 29$cm/s as an estimate for the upper bound.

1.8 Reduction of Complexity

The equations (1.80) governing Langmuir circulations must be supplemented by boundary conditions appropriate to the physical circumstances under study. Since they are evolution equations, initial conditions must also be specified. Typically, the specification of a Stokes drift velocity that is constant in time, and dependent only on the vertical coordinate is reasonable as a model of a random, wind–driven sea. In addition to the initial conditions which specify the density and current structure of the upper layers, the stress imposed by the wind and bottom conditions must be specified.

It is apparent that the CL model (1.80) is no less complex than the full Navier–Stokes equations under the Boussinesq approximation (except, of course, that surface waves are incorporated by the model). For oil spill problems, it is important to know the spatial variation in the windward current caused by Langmuir circulations, the lateral sweeping speeds, and the downwelling speeds. Practical ways to capture this information under a wide range of circumstances dictates a need for a simpler approach than direct simulation. Possible approaches to this question are outlined here.

1.8.1 Structureless equilibria

Under plausible initial and boundary conditions, the equations admit solutions that are simple nonconvective solutions, and depend only on the vertical coodinate and time. The current is rectilinear and unaffected by the vortex force. Since such solutions do not lead to vertical convective motion and the associated patterns, they will be called "structureless" equilibria. If the thermal conditions are destabilizing, then a structureless equilibrium will

be unstable if the thermal Rayleigh number is above critical, and convection will set in.

If the thermal conditions are stabilizing, as they frequently are, then the structureless equilibrium will persist, unless the vortex force, which appears in a role loosely analogous to the gravitational (buoyancy) force, can cause instablity. Simple examples show this to be possible, and these examples and the estimates of the previous section suggest that the instability is typically (that is, under typical wind conditions) much more powerful than typical thermal instability. As a consequence, when active, the Langmuir circulation instability can overcome significant stabilizing density distributions, thereby mixing the upper layers. Furthemore, it is important to note that the CL model, as presented in (1.80) is capable of describing *both* Langmuir circulation and thermal instability, the two active either separately.

1.8.2 Weak instability, amplitude equations, and patterns

Whenever Langmuir circulations or thermal convection cells are absent, the state is by definition structureless, so structureless equilibria may be determined either theoretically or experimentally. An increase of the vortex force, caused by an increase of either wind speed or wave action, above a critical value will lead to instability.

When the forcing only slightly above the critical value needed, the instability is weak. Marginally unstable states may be described by relatively simple computations. For example, for the vertical velocity component, w, in the LC modified current, such a description takes the form

$$w(x,y,z,t) = A(x,y,t)\Phi(z)\exp\left[i\mathbf{k}\cdot\mathbf{x}\right] + c.c., \tag{1.86}$$

where *c.c.* designates the complex conjugate of the preceeding term, Φ gives the vertical structure and is determined by a linear eigenvalue problem, and the complex function A varies slowly with time and horizontal position. For a wide set of physical problems, the amplitude function A is determined by an "amplitude" (or "envelope") equation. For example, in most cases the amplitude equation for marginally unstable systems depending on one horizontal coordinate only (say y) is the so–called Ginzburg–Landau equation,

$$\frac{\partial A}{\partial t} = \lambda A + c_1\frac{\partial^2 A}{\partial y^2} + c_2 A|A|^2, \tag{1.87}$$

where λ, c_1, and c_2 are all in general complex numbers that can be computed from the original system. The coefficient λ, for example, is just the

(complex) linear growth rate (eigenvalue) and is proportional to $\sqrt{R - R_c}$, where we have assumed that the destabilizing parameter is called R and its critical value is R_c.

The amplitude A modulates the plane wave that it multiplies in (1.86). Other amplitude equations arise depending on circumstances. In particular, while the Ginzburg-Landau is in some sense generic for problems restricted to two space dimensions. The generic counterpart in three space dimensions (where the *modulation* is required in two dimensions), requires the addition of another variable, analogous to a pressure term, to enforce mass conservation (originating, it appears, in the work of Davey & Stewartson [16]).

In the simplest case, when A provides modulations in time only, (1.87) reduces to the "Landau", (also known as "Stuart–Landau") equation,

$$\frac{\partial A}{\partial t} = \lambda A + c_2 A|A|^2. \tag{1.88}$$

A description by means of the form (1.86) utilizing an amplitude equation is very much simpler and more flexible than the original set of partial differential equations. Amplitude equations are the principal tool is the study of pattern formation process, since the vertical structure is known at this stage, and the patterns in the horizontal are determined by A.

1.8.3 Strong instability and patterns

When the instability is far above marginal, the motions are fully nonlinear. In interesting developments, amplitude equations have been applied to study horizontal patterns. The most rigorous of this recent work seems to be that of Newell, Passot, and Souli [67], which considers thermal convection.

The basis of this kind of analysis is quite different. Instead of proceeding by a perturbation about a simple known (equilibrium) state based on small departures, the perturbation is based on *slow* horizontal and temporal variations from *exact* nonlinear states of simple (plane wave) spatial form. Although the resulting description requires a great deal more computation (since the "exact" nonlinear states are known only by first computing them numerically), and is necessarily more complex in other ways, an amplitude equation nevertheless emerges, and its study permits pattern formation to be explored.

1.8.4 Applications to Langmuir circulations

There are two ways in which amplitude equations can be used to study fully nonlinear aspects of patterns in Langmuir circulations.

One such approach, much the more difficult of the two, is to carry out a program analogous to that described in §1.8.3. The second assumes that the form of the amplitude equation appropriate in the marginal instability parameter range remains valid, but the coeffients computed from the marginal circumstances are altered when the disturbances are large. An attempt can then be made to alter the coeffients by fitting the results obtained from amplitude equation to flows found from full numerical simulation.

An alternative approach is described in Chapter 7 and used in an "operational model" that forms the subject of Part II of this report. There we assemble a catalog of nonlinear solutions for rolls. This catalog amounts to the basis for the kind of approach outlined in § 1.8.3, but the roll solutions are not permitted to interact, and empirical information is utilized to constrain the number of entries in the catalog.

Chapter 2

Specification of the Sea State and Boundary Conditions

The CL theory permits the prediction of Langmuir circulations for a specified oceanographic environment. To use the theory, one must provide information concerning the wind forcing, sea state, initial thermal structure of the mixed layer, and internal parameters modelling the effects of incoherent turbulence in the mixed layer. The specification of surface wave related quantities is discussed in this chapter. As described in Chapter 1, the development of Langmuir circulations depends on the water wave field through the Stokes drift produced by the water waves. Thus, given a sea state, we need to calculate the Stokes drift associated with it. This leads to a two part task, to decide on a method of specifying the sea state, and then to calculate the relevant Stokes drift to be input to the theory.

The water depth is assumed infinite and of unlimited horizontal extent. The deep water assumption is acceptable so far as orbital motions in water waves are concerned whenever the water depth is greater than a fraction (roughly one–fourth or larger) of the wavelength of the longest water wave of interest.

2.1 Representation of the sea state

The sea surface is too complex for a detailed description. Lack of knowledge of the precise details giving rise to the instantaneous sea state, and its complexity, demands that a practical mathematical representation for the sea state account for its apparently random nature by a statistical represen-

tation. Having adopted such a representation, one must then address the specific forms it should take. A standard reference for the representation of a random sea is Phillips [71].

Suppose x and y are orthogonal coordinates in the plane of the mean sea surface, and z is the vertical coordinate. We imagine a collection, or ensemble, of identical experiments, in which the sea surface is disturbed leading to waves.. Each (thought) experiment constitutes a realization leading to a space–time evolution of the surface displacement and associated velocity field. Although the conditions imposed are identical as far as measureable observables are concerned, we recognize that there are unobserved conditions which will generally differ from one experiment to the next, leading to a different outcome in, for example, the displacement of the air–sea interface at a given time and place. Let the instantaneous displacement of the sea surface for a given realization is $\zeta(\tilde{\mathbf{x}}, t; \alpha)$, where $\tilde{\mathbf{x}} \equiv x\boldsymbol{e}_1 + y\boldsymbol{e}_2$ is the projection of the position vector $\mathbf{x}$onto the horizontal plane. Here α is a parameter that serves to distinguish the various realizations, and we suppose α can take on any value in a set Ω.

Assuming an underlying probability distribution with probability density $p(\alpha)$, the mathematical expectation, or average over the ensemble, of any quantity, $f(\zeta(\mathbf{x}, t; \alpha)$, is defined to be

$$\overline{f} = \int_{\Omega} f(\mathbf{x}, t; \alpha) p(\alpha) d\alpha.$$

We suppose that displacements are measured from the mean sea surface, so by definition,

$$\overline{\zeta(\mathbf{x}, t)} = \int_{\Omega} \zeta(\mathbf{x}, t; \alpha) p(\alpha) d\alpha = 0.$$

The fluid is horizontally unbounded, and the Fourier transform over the two horizontal directions and over time for the surface displacement of a given realization is

$$A(\mathbf{k}, n; \alpha) = \left(\frac{1}{2\pi}\right)^3 \int\int\int \zeta(\mathbf{x}, t; \alpha) \exp\{-\mathbf{k} \cdot \mathbf{x} - nt\} dx_1 dx_2 dt, \qquad (2.1)$$

where A will be a complex–valued generalized function, and

$$\mathbf{k} \equiv k_1 \boldsymbol{e}_1 + k_2 \boldsymbol{e}_2.$$

We also have the inversion formula

$$\zeta(\mathbf{x}, t; \alpha) = \int_{\mathbf{k},n} A(\mathbf{k}, n; \alpha) \exp\{\mathbf{k} \cdot \mathbf{x} - nt\} d\mathbf{k} dn. \qquad (2.2)$$

The notation is meant to indicate that the integrals are taken over the regions covered by the designated variable; for example

$$\int_{\mathbf{x},t}(\cdot)d\mathbf{x}dt = \int_{x=-\infty}^{\infty}\int_{y=-\infty}^{\infty}\int_{t=-\infty}^{\infty}(\cdot)dxdy,$$

and the range of each (scalar) integration variable is $(-\infty,\infty)$. The average

$$\overline{A^*(\mathbf{k},n)A(\mathbf{k}',n')} = \tag{2.3}$$
$$\left(\frac{1}{2\pi}\right)^6\int_{\mathbf{x},t}\int_{\mathbf{x}',t'}\overline{\zeta(\mathbf{x},t)\zeta(\mathbf{x}',t')}\exp\{\mathbf{k}\cdot\mathbf{x}-nt\}\exp\{\mathbf{k}'\cdot\mathbf{x}'-nt'\}d\mathbf{x}dtd\mathbf{x}'dt,$$

and the label α in the argument of random functions is suppressed. Let the relative position vector $\mathbf{x}'-\mathbf{x}=\mathbf{r}$, and the time difference $t'-t=\tau$. For a statistically stationary random process, the two–point, two–time covariance

$$\overline{\zeta(\mathbf{x},t)\zeta(\mathbf{x}',t')} = \overline{\zeta(\mathbf{x},t)\zeta(\mathbf{x}+\mathbf{r},t+\tau)}.$$

depends only on the time lag τ and not on the time itself, and for a homogeneous random field, the covariance depends only on the relative position vector of the two points on which it is based. With this assumption,

$$\overline{\zeta(\mathbf{x},t)\zeta(\mathbf{x}+\mathbf{r},t+\tau)} \equiv Z(\mathbf{r},\tau),$$

and (2.3) may be written

$$\overline{A^*(\mathbf{k},n)A(\mathbf{k}',n')} = \tag{2.4}$$
$$\left(\frac{1}{2\pi}\right)^6\int_{\mathbf{x}',t'}Z(\mathbf{r},\tau)\exp\{-\mathbf{k}\cdot\mathbf{r}-n\tau\}d\mathbf{r}d\tau\int_{\mathbf{x},t}\exp\{-(\mathbf{k}'-\mathbf{k})\cdot\mathbf{x}-(n'-n)t\}d\mathbf{x}dt.$$

The expression involving integrals over $\mathbf{x}$ and t is $(2\pi)^3$ times the delta function $\delta(\mathbf{k}'-\mathbf{k},n'-n)$. Consequently, $X(\mathbf{k}',n')$, given by

$$\begin{aligned}X(\mathbf{k}',n') &\equiv \\ &\int_{\mathbf{k},n}\overline{A^*(\mathbf{k},n)A(\mathbf{k}',n')}d\mathbf{k}dn \\ &= \left(\frac{1}{2\pi}\right)^3\int_{\mathbf{x}',t'}Z(\mathbf{r},\tau)\exp\{-\mathbf{k}'\cdot\mathbf{r}-n'\tau\}d\mathbf{r}d\tau,\end{aligned}$$

is the (multiple) Fourier transform of the covariance and is called the *wave spectrum.* The notation used here is that of Phillips, [71]. In the event the

wavefield may be said to satisfy the deep-water linear dispersion relation, the spectrum may be expressed in terms of either wavenumber alone, or frequency alone. This will be assumed to be justified, and the notation to be used (subsequently) for frequency spectrum is that of Hasselmann et al. [29].

Wave fields are only approximately homogenous and stationary. In particular, as wind waves develop as functions of the time the wind has been blowing (duration) and the distance over which it has been acting (fetch), the wave spectrum evolves as a function of duration and fetch. The fetch and duration leading to significant changes in the spectrum are large compared to the typical wavelengths and periods, and this justifies the invocation of approximate homogeneity and stationarity. Nevertheless, recognizing the dependence on fetch and duration, we include these as arguments of the spectrum $X(\mathbf{k}, n, \mathbf{x}, t)$.

Data on surface wave fields is usually given in terms of the spectrum, and therefore it is necessary to connect the wave-related information that we need, the Stokes drift, to the wave spectrum.

2.1.1 Stokes drift for a random wave field

The Stokes drift is given by the expression (see (31) of Chapter 1)

$$\mathbf{u_s} = \overline{\int^t \mathbf{u}_w(\mathbf{x}, t)dt \cdot \nabla \mathbf{u}_w(\mathbf{x}, t)}. \tag{2.5}$$

The velocity field due to irrotational water waves, $\mathbf{u}_w$, may be written as a Fourier transform in space and time,

$$\mathbf{u}_w = \int_{\mathbf{k},n} i\boldsymbol{\ell}(\mathbf{k})\phi(\mathbf{k}, n)\mathrm{e}^{kz}\mathrm{e}^{i\Theta}d\mathbf{k}dn. \tag{2.6}$$

In this expression,

$$\begin{aligned} \boldsymbol{\ell}(\mathbf{k}) &\equiv \mathbf{k} - ik\boldsymbol{e}_3, \text{ and } \Theta \equiv \mathbf{k}\cdot\mathbf{x} - nt, \\ \text{where} & \\ k &= \left(k_1^2 + k_2^2\right)^{1/2}. \end{aligned}$$

From (2.6), the velocity gradient tensor can be formed, giving

$$\nabla \mathbf{u}_w = -\int_{\mathbf{k},n} \boldsymbol{\ell}\boldsymbol{\ell}\phi(\mathbf{k}, n)\mathrm{e}^{kz}\mathrm{e}^{i\Theta}d\mathbf{k}dn, \tag{2.7}$$

and the water particle displacement vector,

$$\boldsymbol{\xi} = \int^t \mathbf{u}_w dt = -\int_{\mathbf{k},n} \frac{\boldsymbol{\ell}}{n}\phi(\mathbf{k},n)\mathrm{e}^{kz}\mathrm{e}^{i\Theta}d\mathbf{k}dn. \tag{2.8}$$

The surface value of the 3 component of $\boldsymbol{\xi}$ is the surface displacement ζ. Therefore, from (2.2) and (2.8),

$$\zeta = \int_{\mathbf{k},n} A(\mathbf{k},n)\mathrm{e}^{i\Theta}d\mathbf{k}dn = \int_{\mathbf{k},n} \frac{\boldsymbol{\ell}}{n}\phi(\mathbf{k},n)\mathrm{e}^{i\Theta}d\mathbf{k}dn,$$

which relates A and ϕ, with

$$\phi(\mathbf{k},n) = -\frac{in}{k}A(\mathbf{k},n).$$

Since $\boldsymbol{\xi}$ is real, the Stokes drift is

$$\mathbf{u_s} = \overline{\boldsymbol{\xi}^*\cdot\nabla\mathbf{u}_w}$$

or,

$$\begin{aligned}\mathbf{u_s} &= \\ &= \int_{\mathbf{k},n} \frac{\boldsymbol{\ell}^*(\mathbf{k})}{n}\phi^*(\mathbf{k},n)\mathrm{e}^{kz}\mathrm{e}^{i\Theta}d\mathbf{k}dn\cdot\int_{\mathbf{k}',n'} \boldsymbol{\ell}(\mathbf{k}')\boldsymbol{\ell}(\mathbf{k}')\phi(\mathbf{k}',n')\mathrm{e}^{k'z}\mathrm{e}^{i\Theta'}d\mathbf{k}'dn' \\ &= \int_{\substack{[\mathbf{k},n]\\[\mathbf{k}',n']}} \frac{n'}{kk'}\overline{A^*(\mathbf{k},n)A(\mathbf{k}',n')}[\boldsymbol{\ell}^*(\mathbf{k})\cdot\boldsymbol{\ell}(\mathbf{k}')]\boldsymbol{\ell}(\mathbf{k}')\mathrm{e}^{(k+k')z-i(\Theta-\Theta')}d\mathbf{k}d\mathbf{k}'dndn',\end{aligned}$$

which simplifies to

$$\mathbf{u_s} = \int_{\mathbf{k},n} 2n\boldsymbol{\ell}(\mathbf{k})X(\mathbf{k},n)\exp(2kz)d\mathbf{k}dn.$$

The component in the vertical (z) direction clearly must vanish to be physically reasonable, and (because it is imaginary) to be mathematically correct (since $\mathbf{u_s}$ must be real). It may be seen to vanish by virtue of the symmetry relation

$$X(-\mathbf{k},-n) = X(\mathbf{k},n). \tag{2.9}$$

That (2.9) holds arises by virtue of the fact that the covariance $Z(\mathbf{r},\tau)$ is real, and because spatial homogeneity and temporal stationarity require that $Z(-\mathbf{r},-\tau) = Z(\mathbf{r},\tau)$.

Since its z–component vanishes, the Stokes drift is given by

$$\mathbf{u_s} = \int_{\mathbf{k},n} 2n\mathbf{k}X(\mathbf{k},n)e^{2kz}d\mathbf{k}dn. \tag{2.10}$$

For waves on deep water, $n^2 = \sigma^2 = gk$, and the wavenumber–frequency spectrum may be simplified by use of this dispersion relation ([71]), leading to

$$X(\mathbf{k},n) = \Psi(\mathbf{k})\delta(n-\sigma), \tag{2.11}$$

where $\Psi(\mathbf{k})$ is the *wavenumber spectrum.* With this substitution, we arrive at a useful formula for the Stokes drift of a random sea,

$$\mathbf{u_s} = \int_{\mathbf{k}} 2\sigma(k)\mathbf{k}\Psi(\mathbf{k})e^{2kz}d\mathbf{k}. \tag{2.12}$$

The wavenumber spectrum is related to a more readily measured directional–frequency spectrum, $F(f,\theta)$. Here f is wave–frequency, related to the angular frequency, σ, used above by $\sigma = 2\pi f$. Change coordinates in the wavenumber plane from (k_1,k_2) to the polar coordinates (k,θ), where, to be definite, the angle θ is measured from the x–axis. Then the area element in the (k_1,k_2) plane can be written as $kdkd\theta = 32\pi^3(f^3/g^2)dfd\theta$, by use of the dispersion relation. The surface displacement variance may be expressed either in terms of the wavenumber spectrum or the frequency spectrum as follows:

$$\overline{\zeta^2} = \int_0^{2\pi} d\theta \int_0^{\infty} \Psi(k,\theta)kdk \tag{2.13}$$

$$= \int_0^{2\pi} d\theta \int_0^{\infty} F(f,\theta)df. \tag{2.14}$$

Note that, assuming small the waves have small slope, the surface variance is related to the total energy in the wave field: in particular $\rho g\overline{\zeta^2}$ is the wave energy per unit surface area. Thus, except for a constant factor, F is also an energy spectrum.

The identification in (2.13) relates $F(f,\theta)$ to $\Psi(k,\theta)$, and in particular allows us to write the Stokes drift in (2.12 in terms of F as

$$\mathbf{u_s} = \frac{16\pi^3}{g}\int_0^{2\pi}\int_0^{\infty} f^3F(f,\theta)\exp[8\pi^2f^2z/g)](\cos\theta\mathbf{e}_1+\sin\theta\mathbf{e}_2)dfd\theta. \tag{2.15}$$

If the spectrum F is symmetric in θ, the 2-component of $\mathbf{u_s}$ will be identically zero, leading to a Stokes drift entirely in the 1-direction.

For future reference, we note that the frequency spectrum, $E(f)$ is the integral over all possible angles of F, or

$$E(f) = \int_0^{2\pi} F(f,\theta)d\theta, \tag{2.16}$$

so that one can write F as a product

$$\begin{aligned} F(f,\theta) &= E(f)S(f,\theta), \text{ where} \\ \int_0^{2\pi} \hat{S}(f,\theta)d\theta &= 1, \end{aligned} \tag{2.17}$$

and $\hat{S}(f,\theta)$ is sometimes called the "spreading function".

At this stage, we have found an expression, (2.15), for the Stokes drift in terms of the directional–frequency spectrum of the surface waves. In order to fix the Stokes drift input to the Langmuir circulation theory, we must adopt a suitable surface wave spectrum, and this is the subject we next address.

2.1.2 Specification of the wave spectrum and its development in space and time

Once a directional frequency (or a wavenumber) spectrum is specfied, the Stokes drift is determined. The problem of predicting the gravity wave spectrum of ocean waves is one of long standing and on which much effort has been devoted. The earliest attempt is that of Sverdrup and Munk during World War II, and the importance of the problem to operations at sea have led to a continuous refinement and improvement. The monograph by Khandekar [40] briefly reviews the history of the subject, and provides a useful survey of the problem. The current status of the prediction of wind–generated seas is outlined in WAMDI [86].

While ocean waves may be generated by events such as seismic activity, their most common cause is the instability of the air–sea interface caused by wind forcing. The goal of wave prediction is then to determine the statistics of the sea surface given the mean wind stress distribution on the sea surface. Attention has been focussed on the development in space and time of the wave spectrum, $F(f,\theta;\mathbf{x},t)$. The spectrum changes due to several effects. First, under the influence of atmospheric forcing, energy is fed into the wave field, causing an increase of F. Second, given any wave field involving

a superposition of many wavelengths and frequencies, interactions occur between waves of differing wavenumbers, provided they are related by a resonance condition. A consequence of this nonlinear coupling, the spectral content of F can change in time, with energy in a given wavenumber band being both gained and lost to other wavenumbers, so that a "scattering" of wave energy takes place due to (usually weak) nonlinear effects. Third, energy can be lost to the wave field to turbulence by wave breaking, or "whitecapping". Fourth, energy may be transferred to or from existing non-wave motions in the ocean, currents or turbulence for example. The latter components of the motion are those for which the dispersion relation associated to wave motion does not apply.

The most sophisticated spectral models contemplated to date [86] calculate the rate of change of F according to the Boltzmann–like transport equation

$$\frac{\partial F}{\partial t} + \mathbf{v}_g \cdot \nabla F = S. \tag{2.18}$$

Here $\mathbf{v}_g$ is the group velocity of the waves of frequency f, and S is a source representing the possible gains and losses of energy. Generally, it is thought adequate to model the source by a superposition of individual effects, and only the effects of the first three mentioned in the previous paragraph are modelled. In principal, all source terms are nonlinear and generally coupled, and involve complex physical processes which must be modelled in some suitable way. In the newer existing models [86], the contribution due to atmospheric forcing is taken to be a linear function of F, and the energy dissipation term due to wave breaking is taken to be a quasi-linear function of F. The nonlinear source term due to wave interactions is based on the weakly nonlinear resonance analyses (see [71]). The exact evaluation of the interaction term so identified involves an eightfold multiple integral, and this requires more computational work than is feasible for practical purpose, even on modern supercomputers. Consequently, assumptions must be made to simplify the numerical evaluation of this input.

Equation (2.18) relates the problem of wave prediction to the underlying physical mechanisms more closely than had been possible heretofore, and it is thought that by making continuing improvements in the source terms by improved understanding of the physics involved in each, predictions made on the basis of this equation should satisfy most requirements. Nevertheless, the prediction of wind-driven seas must be done numerically, and when done on the basis of (2.18) is a numerically intensive process. While it is important to keep this kind of analysis firmly in mind, it is not currently practical to

consider coupling the development of the wave spectrum as computed on the fundamental basis of (2.18) to the development of Langmuir circulations associated with the spectrum.

Instead, we turn to earlier wave prediction methods which postulate the functional form of the spectrum, which depends on a small number of parameters. For example, the JONSWAP ("Joint North Sea Wave Project") spectrum seems to fit a wide range of experimental wave spectra, and supercedes earlier spectra such as the widely used Pierson–Moscowitz spectrum (see [72]). Let the frequency at the peak of the spectrum be denoted f_m and let the dimensionless version of this frequency be denoted ν, where

$$\nu \equiv \frac{U f_m}{g}, \tag{2.19}$$

where U is the wind speed at anemometer height (10 meters), and let the frequency normalized by f_m be μ, or

$$\mu \equiv \frac{f}{f_m}. \tag{2.20}$$

The JONSWAP frequency spectrum is given by

$$E(\mu) = \frac{\beta}{(2\pi)^4}\frac{U^5}{\nu^5 g}\mathcal{E}(\mu), \text{ where} \tag{2.21}$$

$$\mathcal{E}(\mu) = \mu^{-5}\exp[-G(\mu)], \text{ and} \tag{2.22}$$

$$G(\mu) = \frac{5}{4}\mu^{-4} - (\ln\gamma)\exp[-(\mu-1)^2/2\sigma^2)], \tag{2.23}$$

with

$$\sigma(\mu) = \begin{cases} 0.07 & \text{if } \mu \leq 1, \\ 0.09 & \text{if } \mu > 1. \end{cases}$$

The parameter γ is the "peak enhancement factor", and Hasselmann et al. [29] assert that the best fit to the JONSWAP data may be had by taking $\gamma = 3.3$. When $\gamma = 1$, there is no "peak enhancement", and the JONSWAP spectrum reduces to the Pierson–Moscowitz spectrum.

Figure 2.1.2 shows the experimentally measured fetch–limited spectra for which the JONSWAP spectral form was developed.

Hasselmann el al. [29] describe two models using the JONSWAP frequency spectrum, applicable to developing seas. These models are based on the observation that the shape of measured spectra remain self–similar to a good approximation as the wave field grows under wind forcing, and is

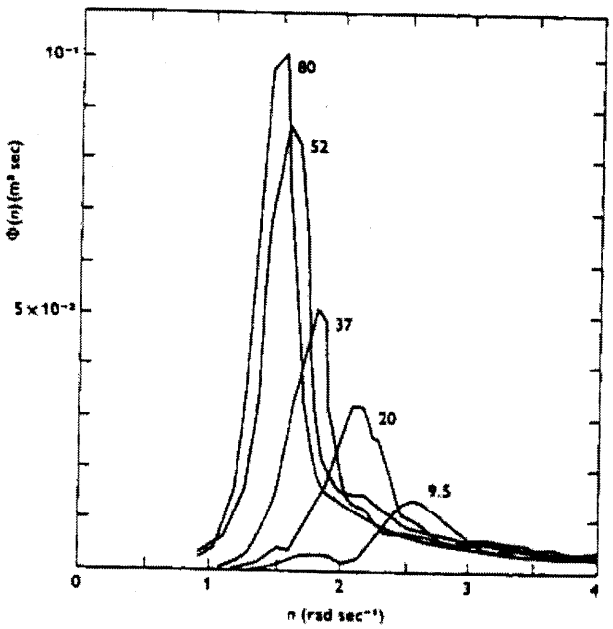

Figure 2.1: Development of the spectrum with increasing fetch (from 9.5 to 80 km, as found by JONSWAP.

well fitted by the JONSWAP spectum. The general level of the spectrum increases as energy is transferred into the wave field, and this may be accounted for by allowing β to vary in space and time, and the location of the spectral peak shifts to lower frequencies as the wave field develops, and this may be accounted for by allowing ν, the dimensionless peak frequency, to vary in space and time. In the first model, two partial differential equations are derived that permit these two parameters to evolve so as to permit the JONSWAP spectrum to approximately satisfy the energy balance equation (2.18). It is found that the solutions to this pair of equations very rapidly is attracted to a functional relation

$$\beta = 0.032\nu^{2/3}, \tag{2.24}$$

which allows a further reduction to a second model entirely controlled by a single parameter, which may be taken to be ν. We adopt this model due to its simplicity, and to the flexible range of conditions that it seems to cover with reasonable reliablility. In both cases, the spreading function is taken to be

$$\hat{S}(f,\theta) = \begin{cases} \frac{2}{\pi}\cos^2\theta & \text{for} \quad 0 \le |\theta| < \frac{\pi}{2}, \\ 0 & \text{for} \quad \frac{\pi}{2} \le |\theta| < \pi, \end{cases} \tag{2.25}$$

where $\theta = 0$ defines the local wind–direction.

According to [29], the single parameter ν is to be determined from an equation may be written as

$$\frac{U}{g\nu}\left(\frac{\partial\nu}{\partial t} + bU\nu^{-1}\frac{\partial\nu}{\partial s}\right) = -\frac{3}{7}a\nu^{7/3} + \frac{1}{g}\left(\frac{\partial U}{\partial t} + b'U\nu^{-1}\frac{\partial U}{\partial s}\right) \tag{2.26}$$

where

$$a = 0.00129, \quad b = 0.064, \quad b' = 1.049b,$$

and s is arclength of a path along the wind direction, so

$$\frac{\partial}{\partial s} = \boldsymbol{e}_{wind}\cdot\nabla \tag{2.27}$$

where

$$\boldsymbol{e}_{wind} = \boldsymbol{U}(\mathbf{x},t)/U(\mathbf{x},t)$$

is a unit vector tangent to the local wind velocity vector $\boldsymbol{U}$. direction

We find it convenient to rewrite (2.26) in the alternative form

$$\frac{\partial}{\partial t}\left[\left(\frac{U}{\nu}\right)^{7/3}\right] + b\frac{U}{\nu}\frac{\partial}{\partial s}\left[\left(\frac{U}{\nu}\right)^{7/3}\right] = U^{4/3}\left(ag - \frac{7}{3}(b'-b)\left(\frac{U}{\nu}\right)^2\frac{1}{U}\frac{\partial U}{\partial s}\right). \tag{2.28}$$

Typically, the term involving $b' - b$ is small compared to ag, primarily because $|U(\partial U/\partial s) \ll g$, and we therefore shall ignore it. This leads to a very tractable equation, which in the general case can easily be integrated along characteristics. For the simpler cases for which the waves are either steady, but *fetch–limited* (so $\partial/\partial t = 0$, or acted upon by a wind field that is independent of distance, so the waves are limited by the *duration* of the wind only, the solution for ν reduces to quadratures. For example, for the steady fetch–limited case, $\nu = \nu(x)$, where we write x for s. It is natural here to suppose the wave energy density vanishes at zero fetch (implying that $\nu(0) = \infty$, so

$$\nu(x) = \frac{U(x)}{\left(\frac{10ag}{7b}\int_0^x U^{4/3}(s')ds'\right)^{3/10}}. \tag{2.29}$$

If the wind is spatially uniform, this result gives

$$\nu(x) = 2.9\left(\frac{U^2}{gx}\right)^{3/10},$$

in acceptable agreement with (5.3) of Hasselmann et al. [29].

For a wind and wave field depending on duration but not fetch, the result corresponding to (2.29) is

$$\nu(t) = \frac{U(t)}{\left(ag\int_0^t U^{4/3}(s')ds'\right)^{3/7}}. \tag{2.30}$$

For a steady wind, the duration–limited (dimensionless) peak frequency develops in time like

$$\nu(t) = 17.3\left(\frac{U}{gt}\right)^{3/7}.$$

This may be compared to the two–parameter model of [29], which is the same, but with the coefficient 17.3 replaced by 16.8.

2.1.3 Stokes drift specification

If the waves are defined in terms of a frequency spectrum and a spread function, then our expression (2.15 may be written on use of (2.17), as

$$\mathbf{u_s} = \frac{16\pi^3}{g}\int_0^\infty f^3E(f)\exp(8\pi^2f^2z/g)df\int_0^{2\pi}\hat{S}(f,\theta)[\cos\theta\mathbf{e}_1 + \sin\theta\mathbf{e}_2]d\theta. \tag{2.31}$$

For waves that are generated locally by the wind, it is reasonable to assume that the spread function is an even function of θ, in which case the component of Stokes drift at right angles to the wind direction vanishes when (2.31) is evaluated.

Sea state data required to obtain the Stokes drift is not routinely available. We therefore need to connect the most readily available observational data, the local wind speed, to sea state. Even if the connection used were exact, such a description would be incomplete. Wind at distant locations and at earlier times may produce waves that can propagate to the area of concern. This *swell* component of the wave field will be missed by predictions based on local conditions. Nevertheless, the locally generated wind waves frequently dominate the energy spectrum.

Here we adopt the JONSWAP spectrum (2.21) for $E(f)$, and the $\cos^2\theta$ used by Hasselmann et al. [29]. In this case, the Stokes drift is simply

$$\mathbf{u_s} = \frac{8}{3\pi^2}\frac{\beta}{\nu}Ue_1\mathcal{I}(\hat{z}) \text{ where} \tag{2.32}$$

$$\mathcal{I} = \int_0^\infty e^{-G(\mu)}e^{\mu^2\hat{z}}\frac{d\mu}{\mu^2}, \tag{2.33}$$

where

$$\hat{z} = 8\pi^2\nu^2\frac{gz}{U^2},$$

and G is given by (2.21).

The integral (2.33) cannot be given in explicit form, but may be readily evaluated numerically.

Ocean wave spectral models do not predict the small wavelength components, and the short wave components nominally predicted by parametric spectral models are incorrect. The short waves are dissipated, and therefore spectral models need to be adjusted if unrealistic consequences follow from the formal extension of these spectra to all wavelengths.

The Pierson-Moscowitz spectrum and the JONSWAP spectrum built upon it both predict that the angular frequency spectrum (where the angular frequency, n, is related to the frequency, f by $n = 2\pi f$) of the short waves goes like

$$E(n) \sim \beta n^{-5}. \tag{2.34}$$

Any spectrum with an algebraic behaviour at high frequency that falls off like n^{-5} or more slowly, like Pierson-Moscowitz or JONSWAP, or indeed most suggested empirical fits to ocean wave data, will lead to infinite values

at the mean water surface of the *gradient* of the Stokes drift.[1] The long algebraic tails in these spectral forms arise from the neglect of scales below which wave energy is heavily dissipated. The most significant dissipative process is thought to be wave breaking. According to Phillips [71], the presence of surface currents acts to enhance wave breaking. This is not important for frequencies

$$n \ll n_{sc} = 2g/u_{*a},$$

where u_{*a} is the air friction velocity, but becomes important for frequencies larger than about $n_c = n_{sc}/10$. The energy spectrum therefore drops off faster than (2.34) indicates, and is better written as

$$E(n) \sim \beta n^{-5} f(nu_{*a}/g). \tag{2.35}$$

where f is a function that decays exponentially fast. Other factors, such as capillary effects, also cause modification and ultimately dissipate the high frequency components.

The net effect is that the wave spectrum should be cut off at values of the frequency comparable to n_c. We may estimate n_c by taking $u_{*a} \sim U/25$, giving $n_c \sim 5g/U$, where U is the local wind speed. This is the assumption we will make, and we will accomplish the cut-off by assuming the wave energy is zero for frequencies larger than n_c.

This alters (2.32) for the Stokes drift profile by substituting n_c for ∞ in the upper limit of the integral required. This is unimportant for this quantity, but is makes an essential difference to its gradient, which with this substitution is

$$\begin{aligned} \frac{\partial \mathbf{u_s}}{\partial z} &= \frac{64\beta}{3}\frac{g\nu}{U}\mathbf{e}_1 \mathcal{J}(\hat{z}) \text{ where} \\ \mathcal{J} &= \int_0^5 e^{-G(\mu)} e^{\mu^2 \hat{z}} d\mu. \end{aligned} \tag{2.36}$$

2.2 Exchange processes at the mixed layer boundaries

The part of the ocean with which we are concerned is the mixed layer. To focus attention on this limited region, we need to isolate it from the

[1] The Stokes drift itself is finite everywhere under these circumstances.

atmosphere above and the water body below. This implies a need to specify boundary conditions which reflect the physical exchanges occuring at the air–sea interface and at the base of the mixed layer. Since imposition of conditions at these boundaries is a process of mathematical idealization, it in itself amounts to and requires the modelling of physical mechanisms which are not fully understood. Any choices of models is therefore at best tentative, and it should be recognized that other choices may later be seen to better reflect the physics.

In this section, we first specify a set of boundary conditions reflecting the exchanges of momentum and heat to the mixed layer. We then give, for the purposes of illustration, a simple steady state current and density stratification field that could arise from this set of exchange processes in an ocean in which the Coriolis acceleration is ignored. The section concludes with an estimation of the parameters which appear in the boundary coupling conditions.

2.2.1 a. Boundary conditions

To fix our problem, we suppose that the wind at some "anemometer" height above the mean water surface is constant in speed and in direction, which we take to coincide with the x–axis. A strong thermocline exists at a depth d below the mean water surface, $z = 0$, and the water above it is either of uniform density, or stratified with a modest density gradient. It is supposed that the thermocline is strong enough to prevent the penetration of any significant convective motion, so that the plane $z = -d$ acts like an impenetrable surface. The water below the thermocline may be moving. If so, its horizontal speed, like that of the wind, is supposed constant in speed and direction with x and y components of u_{below}, v_{below}, respectively.

A stress will be exerted on the water, some of which will provide the momentum radiated away from the local water column by surface waves, and the residual will increase the momentum of the local current system. We suppose that the surface waves are statistically stationary and horizontally homogeneous, and that the associated Stokes drift is rectilinear with speed $U_S(z)$ in the wind direction. Furthermore, we suppose that the wind speed U_a has been discounted for any momentum transferred to the waves, so that only the stress which transfers momentum to the current system is accounted for. The mean surface water speeds are much smaller than the wind speed at standard anemometer heights, typically by a factor of 30 or so, and so the usual practice in estimating the stress applied to the water surface is to

ignore the surface current speed. In this approach, a constant value of U_a implies a constant applied stress. This is a good approximation, but there are clearly small departures from it when the surface current accelerates. It is evident that the stress will be reduced, albeit by a small amount, as the surface current increases.

Let the stress vector be $\boldsymbol{\tau}$. Assume a constant bulk momentum exchange coefficient, C_m, and fix the stress vector applied to the (mean) water surface by the wind to be

$$\boldsymbol{\tau} = C_m \rho_a \sqrt{(U_a - u_s)^2 + v_s^2}\, [(U_a - u_s)\mathbf{i} - v_s \mathbf{j}], \tag{2.37}$$

where u_s and v_s are the components of the mean surface water current in the x (windward, unit vector $\mathbf{i}$) and y (crosswind, unit vector $\mathbf{j}$) directions, respectively, and ρ_a is the air density. The water current speed is small compared to U_a, so we can approximate (2.37) by

$$\boldsymbol{\tau} \approx \rho_w u_*^2 \left[\left(1 - 2\frac{u_s}{U_a} \right) \mathbf{i} - \frac{v_s}{U_a} \mathbf{j} \right], \tag{2.38}$$

where ρ_w is the water density, and u_* is the *water* friction velocity defined here by

$$\rho_w u_*^2 = C_m \rho_a U_a^2.$$

This leads to the surface stress boundary conditions

$$\begin{aligned} \frac{\boldsymbol{\tau}\cdot\mathbf{i}}{\rho_w u_*^2} + \frac{2u_s}{U_a} &= 1, \\ \frac{\boldsymbol{\tau}\cdot\mathbf{j}}{\rho_w u_*^2} + \frac{v_s}{U_a} &= 0. \end{aligned} \tag{2.39}$$

Similar conditions may be applied, albeit more speculatively, to couple the mixed layer to the water below it. Current speeds typically are much smaller below the pycnocline than they are just above it. The higher effective viscosity in the turbulent (or simply the convective) motion in the mixed layer is one way to think of the cause of the boundary-layer character exhibited across the thermocline. The momentum flux from the mixed layer to the water below is modelled here in a way that has been suggested for integral models of the mixed layer (Niiler & Kraus [68]). The two transfer mechanisms contemplated are due first to entrainment at the base of

the mixed layer, with an entrainment velocity, w_e to be specified, and second to downward radiation of momentum in internal waves (Pollard & Millard [74]). Niiler & Kraus suggest parameterization of this effect by means of a constant drag coefficient. We note that if the mixed layer depth remains constant, then any time–independent horizontally–averaged current that may emerge must have the stress imposed at the surface balanced by the stress imposed at the bottom, and with the mechanisms suggested here, this implies that the stress is imposed by internal wave radiation. Accordingly, we will take the contribution of the internal wave drag in the form $\rho_w(mu_*^2\mathbf{i} + C_{IW}u_*(\Delta u\mathbf{i} + \Delta v\mathbf{j})$. Here we have taken $\Delta u \equiv u_{bottom} - u_{below}$ and $\Delta v \equiv v_{bottom} - v_{below}$ to be the difference of the horizontal velocity components at the bottom of the mixed layer (i.e., as $z \downarrow -d$), and the corresponding velocity components in the fixed current below the mixed layer; the "extra" wave stress has been taken in the form of a linear friction.

The dimensionless parameter m is a measure of the fraction of the stress attributable to internal waves. When the mixed layer has constant depth and is in dynamical equilibrium, then all of the stress at the bottom is accounted for by internal wave radiation and m approaches one.

The bottom stress boundary conditions, allowing for entrainment and radiation, are

$$\begin{aligned} \frac{\boldsymbol{\tau}\cdot\mathbf{i}}{\rho_w u_*^2} &= \left(\frac{w_e}{u_*} + C_{IW}\right)\frac{\Delta u}{u_*} + m, \\ \frac{\boldsymbol{\tau}\cdot\mathbf{j}}{\rho_w u_*^2} &= \left(\frac{w_e}{u_*} + C_{IW}\right)\frac{\Delta v}{u_*}, \end{aligned} \tag{2.40}$$

at $z = -d$. In the next section, we shall estimate the entrainment velocity based on the over-all Richardson number across the pycnocline using the experimental data discussed by Phillips [71].

Whenever a nonzero entrainment velocity is invoked, we must allow the mixed layer depth, d, to change with time (since $\dot{d} = w_e$). In the stability analysis to follow, we suppose that any such changes are much slower than the time scales for Langmuir circulation instability to occur, so that the depth variations may be treated quasistatically.

We adopt similar mixed boundary conditions on heat transfer at the upper and lower boundaries to relate heat flux to temperature differences across the interfaces. If T_a, T_s, T_{bottom}, and T_{below} are the temperatures of the air and water corresponding to U_a, u_s, u_{bottom}, and u_{below}, then Newton's

law of cooling gives

$$\kappa_T \frac{\partial T}{\partial z} = h_{aw}(T_a - T_s) \quad \text{at } z = 0, \tag{2.41}$$

and

$$\kappa_T \frac{\partial T}{\partial z} = h_{ww}(T_{bottom} - T_{below}) \quad \text{at } z = -d. \tag{2.42}$$

Here h_{ww} is the heat transfer coefficient across the thermocline (heat flux divided by heat capacity, $\rho_w c_{pw}$, of a unit volume of water), h_{aw} is the heat flux across the air layer divided by the heat capacity of a unit volume of water, and κ_T is the (eddy) thermal diffusivity of water.

2.2.2 b. Structureless equilibrium

The CL theory differs from the Navier–Stokes or Reynolds–averaged Navier–Stokes equations by a term representing the rectified effects of surface gravity waves. These effects reside in a "vortex force"

$$\mathbf{U_S} \times \operatorname{curl} \mathbf{v},$$

where $\mathbf{v}$ is the velocity vector of the complete (rectified) current system. When $\mathbf{U_S} = U_S(z)\mathbf{i}$, the CL equations allow for a nonconvective, rectilinear current and temperature field in which the vortex force does not play a role.

Applications of the theory to date assume constant eddy viscosity and constant eddy thermal diffusivity. Although the theory is not restricted to this representation of the incoherent turbulence, we continue to adopt this parameterization.

Given these preliminary remarks, the problem for nonconvective or "structureless" states in the layer is (quasi)laminar and the vortex force term simply modifies the mean pressure distribution. If we seek steady structureless equilibria, then the velocity vector lies in the horizontal plane, and must be a linear function of z. Similarly, the temperature, $T(z)$, must be a linear function. The boundary conditions are (2.39), (2.40), (2.41), (2.42), supplemented by

$$\frac{\boldsymbol{\tau}}{\rho_w} = \nu_T \frac{\partial \mathbf{v}}{\partial z} \quad \text{at } z = 0, -d,$$

where ν_T is the eddy viscosity and the appropriate expression is substituted for $\boldsymbol{\tau}$ from (2.39) and (2.40).

Defining

$$R_* = \frac{u_* d}{\nu_T},$$

the velocity field satisfying these conditions has x component

$$u = U(z) = U_1 \frac{z}{d} + U_0, \tag{2.43}$$

where

$$U_0 = u_* \frac{(1 - m + \alpha_b)R_* + \alpha_b(u_{below}/u_*)}{\alpha_b + \alpha_t + \alpha_b\alpha_t} \tag{2.44}$$

and

$$U_1 = u_* \frac{(\alpha_b + m\alpha_t)R_* - \alpha_t\alpha_b(u_{below}/u_*)}{\alpha_b + \alpha_t + \alpha_b\alpha_t}, \tag{2.45}$$

where

$$\alpha_t = \frac{2u_*}{U_a}R_*, \quad \text{and} \quad \alpha_b = \frac{dw_e}{\nu_T} + C_{IW}R_* \tag{2.46}$$

are dimensionless parameters.

The y velocity component is

$$v = V(z) = \frac{\alpha_b v_{below}}{\alpha_t + \alpha_t\alpha_b + 2\alpha_b}\left(-\alpha_t\frac{z}{d} + 2\right). \tag{2.47}$$

In the work to follow, we will assume that both α_t and α_b are positive and that $(u_{below}, v_{below}) = \mathbf{0}$. (The latter assumption is always permissible, though not necessarily convenient, since we can always adopt a coordinate system moving with the fluid below at the expense of altering the specification of the wind and surface wave fields.)

The corresponding temperature field is given by

$$T(z) = T_1\left(\frac{z}{d} + \ell_2\right). \tag{2.48}$$

In (2.48),

$$T_1 \equiv \frac{T_a - T_{below}}{1 + \gamma_t^{-1} + \gamma_b^{-1}}, \tag{2.49}$$

and

$$\ell_2 \equiv \frac{T_a + \gamma_b^{-1}T_a + \gamma_t^{-1}T_{below}}{T_a - T_{below}}, \tag{2.50}$$

where

$$\gamma_t = \frac{dh_{aw}}{\kappa_T}, \quad \text{and} \quad \gamma_b = \frac{dh_{ww}}{\kappa_T}, \tag{2.51}$$

are Péclet numbers analogous to $\alpha_{t,b}$. The structureless temperature field may be statically stable or unstable. Density gradients are not necessary to the Langmuir circulation instability mechanism: the motions are not buoyancy driven. We shall think primarily of the situation in which the layer is stably stratified, but the case of unstable stratification is not excluded from the analysis we present.

2.2.3 c. Typical parameter magnitudes

We estimate the parameters $(\alpha_{t,b}, \gamma_{t,b})$ by parameterizing u_* and ν_T in terms of the wind speed, taking $u_*/U_a \sim 10^{-3}$, consistent with an air–sea momentum exchange coefficient $C_m = O(10^{-3})$, as is generally reported (e.g., see Busch [10]) for typical values). This implies

$$\alpha_t \sim 2 \times 10^{-3} R_*.$$

The question of the loss of momentum from the mixed layer to internal waves is too difficult for us to address here. In many cases, we expect that this momentum transfer will be small compared to the direct loss to entrainment (see the discussions of this point by Niiler & Kraus [68], and by Kantha [38]). In any event, for the present purposes, we take $C_{IW} = 0$ in estimating the parameter α_b.

According to the experiments of Kantha & Phillips [39] in a two–layer stratified water body driven by an applied surface stress, the light turbulent upper layer entrains nonturbulent heavy fluid with an entrainment velocity given by

$$w_e = u_* f(Ri).$$

Here the over-all Richardson number is

$$Ri = \frac{gd}{u_*^2} \frac{\Delta\rho}{\rho},$$

$\Delta\rho$ is the difference in density between the heavy and light fluid, and f is a function that at present must be experimentally determined. The data from the Kantha/Phillips experiment, as discussed by Phillips [71] suggests the rough approximation to this function

$$\frac{w_e}{u_*} \sim \frac{6}{Ri}. \tag{2.52}$$

If (2.52) is used to estimate the entrainment velocity in α_b,

$$\alpha_b \sim \frac{6}{Ri} R_*.$$

Relating the friction velocity to the wind speed shows that

$$Ri = \left(\frac{U_a}{u_*}\right)^2 \frac{gd}{U_a^2} \frac{\Delta\rho}{\rho} \sim 10^6 \frac{gd}{U_a^2} \frac{\Delta\rho}{\rho}.$$

For purposes of estimating, we will take $\Delta\rho/\rho \sim 10^{-3}$ as a plausible value for the fractional density "jump" across the pycnocline terminating the mixed layer, then

$$\alpha_b \sim 6 \times 10^{-3} \frac{U_a^2}{gd} \frac{u_* d}{\nu_T}.$$

From this, we arrive at the estimate $\alpha_t/\alpha_b \sim (1/3)gd/U_a^2$. For a wind speed of 25m/s and a mixed layer depth of 50m, the ratio is about 0.26.

Returning now to the estimation of α_t, we assume a parameterization of ν_T similar to that quoted in Leibovich & Radhakrishnan [56], $\nu_T \sim 2.5 \times 10^{-5} U_a^3/g$. Then

$$\alpha_t \sim 10^5 \times \left(\frac{u_*}{U_a}\right)^2 \frac{gd}{U_a^2}.$$

Again assuming $u_*/U_a = 10^{-3}$, a mixed layer depth of 50m and a 25m/s wind, we get $\alpha_t \approx 0.06$. Choosing the eddy viscosity to be proportional to U_a^3/g, as we have done here, makes α_b independent of the wind speed and mixed layer depth. With the specific parameterization introduced above, $\alpha_b \sim 0.24$.

By comparing with the data on the transfer of sensible heat at the air–sea interface given by Busch [10], we find our exchange coefficient to be

$$h_{aw} = \frac{[\rho c_p]_{air}}{[\rho c_p]_{water}} U_a C_\theta,$$

where the conventional bulk exchange coefficient for heat, C_θ, is approximately the same as C_m. Our dimensionless heat exchange coefficient at the surface is

$$\gamma_t \sim \frac{3C_\theta \times 10^{-4}}{(u_*/U_a)} \frac{u_* d}{\kappa_T}. \tag{2.53}$$

This shows that

$$\gamma_t \sim \frac{0.15\alpha_t}{\tau}, \quad \text{where } \tau \equiv \frac{\kappa_T}{\nu_T}.$$

The parameter τ is an inverse Prandtl number. The molecular value of τ is about 0.15, but a more likely value when based on turbulent diffusivities of heat and momentum would probably be around unity. In either event, if α_t is small, so is γ_t.

At the base of the mixed layer, it seems reasonable to set $h_{ww} = w_e$, then

$$\gamma_b = \frac{w_e d}{\kappa_T} = \frac{\alpha_b}{\tau}, \tag{2.54}$$

so γ_b is comparable to α_b.

Chapter 3

Estimates for Turbulent Exchange Coefficients

In the theory as described in Chapter 1, the effects of turbulence are treated by assuming that they may be represented by eddy diffusivities of momentum (ν_T), and heat (κ_T). Our primary concern here will be to estimate ν_T, since our main objective the determination of the velocity in the mixed layer, assuming the layer is itself essentially isothermal. In this case, κ_T will be ignored (or, should a rough estimate be needed, we can take $\kappa_T = \nu_T$).

Of the parameters needed to specify the Langmuir circulation theory, it is about the values of eddy viscosity that least is known. Any attempt to assign values to this parameter requires many assumptions, and a heavy dose of empiricism. There are deveral different avenues we may try.

3.1 Classical estimates

The same issues must be faced whenever an eddy viscosity assumption is invoked in geophysical fluid dynamics. We note that, in the treatment of large–scale oceanographic phenomena in which eddy diffusities are used, one must assume that the eddy diffivities are anisotropic, with much larger values for the "horizontal" diffusivity than the "vertical" diffusivity. This is mainly due to the much larger horizontal length scales in such problems. (See, for example, the review by Bowden [8]. If estimates of eddy viscosities are to be borrowed from this literature, it is the vertical eddy viscosity that is potentially comparable to the eddy viscosity that we need to invoke. In fact, since the large scale phenomena used to assess the vertical eddy viscosity

can reflect mixing accomplished by Langmuir circulations themselves, one can anticipate that the values arrived at will be too large.

3.1.1 Ekman layer fit

An eddy viscosity may be extimated by assuming that surface currents may be related to the simple Ekman layer, adusting the eddy viscosity to accomplish the fit between Ekman's theory and observed currents (see Pond and Pickard [75], and Bowden [9]). The fit indcates that $\nu_T \propto U^2$, where U is the wind speed as before. Such a relationship requires a dimensional constant of proportionality (Bowden [9] cites the constant 1.37 if ν_T is to be given in cm^2/sec, and U in m/sec), and so is fundamentally incomplete. n any event, if we denote this "Ekman–fitted" eddy viscosity by the subscript E, we have

$$\nu_E \sim 1.37U^2,$$

with the understanding that the formula holds only when ν_E and U are given in the special units cited.

3.1.2 Wave associated turbulence

Some empirical estimates for ν_T in the surface layer attempt to correlate it with surface wave characteristics. One of the earliest attempts in this direction is due to Bowden [7]. Another estimate (Ichiye [35]) is

$$\nu_T = C_T H_{1/3}^2 \sigma,$$

where C_T is a numerical constant, σ is the wave angular frequency at the spectral peak, and $H_{1/3}$ is the "significant" wave height, defined to be the mean of the one-third highest waves in the record.

A form like this allows one to express ν_T in terms of the wind speed (see § 2 of this report) as

$$\nu_{LC} = C_V U^3/g. \tag{3.1}$$

This form was also derived by Leibovich and Radharishnan [56] by matching the results of their Langmuir circulation calculations to three observational "rules of thumb": (i) the total surface mean drift current is about 3.5% of the wind speed, (ii), the maximum downwelling speeds in Langmuir circultations is about 0.85% of the wind speed (a "maximum" which seeems to now to be superceded by the results of Weller and Price (see Chapter 1); and (iii) adjusting the near–surface horizontally averaged

Langmuir circulation current speed to measured logarithmic profiles. The three evaluations of C_V done these ways were largely consistent, yielding the values (2.3×10^{-5}, 2.8×10^{-5}, 6×10^{-5}. The average of the first two values leads to an estimate

$$\nu_{LC} = 2.5 \times 10^{-5} U^3/g. \tag{3.2}$$

Values obtained from (3.2) lead to eddy viscosities that are consistent with estimates from other sources.

3.1.3 Estimates from shear flow turbulence

Breaking waves can inject turbulence very near the air–sea interface. The breaking waves are the short waves in the spectrum, with phase speeds typically exceeding $150u_*$ (Phillips [71], pg. 290), where u_* is the friction velocity in the water caused by the stress applied by the wind. This turbulence is injected in a water layer of depth comparable the wavelength of the breaking waves, and will decay in the absence of a turbulence–production mechanism, such as current shear or unstable density distributions.

If it is assumed that the turbulence is maintained by current shear in a mixed layer of depth d, then we can provide an estimate for ν_T on the following grounds. On dimensional grounds (cf. Tennekes and Lumley [84]), one expects the eddy viscosity to be proportional to the product of the rms velocity fluctuations, u', and a length scale, ℓ characteristic of the energy–containing eddies (having velocity scales of order u', a local scale more precisely defined this way is called the integral scale).

In wall–bounded turbulence, the length scale increases linearly away from the wall, at least through the inertial sublayer. Furthermore, the mean velocity gradient is

$$\frac{\partial \bar{U}}{\partial z} = \frac{u_*}{\kappa z},$$

where here κ represents von Kárman's constant, which has value 0.42. Let us write $\ell = \kappa|z|$, near the wall, and is the length scale characterizing the turbulence in this region. The production rate of turbulent kinetic energy density is the Reynolds stress times the mean rate of strain $\partial \bar{U}/\partial z$, which near the wall is precisely u_*^3/ℓ. Furthermore, production and dissipation rates are nearly in balance near the wall (and throughout turbulent flows near equilibrium conditions), so the dissipation rate

$$\varepsilon \approx u_*^3/\ell. \tag{3.3}$$

Evidence shows [2] that this variation of dissipation rate holds in the ocean mixed layer as well, except within a significant wave height of the mean free surface The base of the mixed layer also acts much like a solid surface, and the turbulent intensities become much smaller there. Imagining it to be a solid surface would lead to the requirement that the integral length scale must vanish at both $z = 0$ and at $z = -d$, and near each boundary to vary like κ times the distance from the boundary.

In wall turbulence, it is also known that the rms fluctuating velocity increases with distance from the wall, reaching a maximum comparable to the friction velocity. With this in mind, we expect the eddy viscosity to be

$$\nu_T \propto u_* \ell,$$

with a constant of proportionality that is of order one (with respect to the friction velocity and mixed layer depth). Standard k–ϵ second–order turbulence models fix the eddy viscosity to be

$$\nu_T = C_\mu \frac{k^2}{\varepsilon}, \tag{3.4}$$

where here k represents the turbulent kinetic energy density, which is very nearly $(3/2)u_*^2$, and the usual value assigned to the constant C_μ is 0.09. If (3.4) is used to find the eddy viscosity, we have

$$\nu_T = \frac{9}{4} C_\mu u_* \ell. \tag{3.5}$$

The maximum value of ℓ in the layer, assuming it varies linearly inward from each of the layer boundaries, is $\kappa d/2$, leading to an eddy viscosity in the layer center of

$$\nu_T = 0.043 u_* d.$$

which gives an eddy viscosity estimate based on mixed layer scalings,

$$\nu_{ML} \sim .02 u_* d.$$

In the table below, we compare the values of eddy viscosity that are found from the several estimates above. Values are given for several wind speeds, and in the case of ν_{ML}, for a few values of the mixed layer depth also.

U	ν_E	ν_{LC}	ν_{ML}				
m/s	cm^2/s	cm^2/s	cm^2/s				
			d (meters)				
			10	20	30	40	50
5	34	3	21	42	64	85	106
10	137	25	42	128	191	170	212
15	308	86	64	60	90	255	318
20	548	204	85	170	255	340	425

Table 3.1: "Classical" eddy viscosity estimates.

3.2 Estimates from numerical experiments

Recently, three sets (Skyllingstad and Denbo [78]; McWilliams, Sullivan, and Moeng [64]; and Leibovich and Yang [57]) of numerical experiments have been carried out using large eddy simulation (LES) of turbulent Langmuir circulation. In each case, the vortex force model was used, but the experiments used differing numerical methods and differing assumptions concerning inclusion of the Coriolis acceleration, buoyancy, sub-grid scale (SGS) turbulence models, and lower boundary conditions (the first two papers are very similar in these respects, while differing in initial conditions, while the third differs in all respects).

Bulk eddy viscosity estimates can be made from these experiments, and despite the differences between them, the eddy viscosity estimates (and other measures of the flow states) are quite similar. For example, [78] displays a vertical profile of bulk eddy viscosity based on a model introduced by Deardorff [18],

$$\nu_T = 0.1\ell\sqrt{\bar{E}}, \tag{3.6}$$

where $\bar{E}$ is a turbulent kinetic energy and ℓ is a length scale. Deardorff had proposed this as a SGS eddy viscosity for LES, in which case $\bar{E}$ is the SGS turbulent kinetic energy and is computed by an auxillary evolution equation, and ℓ is the computational grid spacing. Skyllingstad and Denbo [78] use (3.6) to estimate a *bulk* eddy viscosity, interpreting ℓ to be an integral scale for the turbulence and $\bar{E}$ to be the resolved turbulent kinetic energy. The eddy viscosity calculated in this was is largest very near the surface, and then varies about a (dimensional) mean of about .03 m^2/s, which is more

usefully expressed as $\nu_T \approx 0.06\, u * d$.

A bulk eddy viscosity is computed in [64] from the basic definition as the ratio of Reynolds stress to vertical gradient of velocity. This was done with and without the vortex force. With vortex force acting, the peak eddy viscosity is about three times the value without vortex force, showing the large contribution made to the Reynolds stresses by the coherent Langmuir circulation. Presumably, in a constant eddy viscosity model aiming to compute Langmuir circulation, the effects of the coherent motion on the Reynolds stresses should be removed, which implies that the more relevant value to consider is the one computed without vortex force. This again to a peak value of $\nu_T \approx 0.06\, u_* d$.

We can estimate an eddy viscosity based on the numerical experiments [57] by forming $\nu_T \sim \ell_v w'$, where ℓ_v is a integral scale based on the vertical fluctuating velocity component and w' is the rms fluctuating velocity component. The maximum of w' and ℓ_v are approximately $2u_*$ and $0.03d$, respectively, leading to a peak value of this product of $\nu_T \sim 0.06\, u_* d$. A direct computation of the volume averaged eddy viscosity from the SGS model, in this case the Smagorinsky model, led to $\nu_T = 0.055\, u_* d$.

Thus, the LES computations lead to remarkably consistent estimates for the eddy viscosity, or alternatively, for the Reynolds number R_* based on u_*, d, and ν_T, with values of 16 to 18.2. In all of these experiments, these approximate values hold over most of the mixed layer. We choose here to set

$$R_* = 18.2. \tag{3.7}$$

It is important to point out that in none of the estimation methods reviewed above is the effect of wave breaking accounted for.

Chapter 4

Collection of Surface Oil into Windrows

4.1 Introduction

The fate of oil introduced into the sea raises questions of exquisite complexity. The answers to these questions will never be known in detail, as they depend on physical, chemical, and biological processes that are individually complex and which operate interactively. The outcomes depend on the chemical composition of the oil; on the evolution of physical properties as the chemical composition changes by interaction with the environment; on the rate of biological interactions, which depends strongly on the physical environment and especially the temperature; and on the unpredictable nature of the air-sea interfacial region in which the oil is immersed.

Practical considerations of these questions have customarily identified several stages and processes, not all disjoint. These are *spread*[1], which refers to the relative motion of an oil layer to that of the underlying water; *weathering*, which refers to changes in physical properties of the oil phase arising from several processes;*evaporation* of lighter fractions to the atmosphere and the corresponding *dissolution* of soluble components into the water column; the formation of *water-in-oil* emulsions (or "chocolate mousse") and *oil-in-water* emulsions; *aerosol production*, in which minute oil droplets are formed by breaking waves and directly transferred to the atmosphere; *dispersion*,

[1]Spreading itself has been divided into a crude but useful chronological sequence of events, each stage of which is controlled by the balance of a pair of forces driving and resisting the reduction in film thickness.

in which turbulence in the water causes vertical mixing into the water column and random horizontal migration of discrete patches of floating oil; and *biodegradation*, in which oil is utilized by living things and transformed by biological processes.

To study the disposition of oil in the sea resulting from physical processes, we suppose that the history of the physical properties of the oil, which will usually vary with time, is specified as a function of time and perhaps of oil temperature and location. In particular, the problem of how the properties of the oil encountered come to be is put aside.

In this report, the process of collection of floating oil into the windrows created by surface convergences is considered in a preliminary way. We begin in §4.2 by presenting equations appropriate for a thin layer of floating oil. These require information about the underlying water motion. Physical estimates of the water velocity are summarized in §4.3. This leads, in §4.4 to estimates of the time scales required to collect oil into windrows, and to estimates of the effect this has on surface transport.

4.2 Thin films on water

The model to be used to estimate the collection of oil into windrows treats the oil as a continuous thin layer, and is laid out below [2]. In reality, such a layer will be torn, and oil removed from it, when waves break, or when the relative speed of the oil and underlying water exceeds a critical value determining the stability of the oil-water interface (see, for example, [47]). These processes have little effect on the collection process, and will be ignored for the present purposes.[3]

The model is cast in terms of the thickness, $h(x, y, t)$, of the oil layer, and the depth-averaged velocity of oil in the layer, $(u(x, y, t), v(x, y, t)$. Here u and v are the velocity components in the x and y directions. A precise meaning for x and y should account for the fact that the mean (or central, *i.e.*, half-depth) surface of the oil layer is deformed by the deflections of the underlying oil water boundary, and this can be accomplished to some extent by interpreting x and y as local orthogonal coordinates tangent to this central surface of the oil layer, and h is the thickness in the direction

[2] This is the model used in [49].

[3] In point of fact, model described does not properly account for the acceleration of the layer due to the wavy water "substrate". This poses interesting questions that have yet to be considered in the literature, but may well repay any attention given to it.

(z) normal to the central surface. This, however, seldom causes practical complications, since the orientations of these two coordinates usually differ only slightly from the horizontal coordinate directions.

Suppose the oil-water interface is located at $z = z_1(x, y, t)$ and the oil-air interface is at $z = z_2 = z_1 + h(x, y, t)$. Let an overbar signify a depth average over the oil layer, or for any function f,

$$\overline{f} \equiv \frac{1}{h} \int_{z_1(x,y,t)}^{z_2(x,y,t)} f(x, y, z, t) dz. \tag{4.1}$$

If w is the z-component of velocity in the oil, the continuity equation, in Cartesian coordinates (x, y, z), when averaged over the depth of the layer and rearranged gives

$$\frac{\partial h}{\partial t} + \left[\frac{\partial h\overline{u}}{\partial x} + \frac{\partial h\overline{v}}{\partial y} \right] = 0, \tag{4.2}$$

exactly.

If we do the same to the momentum equation, then again without approximation (assuming z is the vertical direction),

$$\frac{\partial h\overline{\mathbf{u}}}{\partial t} + \nabla \cdot h\overline{\mathbf{u}\mathbf{u}} = -h\overline{\nabla \left(\frac{p}{\rho_o} + gz \right)} + \frac{h}{\rho_o} \overline{\nabla \cdot \mathbf{T}}, \tag{4.3}$$

where $\mathbf{u}$ is the velocity vector in the oil, $\mathbf{T}$ is the stress tensor with the pressure removed, and all quantities with overbars are functions only of (x, y, t). The subscript "o" indicates properties evaluated for the oil, "w" and "a" will have the corresponding meanings for water and air.

Now the thinness of the layer is invoked. This implies that

$$\overline{\mathbf{u}\mathbf{u}} = \overline{\mathbf{u}}\,\overline{\mathbf{u}} \left(1 + O(h/L)\right),$$

where L is a typical length over which the layer has appreciable horizontal variability, and

$$\overline{\nabla \cdot \mathbf{T}} = \boldsymbol{e}_z \cdot \left[\mathbf{T}(x, y, z_2, t) - \mathbf{T}(x, y, z_1, t) \right] \left(1 + O(h/L)\right).$$

Since continuity implies that $w = O(hu)$ and similarly is of $O(hv)$, the vertical component of the Navier-Stokes equation implies that the oil is in hydrostatic equilibrium in that direction, so

$$\frac{p_o}{\rho_o} + gz = H(x, y, t).$$

Equating pressures at the air-oil interface and at the oil-water interface then implies that

$$H(x,y,t) = \chi g h, \text{ where } \chi = \frac{\rho_w - \rho_o}{\rho_w}.$$

The horizontal components of the depth-averaged Navier-Stokes equations then take the form

$$\frac{\partial h\overline{u}}{\partial t} + \frac{\partial h\overline{u}\,\overline{u}}{\partial x} + \frac{\partial h\overline{u}\,\overline{v}}{\partial y} = \chi g h \frac{\partial h}{\partial x} + (\rho_o)^{-1} t_x \tag{4.4}$$

$$\frac{\partial h\overline{v}}{\partial t} + \frac{\partial h\overline{u}\,\overline{v}}{\partial x} + \frac{\partial h\overline{v}\,\overline{v}}{\partial y} = \chi g h \frac{\partial h}{\partial y} + (\rho_o)^{-1} t_y, \tag{4.5}$$

where (t_x, t_y) are the two horizontal components of $\mathbf{t}$, which is the sum of the stress vectors imposed on the oil at the air-oil and oil-water interfaces. Using (4.2), we may rewrite this equation, if desired, as

$$\frac{\partial \overline{\mathbf{u}}}{\partial t} + \overline{\mathbf{u}} \cdot \nabla \overline{\mathbf{u}} = \chi g \nabla h + (\rho_o h)^{-1} \mathbf{t}. \tag{4.6}$$

The motion of the oil layer is then prescribed by (4.2) and (4.6), and the specification of the stress vector $\mathbf{t}$ imposed by the fluids outside the layer. This can be done by specifying "friction coefficients", C_a and c_w for the air-oil and oil-water interfaces, from which the stress vector is given by

$$\mathbf{t} = C_a \rho_a |\mathbf{u}_a - \overline{\mathbf{u}}| \, (\mathbf{u}_a - \overline{\mathbf{u}}) + C_w \rho_w |\mathbf{u_s} + \mathbf{u}_w - \overline{\mathbf{u}}| \, (\mathbf{u_s} + \mathbf{u}_w - \overline{\mathbf{u}}). \tag{4.7}$$

Here $\mathbf{u}_a$ and $\mathbf{u}_w$ refer to the velocity vectors of the air and water at the corresponding interfaces with the oil. The value of C_w depends on oil type (see [61], [15]), but typically ranges from 10^{-3} to 4 or 5×10^{-3}. Of course, the values of C_a and C_w are nonzero only if there oil on the surface - in fact, the oil must be thick enough to be treatable as a macroscopic layer for it to be treated as we have here. On portions of the surface swept clean of oil, these coefficients should be set to zero in our macroscopic model.

The filtered effect of the stress on the oil-water surface, undulating with the waves, is accounted for in (4.7) in an *ad hoc* fashion by incorporating the Stokes drift into the relative velocities that appear.

Now, C_a relates to an average *shear* stress exerted by the air on the oil. If its value was to be fixed by the momentum transport from the atmosphere to the ocean, then it would be estimated by $C_m \approx 10^{-3}$ (as § 2.2 in Chapter 2 - also see [10], or Large and Pond [45]). The total momentum transport is set both by pressure forces on waves and by skin friction, and quite plausibly

mostly by the former. Consequently, we would expect $C_a \ll C_m$. Because of this, and because here our analysis applies to an average over several wave periods that is difficult to assess but which is here parameterized by the dependence on $\mathbf{u_s}$, we will set $C_a = 0$.

4.3 Estimates of surface water velocity

The purpose of this section is to estimate, based on earlier reports in this series, a parametric dependence of the surface water velocity, especially the sweeping component, with wind speed.

According Chapter 1 [4], the maximum speed in Langmuir circulations is not expected to exceed

$$U_{LC} = \sqrt{\mathcal{U}_s \frac{u_*^2}{k_p \nu_T}}, \tag{4.8}$$

where $\mathcal{U}_s$ is the surface value of the Stokes drift speed, k_p is a characteristic wavenumber of the surface waves, say the wavenumber of the spectral peak, u_* is the friction velocity of the applied wind stress, and ν_T is the eddy viscosity. This can be expressed in terms of the Reynolds number, $R_* = u_* d/\nu_T$, where d is the mixed layer depth,

$$U_{LC} = \sqrt{\mathcal{U}_s u_* \frac{\lambda}{2\pi d} R_*}. \tag{4.9}$$

From Chapter 3, $R_* \approx 18.2$ is a plausible value, so

$$U_{LC} \sim \sqrt{\frac{18.2}{k_p d} \mathcal{U}_s u_*}. \tag{4.10}$$

Now introduce a correlation of the surface wave field with the wind, which will allow $\mathcal{U}_s$ and k_p to be replaced by the wind speed (or wind stress). This clearly cannot be universal, since the wave field depends not only upon the wind, but also on the wind origin and history. Here we take two examples, which we think should provide an acceptable idea of the appropriate scales. The first example is the Pierson-Moskowitz wave spectrum (or "PM"), which has an angular frequency at the spectral peak of

$$\omega_{PM} = \frac{0.88g}{U}, \tag{4.11}$$

[4] See equation (85).

where U is the wind speed at anemometer height. The wavenumber corresponding to angular frequency ω in deep water waves is

$$k = \omega^2/g$$

so for the PM spectrum,

$$k_p = \frac{0.774g}{U^2}.$$

The Stokes drift at the surface in the Pierson-Moskowitz spectrum is

$$\mathcal{U}_s = 0.013U, \tag{4.12}$$

which gives an upper bound for the Langmuir circulation (vertical) velocity of

$$U_{LCPM} = .55U\sqrt{\frac{Uu_*}{gd}}. \tag{4.13}$$

The second example is the JONSWAP-based parametric model (J) described in Chapter 2. When wind duration (t) limited, this model gives

$$\omega_J = 108.7\frac{g}{U}\left(\frac{U}{gt}\right)^{3/7},$$

so that

$$k_p = 1.18 \times 10^4 \frac{g}{U^2}\left(\frac{U}{gt}\right)^{6/7}.$$

The surface value of the Stokes drift for the J-model is

$$\mathcal{U}_s = 0.0026\left(\frac{gt}{U}\right)^{1/7}U, \tag{4.14}$$

so that our Langmuir circulation bound is

$$U_{LCJ} = .002U\sqrt{\frac{u_*t}{d}}. \tag{4.15}$$

In both of these examples, it is sufficiently accurate to take $u_* = .001U$. Therefore, if $U = 10\text{m/s}$ and $d = 40\text{m}$, then the Pierson-Moskowitz estimate gives

$$U_{LCPM} = 0.086\text{m/s}$$

and the J-model gives

$$U_{LCJ} = 0.00032\text{m/s}\sqrt{t/\text{s}}.$$

After one hour, $U_{LCJ} = 0.019\text{m/s}$, and builds up to the Pierson-Moscowitz value when the wind duration in about 21 hours.

4.4 Oil in windrows and its surface transport

First, an estimate is given for the process of collection of oil into windrows. Second, the implications for downwind surface transport will be assessed.

Estimates for the maximum values of each component of the Langmuir circulation Eulerian current are given by the speed estimates of the previous section.

4.4.1 Sweeping of oil into windrows

Suppose oil is initially uniformly distributed on the surface, in the form of a layer of thickness h_0, and is then subject to lateral sweeping by the y component of a Langmuir circulation system. Let the component of the water velocity in the y-direction be v_{LC}, and suppose it is time-independent, and essentially independent of the coordinate in the wind or x-direction (so the circulations are in the form of long rolls parallel to the wind. Let the distance between surface convergence lines be $2L$, so a single cell of the convective system will have a width L, corresponding to the distance between upwelling (below surface divergence lines) and downwelling (below surface convergence lines). To be definite, suppose a surface divergence line is located at $y = 0$ then the adjacent surface convergence lines will be at $y = \pm L$.

Adopting the model in § 4.2, we can suppose the oil velocity is also independent of x. In this case, the oil moves according to the equations (4.4) and (4.2)

$$\frac{\partial h\overline{u}}{\partial t} + \frac{\partial h\overline{u}\,\overline{v}}{\partial y} = +(\rho_o)^{-1} t_x \tag{4.16}$$

$$\frac{\partial h\overline{v}}{\partial t} + \frac{\partial h\overline{v}\,\overline{v}}{\partial y} = \chi g h \frac{\partial h}{\partial y} + (\rho_o)^{-1} t_y \tag{4.17}$$

$$\frac{\partial h}{\partial t} + \frac{\partial h\overline{v}}{\partial y} = 0. \tag{4.18}$$

This problem has a time–independent solution to which the initial value problem will approach for sufficiently large time. In this case "large time" corresponds to times large compared to the time scale characteristic of the lateral sweeping, which is clearly

$$t_{sweep} = L/U_{LC}. \tag{4.19}$$

This in turn can be estimated in terms of the wind speed U by adopting the Pierson-Moscowitz form (4.13) for U_{LC}.

$$t_{sweep} = 57.5\frac{L}{U}\frac{\sqrt{gd}}{U}. \tag{4.20}$$

Choosing a typical ratio $L/d = 3/2$, $d = 40$m and $U = 10$m/s leads to the estimate $t_{sweep} \sim 11$ minutes.

Now examine the asymptotic steady state. From (4.18), this asymptotic solution requires that $h\overline{v}$ be a constant. At some point in the windrow $\overline{v} = 0$, which implies that $\overline{v} = 0$ for all values of y. This in turn implies, from (4.16) that the net shear stress on the oil in the x-direction vanishes,

$$t_x = 0, \tag{4.21}$$

and that the net shear stress in the y-direction is balanced by the hydrostatic pressure variation,

$$\chi g h\frac{\partial h}{\partial y} + (\rho_o)^{-1}t_y = 0. \tag{4.22}$$

Remembering that the friction coefficient C_w is zero for the oil-free portions of the surface, the oil thickness variation in any given Langmuir cell $(0 < y < L)$ can be found from (4.22) to be

$$h(y) = \sqrt{\frac{2}{g\chi}\int_{y_0}^{y}\frac{t_y}{\rho_o}dy}, \tag{4.23}$$

where the part of the surface $0 < y_0$ is free of oil layer. The total volume of oil is conserved. Since the unswept thickness is h_0, the total oil volume per unit length in the wind direction is $h_0 L$. Consequently,

$$\int_{y_0}^{L} h(y)dy = h_0 L, \text{ or } \frac{1}{L}\int_{y_0}^{L}\frac{h(y)}{h_0}dy = 1. \tag{4.24}$$

The stress components are given by (4.7). Consequently, the stress vector component t_y is given approximately by

$$\frac{t_y}{\rho_o} \approx C_w\frac{\rho_w}{\rho_o}\sqrt{(\mathcal{U}_s + u_w - \overline{u})^2 + (v_w - \overline{v})^2}\,(v_w - \overline{v}),$$

and

$$\frac{t_x}{\rho_o} \approx C_w\frac{\rho_w}{\rho_o}\sqrt{(\mathcal{U}_s + u_w - \overline{u})^2 + (v_w - \overline{v})^2}\,(\mathcal{U}_s + u_w - \overline{u}).$$

The condition $t_x = 0$ then requires

$$\overline{u} = \mathcal{U}_s + u_w, \tag{4.25}$$

which simply says that the average speed of the surface oil in the downwind direction is given by the average Lagrangian velocity of the underlying water.

Since $\overline{v} = 0$,

$$\frac{t_y}{\rho_o} = C_w \frac{\rho_w}{\rho_o} |v_w| \, v_w. \tag{4.26}$$

This now permits $h(y)$ to be estimated from (4.23), provided $v_w(y)$ is provided.

For two dimensional, time independent Langmuir circulation, the sweeping speed can be written as

$$v_w(y) = U_{LC} \mathcal{V}(\eta), \text{ where } \eta \equiv \frac{y}{L}, \tag{4.27}$$

and where $\mathcal{V}(\eta)$ is a dimensionless function. A theoretical value for v_w (or $\mathcal{V}(\eta)$ requires the solution of the Langmuir circulation problem. Such theoretical estimates will be incorporated in our final model. As a simple illustration, however, suppose that

$$\mathcal{V}(\eta) = \beta \left(\frac{y}{L}\right)^3 (1 - \frac{y}{L}), \tag{4.28}$$

where β is a constant factor.

This form for $v_w(y)$ has the property that the maximum sweeping speed is attained one-quarter cell width from the convergence line - a behavior not dissimilar from the calculations reported by Leibovich and Paolucci [54]. Furthermore if $\beta = 256/27$, then the maximum sweeping speed is U_{LC}. We expect the maximum value of v_w to be near to that for the maximum downwelling speed (again, from [54]). While this is not expected to be as large as U_{LCPM}, this value should be of the right order of magnitude, so for the purpose of illustration, take $\beta = 256/27$. Figure 4.4.1 shows the hypothesized form of $\mathcal{V}(\eta)$.

For any $\mathcal{V}(\eta)$, in a given Langmuir cell, $h(\eta) = 0$ for η smaller than some value η_0, which remains to be determined, and

$$\frac{h(\eta)}{h_0} = \sqrt{\Gamma \int_{\eta_0}^{\eta} \mathcal{V}^2(\eta) d\eta}, \tag{4.29}$$

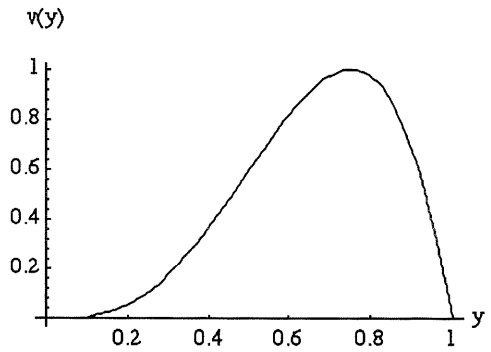

Figure 4.1: Sample water sweeping speed.

for $\eta > \eta_0$. Here

$$\Gamma = C_w \frac{\rho_w L^2}{\rho_o h_0^2} \frac{U_{LC}^2}{\chi g L} \tag{4.30}$$

is the square of a weighted densimetric Froude number based on the Langmuir circulation speed scale and cell width. If U_{LC} is related to the wind speed U by taking the Pierson-Moskowitz form from §4.3,$C_w = 0.004$, $\rho_o/\rho_w = 0.98$; and by taking $u_* = 0.001U$, and $L/d = \pi/2$ (consistent with the results of [83]), then

$$\Gamma = \left(\frac{10^{-2} U^2}{g h_0} \right)^2, \tag{4.31}$$

and typically $\Gamma \gg 1$ (for example,if taking even the substantial value of $h_0 = 1\text{mm}$, and $U = 10\text{m/s}$, then $\Gamma \approx 10^4$). For the example,

$$\frac{h(\eta)}{h_0} \approx \sqrt{\Gamma \left(\frac{\eta^7 - \eta_0^7}{7} - \frac{\eta^8 - \eta_0^8}{4} + \frac{\eta^9 - \eta_0^9}{9} \right)}.$$

The value of η_0 may be determined by conservation of volume. From (4.24),

$$\int_{\eta_0}^{1} \sqrt{\Gamma \left(\frac{\eta^7 - \eta_0^7}{7} - \frac{\eta^8 - \eta_0^8}{4} + \frac{\eta^9 - \eta_0^9}{9} \right)} d\eta = 1. \tag{4.32}$$

When Γ is large, eta_0 is close to the surface convergence line, $\eta = 1$. This suggests that eta_0 may be found by perturbation methods. The lowest

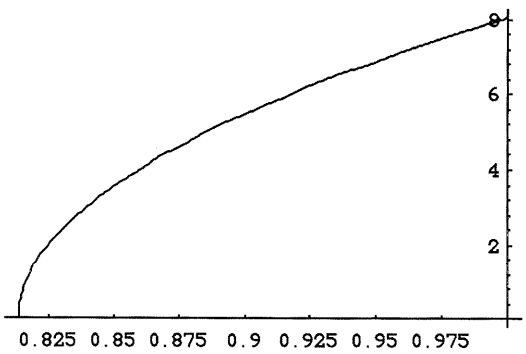

Figure 4.2: Film thickness variation for the example in text.

approximation in an expansion in inverse powers of Γ produces

$$\eta_0 = 1 - \left(\frac{3}{2}\right)^{2/5} \Gamma^{-1/5}. \tag{4.33}$$

The variation of film is then

$$\frac{h(\eta)}{h_0} \approx \begin{cases} 0, & \text{for } \eta < \eta_0 \\ \left(\frac{3}{2}\right)^{2/5} \Gamma^{3/10} \sqrt{\eta - \eta_0}, & \text{for } \eta > \eta_0 \end{cases} \tag{4.34}$$

where η_0 is given by (4.33). This approximation can be systematically improved. For the example with $U = 10\text{m/s}$, $h_0 = 1\text{mm}$,

$$\frac{h(\eta)}{h_0} \approx \begin{cases} 0, & \text{for } \eta < 0.81 \\ 8.05\sqrt{\eta - 0.81}, & \text{for } \eta > 0.81 \end{cases} \tag{4.35}$$

The oil thickness in the windrow for this example is shown in Figure 4.2. Notice that the maximum film thickness, occurring at the surface convergence, is about 8 times the uniform oil thickness h_0, and that the oil is concentrated in windrows occupying only 20% of the surface area.

4.4.2 Collection effects on downwind transport

Because oil is collected into windrows, its surface transport is not the same as the horizontally averaged surface motion.

From (4.25), surface oil moves in the downwind direction with the downwind mean speed of the water particles, which is the sum of the Stokes drift

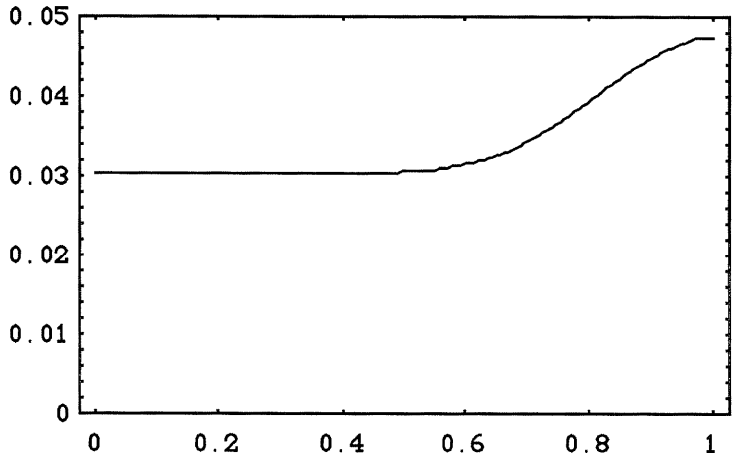

Figure 4.3: Mean Lagrangian downwind current at surface.

and the Eulerian-mean velocity component, u_w. As with v_w, u_w is found by solving for the Langmuir circulation current field. To illustrate, however, we can construct an artificial form for u_w. Since the current variations scale with U_{LC} and u_w peaks at surface convergence lines, in the Langmuir cell discussed in the previous subsection, it is reasonable to take

$$u_w(y/L) = U_{LC}\mathcal{U}(\eta), \quad \eta = y/L,$$

with

$$\mathcal{U}(\eta) = \mathcal{U}_0 + \mathcal{U}_1 \exp[-16(1-\eta)^2],$$

with $\mathcal{U}_0$ and $\mathcal{U}_1$ constants. The factor in the exponent is chosen so that the surface jet in the windrows e-folds where v_w is maximum. The ratio of $\mathcal{U}_0$ to $\mathcal{U}_1$ is not known and presumably depends on the details of the Langmuir circulation field. Nevertheless, they are order one numbers, and here we take them to have the common value 2.

Assuming the Pierson-Moskowitz spectrum and (as before) $u_* = 0.001U$, this choice yields

$$\frac{u_w(\eta)}{U} = 0.013 + 0.034\frac{U}{\sqrt{gd}}\left(1 + \exp[-16(1-\eta)^2]\right),$$

which is shown in the graph of figure 3 for the case $U = 10\text{m/s}$, $d = 40\text{m}$. For the example in Figure 4.4.2, the horizontally averaged surface current

speed is $0.034U$. The rate of downwind transport of oil is

$$\int_{y_0}^{L} u_w(y)h(y)dy, \tag{4.36}$$

and we can now compare this when the oil has a uniform thickness (no surface sweeping), and when the oil is collected into windrows as in the previous section.

In the absence of windrow collection, the downwind rate of volume transport for the example discussed is

$$0.034h_0LU$$

while in the case of oil collected in windrows, the downwind rate of volume transport is - upon numerically evaluating the integral in (4.36) -

$$0.045h_0LU,$$

an increase of 32%. This increase is the same as the downwind speed increase of the oil for trajectory analysis.

While the particular example is artificial, the same kind of analysis can be done with currents generated by the Langmuir circulation model. The results are expected to be qualitatively similar to the artificial example. Whether the results will turn out to be quantitatively similar remains to be seen, but the prospect seems plausible.

Chapter 5

Oil Suspended in the Water Column

Vertical mixing of oil into the water column by small scale turbulent fluctuations can be treated by standard methods, and results in a smearing of oil that is horizontally homogeneous. When coherent turbulent features with large spatial scales are present, such as Langmuir circulation, then the distributions of oil both in the horizonal and in the vertical may be substantially altered. In particular, oil can be found at much greater depths, can be held in suspension for relatively long times, and can be concentrated in horizontally compact zones. Such subsurface distributions are discussed in this Chapter, together with ways to estimate the oil particle sizes to be expected from the breakup of large floating oil masses.

5.1 Introduction

When coherent masses of floating oil are fragmented by oceanic turbulence, the distribution of oil in the water column follows the same history as any other buoyant particle of similar density, size and shape. The physically significant aspects are the particle buoyancy and fluid mechanical drag. Because oil properties change with due to weathering, these physically relevant features will change with time for oil particles, but this change is relatively slow after oil water contact, and especially after the first few minutes of oil fragmentation.

Fragmentation and the initial dispersion of oil depend heavily on small scale turbulence. However, the dispersion produced by the small scale tur-

bulence is limited to a relatively shallow layer close to the air/sea interface. Persistent *large* scale vertical motions, on the other hand, notably thermal convection and Langmuir circulations, may lead to a permanent suspension, and spatial concentration, of buoyant material in a subsurface trapping zone. These subsurface effects and consequent great penetration depth of buoyant particles was first recognized by Stommel [82], and it is likely that the phenomenon he decribed is ubiquitous. We call these trapping zones, regardless of the physical mechanism that engenders the convection, "Stommel retention zones", and abbreviate this by SRZ in what follows.

Evidence exists of the role of convective activity leading to anomalously large submergence of oil. The blowout of the Ixtoc I oil well in the Gulf of Mexico, beginning in June, 1979 and continuing for more than four months (the largest oil spill in history), allowed prolonged observation of an oil spill well away from surf zones and hundreds of miles away from the spill source. Visual observations of subsurface oil were recorded by divers. Although few in number, these observations were remarkable (Williams [91]; Robinson [76]; Galt, [25]; Hooper [32]). Apparently oil, in the form of flakes (thought to be the fragmented semi-solid skin of oil "pancakes", was mixed to depths of at least 40 feet. The explanation for the existence of buoyant particles in substantial numbers, originating at the surface and mixed to such depths, defies ordinary turbulent transport models [46]. It seems almost certain that the explanation lies in the presence of a mixing mechanism of larger scale. In point of fact, windrows of oil associated with Langmuir circulations were a notable feature in the Ixtoc-I spill, and are carefully described by Atwood et al.[5], and had been described in accounts of earlier oil spills as well (see the 1969 Batelle review [36] of the Santa Barbara blowout, and Galt's [24] discussion of the AMOCO CADIZ and HAWAIIAN PATRIOT tanker spills). The joint features of banded surface structure and oil at depth clearly are likely to be related, and that connection has been explored by Leibovich and Lumley [53].

The ability of large–scale convection to maintain suspension zones depends in part on the spatial scale, intensity, and most likely the coherence, of the convective activity, as noted by Stommel [82]. A more complete treatment [53] shows that the effectiveness of suspension also depends on the small scale turbulence. This relevant aspects of the the features found by [53] are reviewed here.

5.2 Oil breakup

Continuous floating sheets of oil can be broken into smaller pieces by forces exerted by the underlying or surrounding water. The dispersion of oil into the water column depends on the degree to which the oil is fragmented into small volumes, and the dispersion, for a given water dynamical state, is maximal when the oil particles have reached the smallest size that can be expected [1].

Consequently, we need an estimate of the distribution of oil particle sizes in a turbulent water medium. Kolmogorov has provided a start on this question, which is explained by Levich [59], together with additional considerations. The Kolmogorov theory is reviewed and extended in Chapter 6. At this point, we simply note Kolmogorov's result

$$a_{max} = b_f \left(\frac{\sigma}{\rho}\right)^{3/5} (\epsilon)^{-2/5}, \tag{5.1}$$

where $b_f = \left(16/k_f^3\right)^{1/5}$, where b_f is a constant and ϵ is the dissipation rate of turbulent kinetic energy, for the maximum stable drop size. Equation (5.1) depends only on the interfacial tension of the oil in seawater, and the turbulent kinetic energy dissipation rate. The mechanical properties of both refined and crude oils depend on temperature and degree of weathering, as might be expected. They also depend critically on the chemical composition of the oil: for crude oils, this varies over time for oil from the same well, and generally from well to well at any given time for oils in the same region and bearing the same name, as described in the MMS/EETD Catalog of Crude Oil and Oil Products Properties [1]. For example, the density of Prudhoe Bay Crude at $15°C$ was 0.8936 gm/cc in 1975 and 0.905 gm/cc in 1982, while its interfacial tension against seawater at this temperature was 9.7 dynes/cm in 1985 and 27.4 dynes/cm in 1989. While one can imagine several reasons for variations like this, the available information on any particular "type" of oil clearly can not be presumed to be known with precision. In the temperature range $0 - 15°C$ which is of interest for oil in the ocean, a typical range of σ is 7-25 dynes/cm, depending on oil type and degree of weathering. This range of variation, while substantial, leads only to a factor of two variation in the drop radius predicted by (5.1). On the other

[1] It is assumed throughout that the oil volume is negligible compared to that of the water, and that the motion of the water is unaffected by the presence of the oil. This assumption does not always reflect the facts.

hand, the dissipation rate in (5.1) is both difficult to estimate and can lead to substantial variation in a_{max}. This point will be addressed again in Chapter 6.

5.3 Subsurface Trapping of Oil

We first describe the idealized problem introduced by Stommel, and then explain the refinements shown in [53] to be needed to maintain buoyant material in subsurface suspensionl.

5.3.1 Stommel's model problem

Stommel [82] actually addressed the distribution of heavy particles suspended by upwelling motions in Langmuir circulation cells, but our considerations can apply (with caveats which will be explained later in this section) to this mirror image of the situation that we have so far presented. Stommel approached the issue by supposing the existence of a simple, artificial, velocity field simulating steady, two dimensional convection, and we explain his idea in the context of light particles.

Let a two-dimensional velocity field be represented by a streamfunction, $\psi(y, z, t)$, where z measures distances vertically (upwards) from the mean free surface. Then (y, z) velocity components (v, w) in the water are given by

$$v = \frac{\partial \psi}{\partial z}, \; w = -\frac{\partial \psi}{\partial y}. \tag{5.2}$$

In Chapter 7, the streamfunction arising from Langmuir is computed for a number of cases for a monochromatic surface wave spectrum. In that chapter, the problem is made dimensionless by taking lengths to be scaled by the depth, d of the water layer, velocities in the (y, z) plane perpendicular to the wind direction are scaled by ν_T/d (which may be more conveniently written as u_*/R_*, where u_* is the friction velocity and R_* is the Reynolds number based on u_*, ν_T, and d). As a consequence, the scale for the streamfunction is ν_T. In the discussion of this chapter, we assume the problem has been made dimensionless in this way.

The dimensionless problem for ψ then depends on the shape of the Stokes drift profile, and on the ratio of the magnitude of the maximum Stokes drift speed to the friction velocity – the latter may also be represented by a "Rayleigh number", R, and this is how it is accounted for in Chapter 7. In the case of considered in Chapter 7 with a dimensionless gravity wavenumber

κ, the Stokes drift is an exponentially decaying function of depth, and the dimensionless streamfunction is then a function of κ and R. Furthermore, these two parameters combine to make the dimensionless streamfunction proportional to

$$\sqrt{\frac{R - R_c(\kappa)}{R_c(\kappa)}},$$

where $R_c(\kappa)$ is a function given by (7.9).

Suppose buoyant particles are placed in the water, having a buoyant velocity in still water of V_T, and suppose, with Stommel, that in the presence of water motion, the velocity of a particle relative to the surrounding water is always in the vertical with speed V_T. The dimensionless representation for the trajectory of a particle is then given by $(Y(t), Z(t))$, where

$$\frac{dY}{dt} = v = \frac{\partial \psi}{\partial z}; \frac{dZ}{dt} = w + R_T = -\frac{\partial(\psi - R_T y)}{\partial y}, \tag{5.3}$$

where

$$R_T = \frac{V_T d}{\nu_T}$$

is the dimensionless form of the terminal velocity of rise in the system of units adopted. If the water motion is steady, then the trajectories are given by the level curves of the function

$$\Psi(y, z) = \psi(y, z) - R_T y. \tag{5.4}$$

If the maximum downwelling water speed is greater than V_T, then particles placed in certain regions near downwelling planes will remained trapped (forever) in a closed zone (the SRZ). Furthermore, the SRZ does not connect to the surface. This is easily understood by realizing that the downwards speed on a downwelling plane increases from zero at the surface to a maximum value $|w_{max}|$ at some depth and then decreases to zero again. Provided $V_T < |w_{max}|$, there will be two points, say z_t and $z_b < z_t$, on the plane at which the vertical velocity of a buoyant particle is zero. The SRZ is bounded in the vertical by these two points, so the size of the trapping zone is determined by the intensity of the convection $|w_{max}|$ and by the buoyant velocity of the particle. This is illustrated in the figure below, which is calculated for one of the Langmuir circulation fields computed in Chapter 7 for the case of monochromatic surface waves with dimensionless wavenumber $\kappa = 10$ and Rayleigh number (see Chapter 7) $R = 25,000$, and $R_T = 1$. Note that the

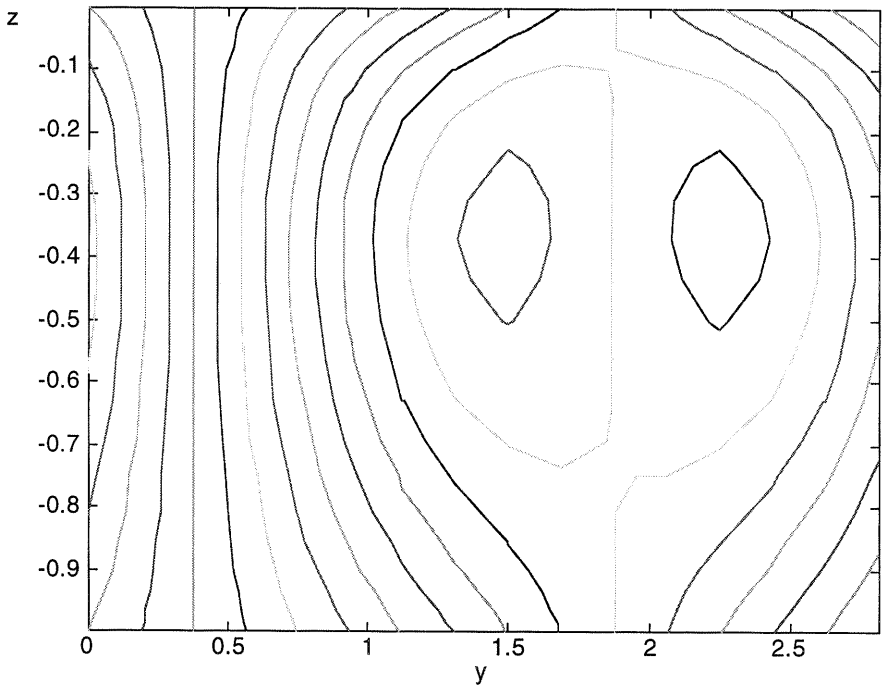

Figure 5.1: Variation of the perturbation windward velocity component profile at the surface with κ for fixed R(=10,000).

nearly closed curve should in fact be closed, and the break in it is an artifact of the contour plotting routine. Particles move on these lines from the bottom of the figure to the top with the exception of those trapped inside the region of nested closed curves. Note that the closed region in Stommel's idealized case is associated with two points of zero particle speed, $w + R_T = 0$. One of these zeros is near the surface at $z = z_{top}$ and the other below that point at $z = z_{bottom}$.

5.3.2 Transport across the retention zone boundary

How does a particle get into the SRZ? In Stommel's idealized problem, a particle is either in or out; it cannot cross the boundary of the trapping

zone. Of course, if a particle were able to get in, it would presumably also be able to get out, so the trapping is not complete. The idealized problem, as Stommel himself noted, neglects velocity fluctuations in the water: such fluctuations, due to turbulence and to surface waves, are always expected, and these must be accounted for to describe the degree of trapping realized.

In the absence of organized convection, all the particles would be in a layer near the surface. The layer has a finite thickness due to the the presence of velocity fluctuations. If the fluctuations are parameterized by an eddy diffusivity, D, then this surface layer would have thickness comparable to $\ell = D/V_T$.

When organized convection is present, the particles in the surface layer are swept towards lines of surface convergence. Most particles that initially may be present below the surface layer but outside the SRZ will rise to the surface layer. Some particles rising outside but very near the SRZ will be entrained into the trapping zone by velocity fluctuations that carry them inside. At the same time, some of the particles initially inside the SRZ will be detrained and rise to the surface. Suppose $|z_{top}| >> \ell$, then there is no way for particles in the surface layer to be entrained into the SRZ, and when the bulk of the water column outside the SRZ is swept clean of particles, there is no further source for entrainment into the SRZ. In time, the SRZ itself will lose all of its particulate content in this case. A balance in which the average number of particles in the SRZ remains constant is therefore only possible if the $|z_{top}|$ is comparable to or smaller than ℓ. In this case, the SRZ can feed on the surface layer. Due to the long residence times within the SRZ, the concentration of particles within it can be assumed to be spatially uniform, and depends on the ratio $\gamma = |z_{top}|/\ell$. In any event, if a fixed amount of oil is present, ultimately all of it will be in the feeder layer confined to the part of the surface near convergence lines and, if γ is not large to prevent exchange, in the SRZ below.

The analysis of [53] is based on this picture, and the concentration within the has been determined as a function of γ. This is conveniently expressed as a ratio, C_*, of the concentration of particles in the SRZ to the maximum concentration in the feeder region. The results of the calculations are given in Figure 5.3.2 by the points marked with x's, and the a least squares fit to the data given by the solid line is

$$C^* = 6.7\gamma^2 + 1.62\gamma + 1. \tag{5.5}$$

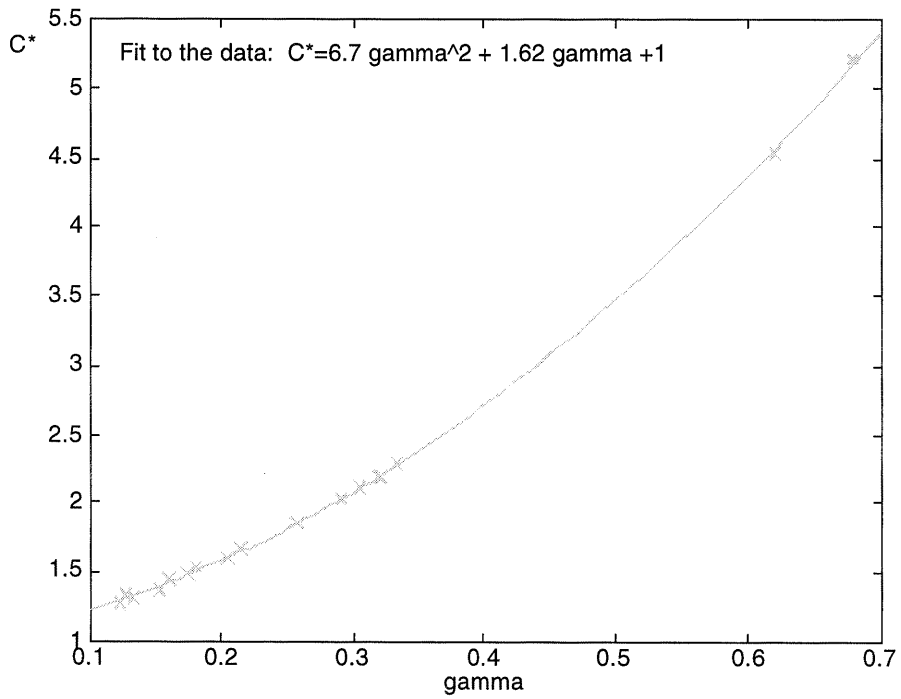

Figure 5.2: Peak concentration in the "feeder" layer. Points marked by the symbols are data from [53], and the solid line is the fit given by (5.5).

Chapter 6

Disintegration of Coherent Oil into Droplets

Oil spilled in the ocean will tend to be concentrated near the surface, but depending on the intensity of turbulence in the upper portion of the water column, the oil may be dispersed over a greater or lesser depth. In severe environmental conditions, it may not even be apparent from surface observations that oil is present.

To determine the subsurface distribution and transport of oil at sea, the size distribution of oil particles must first be known or estimated. Oil size distribution depends on a number of factors - interfacial properties between oil and the ambient seawater, oil density and viscosity, and the turbulent kinetic energy spectrum of the sea.

Continuous floating sheets of oil can be broken into smaller pieces by forces exerted by the underlying or surrounding water. The dispersion of oil into the water column depends on the degree to which the oil is fragmented into small volumes, and the dispersion, for a given water dynamical state, is maximal when the oil particles have reached the smallest size that can be expected. [1]

The theoretical models of Kolmogorov [41] and Hinze [31] for the drop size of the dispersed phase in turbulent flow remain the conceptual basis for work in this field. Published work ([77], [4], [17], [43], [11], [12]) which has followed has attempted to correct for the viscosity of the dispersed phase,

[1] It is assumed throughout that the oil volume is negligible compared to that of the water, and that the motion of the water is unaffected by the presence of the oil. This assumption does not always reflect the facts.

and for coalesence of particles of the dispersed phase. Coalescence needs to be accounted for when the volume fraction of the dispersed phase is large, as in emulsions produced for pharmaceutical or commercial products, but is of little consequence when the volume fraction of the dispersed phase is small, as it usually is in oil spills (and where we think of any coherent floating mats of oil as a separate entity rather than dispersed phase, so that droplets rising to the surface and rejoining floating mats are considered to be removed from the dispersed phase).

All of the work done on this problem to date focusses on the *maximum stable* droplet size. No theoretical model appears to have been proposed for the distribution of droplet sizes that can be expected. Furthermore, existing models do not account for the intermittency of the turbulence. In the upper ocean the intermittency depends on wave breaking, itself a highly intermittent process in space and time, and the resulting fluxes therefore are as well. Consequently, the instantaneous peak values of turbulent kinetic energy, q and its rate of dissipation, ϵ, are much higher than their averaged values, $\bar{q}$, and $\bar{\epsilon}$. It is presumably necessary, therefore, to account for the intermittency and distribution of turbulent quantities in a rational model for transport in the sea. In this Chapter, a statistical model for oil droplet size distribution is presented that accounts for these factors, and proceeds further to attempt to link the sizes to oil type and to the most basic meteorological data, the local wind speed. This requires assumptions on the mechanisms of oil disintegration, on the relation of sea state to wind speed, and the connection between sea state and turbulent kinetic energy to the wind.

A limited amount of laboratory and field data on the size of oil droplets suspended in a turbulent seawater is available, but its reliability remains controvesial (M. Fingas, private communication). Moreover, the work has been done on this problem with oil spills (see Fingas et al. [21], [22], [22]) in mind, have mostly been concerned with the overall effectiveness of dispersants, with most of the effort on laboratory studies. It does not seem to have addressed the the linkage between the wind and sea state, which is a key issue for risk assessment.

Nevertheless, we use what data is available to us to adjust our model. The factors entering the modelling considerations suggest the kinds of laboratory and field data that would be helpful in the future. We conclude by discussing the terminal velocity of oil droplets in turbulent seas for a wide variety of oil types of interest in oil spill questions.

6.1 A statistical model for droplet size

Consider a volume of oil introduced into a water column in turbulent motion. In general, the rate of energy supply, and therefore its dissipation rate per unit mass, $\epsilon(\mathbf{x}, t)$, must be treated as a stochastic function of space and time. Let

$$\epsilon_r = \frac{3}{4\pi r^3} \int_{\odot} \epsilon dV$$

be the volume average of dissipation rate over a sphere (indicated by $\odot$) of radius r, where r is in the inertial range of the turbulence. We will designate mean quantities by an overbar, so the expected value of ϵ is $\bar{\epsilon}$, which is also the mean value for ϵ_r.

6.1.1 Conditional probability density

Suppose for the moment that ϵ is constant, then ϵ_r also is constant and equal to ϵ. This corresponds to the picture contemplated in Kolmogorov's analysis of droplet size and leading to the estimate (5.1). This result represents the largest droplet size emerging after an indefinitely long exposure to the fluid turbulence.

Let us take up the picture of oil breakup at a stage when the oil has been fragmented into pieces comparable to the size of eddies in the inertial range. We suppose, as before, that the viscosities of the water and the oil play no role in the force (or energy) balances. If a drop is exposed to an eddy of a much larger length scale than its own radius a, then the droplet will be moved bodily by the eddy and will be only slightly distorted in the process. If the eddy is exposed to a field of eddies of much smaller scale than a, then the pressure fluctuations felt over the droplet will by and large cancel out, again producing only small distortions. The greatest distortions experienced by a droplet are therefore expected to arise when it interacts with eddies having a size comparable to its diameter. The characteristic time that an oil drop will be exposed to an eddy of size ℓ is the eddy turnover time, $\tau_\ell = \ell / v_\ell = \ell^{2/3} \epsilon^{-1/3}$, and in this interval of time, the fluid is capable of accomplishing an amount of work per unit mass (of water)

$$\epsilon \tau_\ell = (\epsilon \ell)^{2/3} .$$

If this amount of work exceeds the surface free energy, the drop can be expected to fragment into (at least) two parts. The size of an eddy of interest

in our context is approximately the diameter of the drop, so fragmentation is anticipated when[2]

$$(\epsilon\ell)^{2/3} \sim (2\epsilon a)^{2/3} > \frac{4\pi\sigma a^2}{\text{mass}} = 3\frac{\sigma}{\rho a},$$

where σ is the interfacial surface tension coefficient and ρ is the water density.

Thus, a drop with radius exceeding

$$a_\epsilon = b_f \left(3\frac{\sigma}{\rho}\right)^{3/5} (2\epsilon)^{-2/5}, \tag{6.1}$$

or volume exceeding

$$V_\epsilon = \frac{4\pi}{3} a_\epsilon^3, \tag{6.2}$$

will ultimately undergo further division. The drop size given by equation (6.1) is the result found by Kolmogorov [41] and Hinze [31], arrived at by a different route. The the undetermined multiplicative factor, b_f, presumably depends on the detailed dynamical process during the rupturing events and estimates in the literature vary widely. Data reviewed by Hinze, for example, suggests $b_f \approx 0.36$, which is an order of magnitude less than one inferred from Levich [59]. The matter remains in doubt – for example, Sleicher [79] has raised plausible questions about Hinze's interpretation of the available data. Nevertheless, Hinze's value is assumed in the estimates we make later in this Chapter.

Total volume is conserved in a division, so if the original volume is V_0, then the volume of one (of an assumed two-) part of the fission product is $\alpha_1 V_0$ and the second part has volume $(1-\alpha_1)V_0$, where α_1 is a fraction less than one.

The ratio of surface free energy after the division to that before the division is

$$\alpha_1^{2/3} + (1-\alpha_1)^{2/3} - 1.$$

The maximum surface energy increase in a two-part division therefore occurs when the product drops are of equal volume, and this occurs when the surface free energy after the division is 1.26 times the original surface energy. Therefore if the work done on a drop exceeds its free energy by 26%, then on energetic grounds at least, the value of α_1 can be *any* value in the interval

[2]The argument accounts only for inertial (pressure) work, which is valid in turbulent flow only when the length scales are large compared to the Kolmogorov scale, η. It therefore applies for lengths in the inertial range and larger.

$(0, 1)$. The details of the splitting are not known, and so we assume that when division occurs, it does so with α_1 being equally likely to assume any of the values between 0 and 1.

If either (or both) of the subvolumes $\alpha_1 V_0$ and $(1 - \alpha_1)V_0$ is greater than V_ϵ, then it (or they) will eventually split again, into an equally likely fraction $0 < \alpha_2 < 1$ of its previous volume, and so on. If this process goes on forever, one can expect all of the oil to be distributed in drops of volume less than V_ϵ. The nature of the process contemplated here is reminiscent of that shown by Kolmogorov in 1941 to lead to the so-called logarithmic-normal distribution (see [66], pp. 317-319 and also Halmos [28].). There is, however, one significant difference: in the related examples, every particle, regardless of its size, is subject to breakage, while in the case we are considering, there is a special role played by particles of volume V_ϵ or smaller, which are not subject to further breakage. To determine the role of V_ϵ in this process, the probability distribution for the process was determined by a computer simulation. The result, which no doubt we should have been able to see without empiricism, is simple — the oil is uniformly distributed into drops with volumes less than V_ϵ.

Thus, the conditional probability for oil volume size, V, given the dissipation rate per unit mass (which is used as a measure of the rate at which the water is capable of doing work on suspended oil), is the uniform distribution,

$$Pr\{V_1 < v < V_2 | \epsilon_r = \epsilon\} = \begin{cases} 0, & \text{if } V_2 < 0 \\ (V_2 - V_1)/V_\epsilon, & \text{if } 0 < V_1 \leq V_2 \leq V_\epsilon \\ 0, & \text{if } V_1 > V_\epsilon. \end{cases}$$

The expected value of volume holding ϵ fixed is then $\frac{1}{2}V_\epsilon$.

6.1.2 Allowing for energy supply rate variability

In 1962, Obukhov [69] and Kolmogorov [42] argued that the probability distribution for logarithm of the dissipation rate averaged over a sphere of radius r, is distributed normally, with a size-dependent variance σ_r. More specifically, the probability density for ϵ_r they proposed is

$$p(\epsilon_r) = \frac{1}{\sqrt{2\pi}} \frac{\epsilon_0}{\sigma_r \epsilon_r} \exp\left[-\frac{(\log(\epsilon_r/\epsilon_0) - m_r)^2}{2\sigma_r^2} \right], \tag{6.3}$$

where m_r is expectation of $\log(\epsilon_r/\epsilon_0)$ and ϵ_0 is a constant reference value of dissipation rate related to the m_r and σ_r. This concept is developed in

more concrete form by Gurvich and Yaglom [27]. They argue that σ and m_r are determined by the flow according to

$$\sigma_r^2 = \mu \log\left(\frac{L}{r}\right) + A(\mathbf{x}, t), \tag{6.4}$$

where μ is a constant, L is the scale of the energy-containing eddies, and it is assumed that $r \ll L$. The term $A(\mathbf{x}, t)$ here and in the expression for m_r to follow, represents the effects caused by the large scale variations. The parameter m_r, the mean value of $\log(\epsilon_r/\epsilon_0)$, can be expressed (see [27]) as

$$m_r = \log \bar{\epsilon} - \frac{1}{2}\left[\mu \log\left(\frac{L}{r}\right) - A(\mathbf{x}, t)\right].$$

Gurvich and Yaglom review data in the atmospheric boundary layer [27] that suggest that $\mu \approx 0.4$. Yamazaki [93] provides additional discussion, while Yamazaki and Lueck [94] show that standard methods of computing ϵ from oceanic measurements fail to reveal a lognormal distribution due to inconsistencies in the assumptions used in the computation, and that if appropriate methods are used, the lognormal distribution is supported by oceanic data.

The smaller the averaging volume, the larger the variance σ_r^2, as one would expect. The averaging volume of interest to us presumably is somewhat larger than the size of drops produced. Some conclusions about inertial ranges turbulence drawn from the logarithmic normal distribution have been established to be correct, and the same distribution has been claimed to fit the dissipation rate measured under waves in the ocean [2]. We therefore adopt it to estimate dropsize.

As σ increases, the tails of the distribution are elevated, so extreme events are more likely to occur. This is manifest in a more intermittent process, and in fact, Kolmogorov called σ^2 "the intermittency". The elevation of the tails is illustrated in Figure 6.1.2, in which the lognormal distribution of a random variable x with distribution mean of $m = 1$ is plotted for two values, 0.1 and 1 of the standard deviation, σ.

6.1.3 Simulation of stochastic breakup

Suppose the averaged dissipation rate is $\bar{\epsilon}$, and the maximum stable drop volume (abbreviated henceforth by MSDV) based on this is $V_{\bar{\epsilon}}$. A lognormal distribution for ϵ will be determined by two parameters, the distribution mean and variance. Starting with an oil volume V_0 much larger than $V_{\bar{\epsilon}}$, we

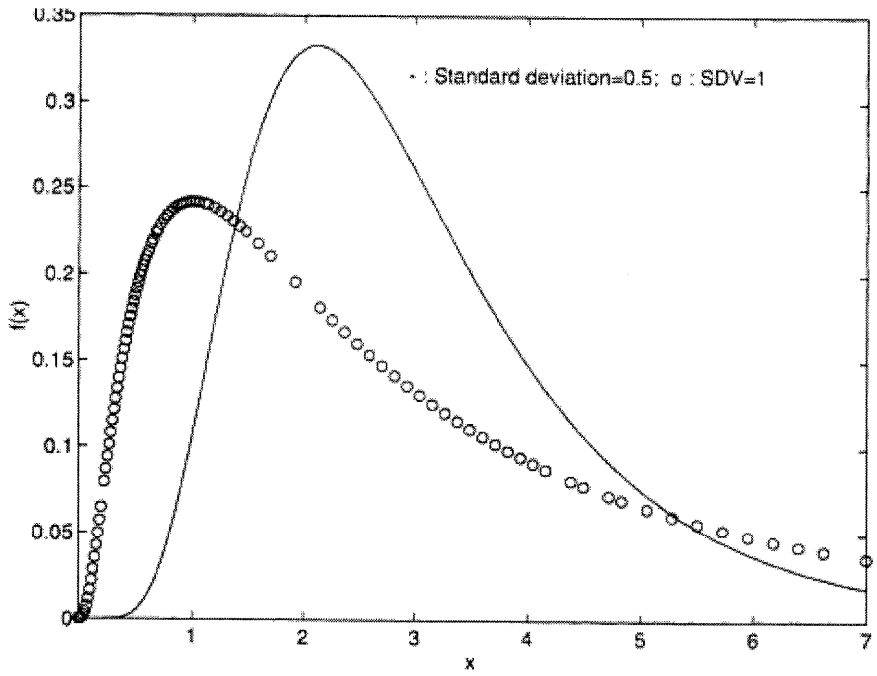

Figure 6.1: Lognormal distributions with the same mean and different intermittencies.

select a sample dissipation rate ϵ from a specified lognormal distribution, and calculate the MSDV V_ϵ for the sample dissipation rate. If $V_0 < V_\epsilon$, we leave the drop in its original state, repeat the process starting from a new sample for ϵ. If $V_0 > V_\epsilon$, the drop is divided into two by a random choice from the uniform probability distribution, while conserving volume in the splitting. The dissipation rate is then sampled again, and each droplet in the collection is tested and is either left undivided, or is divided, depending upon the relation of its individual volume to the MSDV based on the current realization of ϵ. The procedure continues until no further divisions appear to occur.

The resulting ensemble of droplets is then examined for its statistics. Histograms and frequency (probability) distributions, means and variances, of the droplet volume have been produced, using simple numerical codes written in MATLAB.

A sample histogram is shown in Figure 6.1.3, produced for $\sigma = 4$. In typical simulations, the original oil volume has split a large number of times. For example, the simulation corresponds to $V_0/V_{\bar{\epsilon}} = 100$, and 5992 drops emerge before the process appears to terminate. The mean drop size appears insensitive to $V_0/V_{\bar{\epsilon}}$, provided this is 20 or greater, but depends in an important way on σ.

The results of the simulations for mean drop volume for a range of distribution standard deviations, σ,is shown in Figure 6.1.3, where the volumes have been normalized by $V_{\bar{\epsilon}}$. A curve,

$$\frac{\bar{V}}{V_{\bar{\epsilon}}} = \exp\left[-0.1664\sigma^3 + 1.465\sigma^2 - 4.06\sigma - 0.75\right],$$

fits the variation over the range $0 < \sigma < 4$, and for $\sigma > 2$, the ratio

$$\frac{\bar{V}}{V_{\bar{\epsilon}}} = 0.013 \tag{6.5}$$

to very good accuracy. The value at $\sigma = 0$ is 0.47 according to the fit, but here the exact answer can be calculated to be 0.5.

6.2 Dissipation rate near the sea surface

According to the model developed in the previous section, the mean droplet size depends on the mean dissipation rate, $\bar{\epsilon}$, and on the standard deviation σ of the lognormal distribution, as it occurs in the ocean.

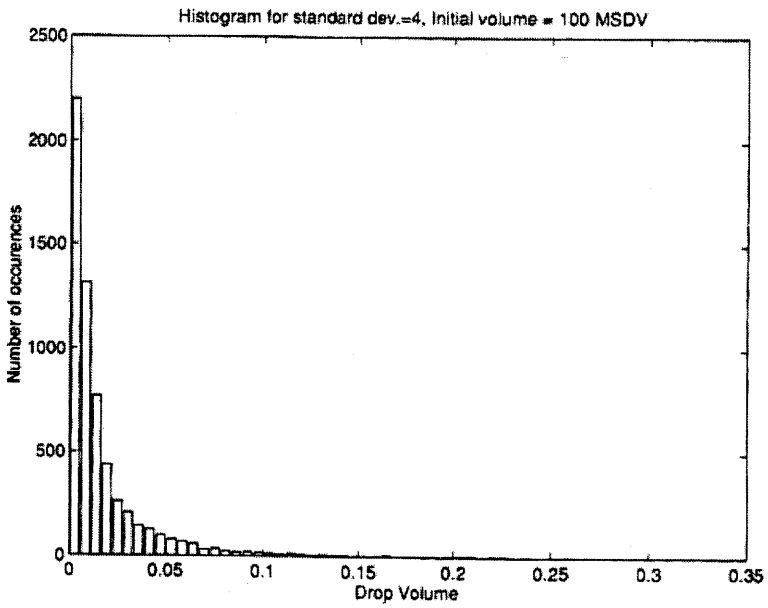

Figure 6.2: Histogram resulting from fragmentation experiment with $\sigma = 4$.

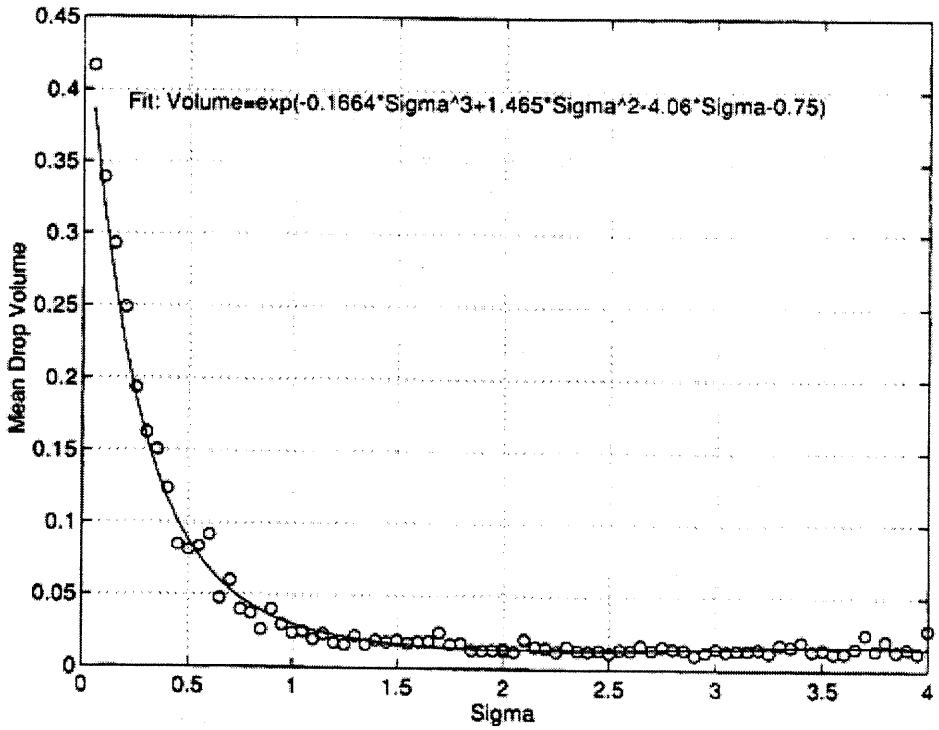

Figure 6.3: Mean drop volume for range of σ.

In the surface mixed layer, both the mean supply of turbulent kinetic energy and its variance are anticipated to be strongly affected by wave breaking. Wave breaking produces turbulence. Since it occurs at the boundary of the water body, wave breaking can be regarded as providing a surface flux of turbulent kinetic energy, and other turbulent statistics. The challenge is to model the fluxes arising from this process in a tractable way. Previous efforts by the community to address this question were frustrated by the lack of adequate means of measurement; better instrumentation now available has altered this situation in the laboratory, and perhaps in the field. There has been recent progress and good reasons to believe ([26], [71], [65], [85], [87]) that significant improvements in the understanding of the effects of wave breaking are on the way.

Early views of the process associated wave breaking with the attainment of a local acceleration of the water surface in excess of $\frac{1}{2}g$ (see Longuet-Higgins, [63]), which corresponds to the acceleration of the Stokes wave of maximum slope. This is now thought (see [71]) to be an oversimplification, and it is now recognized that breaking can occur at much smaller surface accelerations, and is determined by the time history of the interfacial displacement,[3] the local surface drift due to wind stress, and no doubt other effects as well.

The effects of *wave age*, defined as $\beta = c_p/U$, where c_p is the phase speed at the spectral peak of the wave spectrum and U is the wind speed,[4] have come to the forefront ([65], [85]) as an important factor in wave breaking and its associated energy transfers from waves to turbulence. A firm determination of the role of wave age remains an active subject of research. A model for the

The part of the water column that determines the disintegration of oil is near the air–sea interface, and this is where measurements of turbulent characteristics are most difficult. Measurements [37] *below* the wave zone have indicated that the dissipation rate can be represented as if the interface were a smooth no–slip surface, or $\bar{\epsilon} = u_*^3/(\kappa|z|)$ where $\kappa \approx 0.4$ is von Kárman's constant, u_* is the friction velocity in the water, and $|z|$ is the depth below the mean water surface. This is called "wall-layer" scaling.

Recently, it has become possible to measure [2] in the active wave zone, much closer to the free surface. Such measurements reveal a dissipation

[3] With the orbital speeds of large waves affecting the local dynamics of smaller waves riding upon them.

[4] An alternate definition of wave age replaces U by the air friction velocity at the air/sea interface.

rate up to two orders of magnitude higher in this region, which has been attributed to injection and dissipation of turbulence by breaking waves. In a recent analysis of the data, [85], the same group suggests a parameterization that gives for the dissipation rate near the mean free surface of

$$\bar{\epsilon} = \frac{u_*^2\, \bar{c}}{1.2 H_s}, \tag{6.6}$$

where H_s is the significant wave height, and $\bar{c}$ is an effective wave phase velocity. The velocity $\bar{c}$ is a function of "wave age", $\beta = c_p/U$, where c_p is the phase speed at the spectral peak. For $\beta < 0.5$, $\bar{c}$ is approximately constant with value $\bar{c} \approx 0.5$, while if $\beta > 0.5$, $\bar{c}$ is a linear function of wind speed[5] $\bar{c} \approx 0.6 c_p$ for the fetches examined in [85].

The significant wave height by definition is the mean height of the 1/3 highest waves in the spectrum. According to Longuet–Higgins [62], the significant wave height is 2.83 times the r.m.s. surface displacement. For a spectrum with the Pierson-Moskowitz *shape*, this leads to

$$H_s = 2.83 \sqrt{\frac{\alpha}{5}} \frac{g}{\omega_p^2}, \tag{6.7}$$

where ω_p is the angular frequency at the peak of the frequency spectrum, and α is the parameter used in the wind-wave development model of Hasselmann et al. invoked in Chapter 2. [6]

With $\bar{c} = 0.6 c_p$ and $c_p = g/\omega_p$ (for deep water waves), the spectral shape assumption leads to

$$\bar{\epsilon} = \frac{0.395}{\sqrt{\alpha}} \omega_p u_*^2. \tag{6.8}$$

In a developing sea, α and ω_p vary with duration and fetch, and a rational operational procedure is to use an appropriate model for the development of these parameters – such as the parametric wave model discussed in Chapter 2 – while fixing the spectral shape to be Pierson-Moscowitz. The data for the "fully developed sea" to which the Pierson–Moscowitz model was intended to apply gives $\alpha = 0.0081$ is a constant, and $\omega_p = 0.88\, g/U$. For the present purposes, we adopt this choice without verification of the sensitivity of the conclusions to variation of these parameters; this leads to a significant wave

[5] We have replaced the friction velocity in the air by U/28 in converting the data of [85], and otherwise have "rounded off" the values given there.

[6] Where it was called β.

height

$$H_s = 0.147\frac{U^2}{g}$$

and a dissipation rate of

$$\bar{\epsilon} = 3.86u_*^2\frac{g}{U} \approx 4.7 \times 10^{-6}gU \tag{6.9}$$

on replacing $u_* \approx 1.1 \times 10^{-3}U$.

This information provides us with an estimate for $\bar{\epsilon}$. To determine mean drop size from out model, we also need an estimate for the intermittency, σ^2. That the dissipation rate is lognormal, with intermittency due to wave breaking, has been suggested by Agrawal et al. [2]. The connection derives from the intermittent behavior exhibited by 13 second time averages (as close to instantaneous as the experimental method permitted) of dissipation rate, and is summarized in Figure 6.2 4 for one value of the wind speed. A more definitive determination that a lognormal distribution is an accurate representation of the statistics was not made (Terray, private communication), and the parameters of the distribution are unknown.

A more specific indication of lognormality in dissipation rate under breaking waves is provided by George et al. [26]. They have fitted measurements of the dissipation rate in a surf zone to a lognormal distribution, reproduced in Figure6.2. The utility of this work for our purposes derives from the estimates ([26], pg. 805) for the intermittency in the natural surf zone of σ^2 between 2 and 12, and between 3 and 7 for the deep ocean. If this is the case then $\sigma > 1$, and it is not unreasonable to adopt (6.5) to relate the mean drop volume to the maximum stable drop volume based on the mean dissipation rate, $\bar{\epsilon}$.

6.3 Terminal velocity by oil product type

We are now in a position to calculate particle sizes as a function of wind and oil type. Our model provides us with the estimate

$$\bar{V} = 0.013V_{\bar{\epsilon}} = 0.013b_f^3\frac{4\pi}{3}\left(3\frac{\sigma}{\rho}\right)^{9/5}(2\bar{\epsilon})^{-6/5}, \tag{6.10}$$

with $\bar{\epsilon}$ correlated with wind speed through

$$\bar{\epsilon} \approx 4.7 \times 10^{-6}gU. \tag{6.11}$$

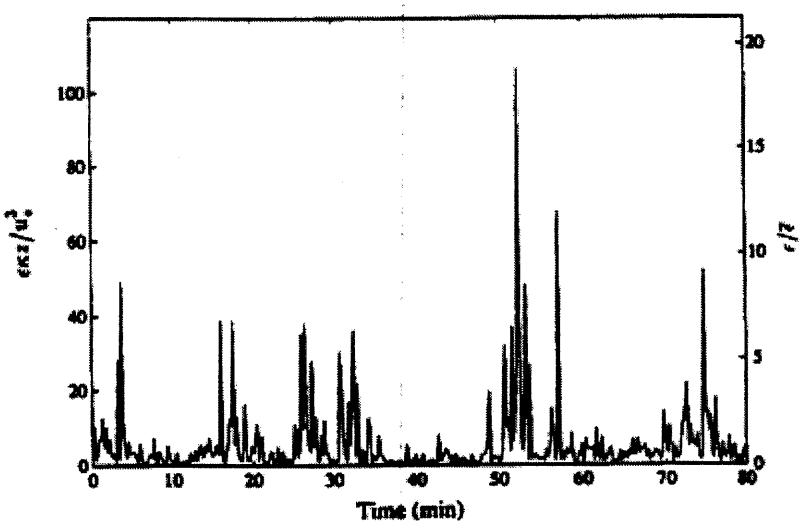

Figure 6.4: Time-dependent dissipation estimates, $\epsilon\kappa z/u_*^3$, or $\epsilon/\bar{\epsilon}$, based on intervals of 13 s, the shortest data length yielding spectra that can be interrogated for ϵ. Wind speed was 12 m s^{-1}. From [2].

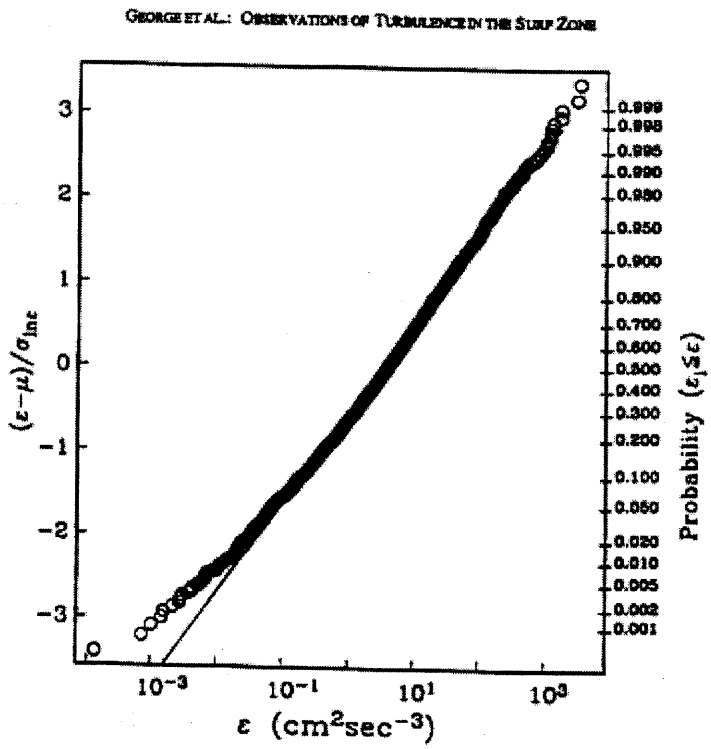

Figure 6.5: From [26].

This produces an estimate for average droplet size that is $0.235\,(=0.013^{1/3})$ times the maximum stable drop radius (5.1).

Let the density difference between the water and oil be $\Delta\rho$, and let the drag coefficient for a sphere of radius a in steady motion at speed V be $C_D(Re)$, where $Re = 2Va/\nu$ is the Reynolds number based on sphere diameter. The terminal velocity of thea sphere is found by balancing the buoyancy and drag, and leads to the equation

$$\sqrt{C_D(Re)}V = \sqrt{\frac{8\Delta\rho}{3\rho}ga}, \tag{6.12}$$

where g is the acceleration of gravity.

The Reynolds number turns out to be of order 10^2 to 10^3, well beyond the Stokes regime. A curve–fit to empirical data for C_D suggested by White [90] (pg.209),

$$C_D = \frac{24}{Re} + \frac{6}{1+\sqrt{Re}} + 0.4 \tag{6.13}$$

is as accurate as the experimental data over the range $Re < 2 \times 10^5$.

In [1], properties of 195 types of oil and oil products are given. In Table 6.3, we list the maximum and minimum values cited for product density and interfacial tension of the product against seawater for the 53 products of [1] for which both types of data are provided. The oil density does not enter expression (5.1), but is listed because the drop buoyancy and therefore its terminal velocity directly depend on oil density. Both density and interfacial tension depend on the precise chemical composition and thermal states of the oil and water. So, for example, when an interfacial tension against "seawater" is quoted, the salt content of the seawater is not known, and so such a quantity presumably is subject to variability when measured for the same oil in seawater obtained from different locations. Of course, the variability of the petroleum mixture is extremely wide, as emphasized in our last report, and so one should expect the quoted data to be subject to significant and so far unquantified error bars.

From this data, we have computed the particle size, as determined from the formulas (6.5) and (5.1) with $\bar{\epsilon}$ parameterized in terms of wind speed and sea state by (6.9). The numerical evaluation is based on a single wind speed of 10m/s, and the range of particle radius (a_{low} to a_{high}) is based on the range of interfacial tensions reported for each oil type. To find the drop sizes for any other wind speed, multiply the radius by $(10/U)^{1.2}$, with U expressed in meters/second.

The table also includes high and low values of the terminal velocity. This depends on the drop size, and on the ratio $(\rho - \rho_{oil})/\rho$, where ρ, the density of seawater; in the calculations, ρ was taken to be 1.02 gm/cc. The terminal velocities were found by solving (6.12) numerically, using (6.13) for the drag coefficient.

The droplet sizes indicated for natural breakup at a wind speed of 10m/s are much larger than the drop sizes reported in laboratory studies of dispersant effectiveness, which appear to be a few tens of microns (see [21]-[23]). This partially reflects the results of the preliminary treatment of the oil with the chemical additives being investigated.

There is no doubt that, had the interfacial tension of the oil products reviewed in Table 1 been measured after being pretreated with dispersants, the droplet size predicted in the Table would be substantially smaller. Nevertheless, it is unlikely that the average droplet size would be in the 100 micron or less range.

This brings to the forefront the question of correlating the mixing energy applied in the laboratory and that actually realized in the ocean. Whether dispersants are used or not (and in risk assessment studies, disperant use presumably would decidedly *not* be assumed), it is not possible to assess droplet sizes, and hence vertical mixing and dispersion of oil, unless reasonable estimates of naturally encountered mixing energy can be made as a function of easily observed environmental parameters. Short of relating the mixing energies applied in the laboratory to those occuring in the field, laboratory dispersant studies are of valuable in comparing the relative merits of additives, but would seem to be of lesser value for risk assessment purposes. This is especially true of existing data, in which the turbulence realized in experimental apparatus is not measured or characterized, making it impossible to translate these results into a more fundamental mechanical description.

It is possible that our model results overestimate the oil particle sizes to be expected in the ocean. We have accounted in part for the observation that turbulence in the upper ocean is highly intermittent. However, the parameterization of the data used averages over the significant height of the waves. It would not be a startling surprise to discover that virtually all of the drop formation results from wave breaking and occurs locally within breaking events. If this were the case, the turbulence is far from equilibrium, the turbulent kinetic energy density is at much higher than our estimates. Furthermore, the parameterization of turbulent kinetic energy by its dissipation rate, as contemplated in the models of Kolmogorov, Hinze,

Oil Type	ρ_{low} gm/cc	ρ_{high} gm/cc	σ_{low} dynes/cm	σ_{high} dynes/cm	a_{low} cm	a_{high} cm	V_{low} cm/s	V_{high} cm/s
Adgo Crude	0.952	0.967	6.9	21.5	0.14	0.29	0.35	8.74
Alberta Sweet Mixed Blend Crude	0.839	0.888	8.4	17.5	0.16	0.25	0.54	13.42
Amauligak Crude	0.890	0.9156	15.0	21.1	0.23	0.28	0.78	12.08
Arabian Heavy Crude	0.887	0.951	15.0	20.0	0.23	0.27	0.73	11.79
Atkinson Crude	0.906	0.924	7.1	18.7	0.15	0.26	0.41	10.46
Avalon Crude	0.844	0.897	20.5	33.2	0.28	0.37	1.72	16.61
Aviation Gasoline 80	0.695	0.708	32.1	33.1	0.36	0.37	3.08	23.16
Aviation Gasoline 100	0.715	0.728	40.0	42.2	0.41	0.43	4.29	24.35
Bent Horn A-02 Crude	0.815	0.874	1.7	34.4	0.06	0.38	0.42	18.38
Bent Horn Crude	0.818	0.874	2.2	53.5	0.07	0.49	0.73	21.22
Cohasset Crude	0.779	0.847	12.5	16.5	0.21	0.24	0.77	15.32
Cold Lake Dilbit	0.917	0.927	16.3	28.1	0.24	0.34	0.97	11.86
Cold Lake Diluent	0.704	0.716	6.8	7.5	0.14	0.15	0.27	12.70
Diesel Fuel	0.827	0.845	28.0	28.2	0.33	0.34	1.88	16.76
Electrical Insulating (Virgin)	0.867	0.892	14.2	17.7	0.22	0.25	0.67	12.13
Electrical Insulating (Used)	0.867	0.878	16.7	23.9	0.25	0.30	1.03	13.67
Electrical Lubricating (Virgin)	0.872	0.882	13.6	19.0	0.22	0.27	0.76	12.77
Electrical Lubricating (Used)	0.873	0.883	11.4	21.8	0.20	0.29	0.75	12.88
Endicott Crude	0.915	0.952	25.8	29.0	0.32	0.34	1.29	11.86
Federated Crude	0.826	0.886	22.2	23.1	0.29	0.30	1.35	15.54
Fuel Oil No. 1 (J.P.-4)	0.755	0.767	9.3	17.0	0.17	0.25	0.67	16.43
Fuel Oil No. 1 (Jet Fuel A-1)	0.804	0.816	37.4	38.4	0.40	0.40	3.11	19.42
Fuel Oil No. 1 (Jet Fuel B)	0.757	0.802	10.8	10.8	0.19	0.19	0.49	13.67
Fuel Oil No. 2	0.840	0.876	26.2	29.0	0.32	0.34	1.77	16.28
Fuel Oil No. 4	0.895	0.938	30.2	—	0.35	0.35	1.63	13.34
Gasoline	0.729	0.750	18.6	19.8	0.26	0.27	1.28	18.28
Gullfaks Crude	0.882	0.914	13.0	17.0	0.21	0.25	0.61	11.67
Hibernia Crude	0.836	0.925	13.5	24.2	0.22	0.31	1.05	15.40
Issungnak Crude	0.828	0.890	12.5	28.2	0.21	0.34	1.20	16.76
Kuwait Crude	0.872	0.928	13.4	24.5	0.22	0.31	0.95	13.95
Lago Medio Crude	0.872	0.898	12.4	17.1	0.21	0.25	0.64	12.13
Lubricating Oil (Extreme pressure)	0.883	0.893	2.8	3.2	0.08	0.09	0.04	4.90
Lubricating Oil (Virgin crankcase)	0.878	0.889	16.6	18.2	0.24	0.26	0.75	11.98
Lubricating Oil (Used crankcase)	0.8845	0.895	21.0	24.2	0.28	0.31	1.12	12.91
Marine Intermediate Fuel Oil	0.971	0.991	35.5	–	0.39	0.39	1.35	8.86
Murban Crude	0.822	0.838	14.3	16.3	0.22	0.24	0.71	13.46
Naptha (Mineral Spirits)	0.793	0.804	43.1	43.2	0.43	0.43	3.83	20.73
Naptha (Petroleum Ether)	0.640	0.655	43.8	44.8	0.44	0.44	5.32	27.48
Nektoralik K-59 Crude	0.854	0.917	14.8	15.1	0.23	0.23	0.63	11.87
Nerlerk M-98A Crude	0.920	0.923	5.2	11.0	0.12	0.19	0.18	7.75
Norman Wells Crude	0.829	0.881	16.4	16.5	0.24	0.24	0.78	13.46
Primer Asphalt	0.942	0.953	24.7	26.8	0.31	0.33	1.05	10.29
Prudhoe Bay Crude	0.881	0.950	9.7	27.6	0.18	0.33	0.83	13.98
Sable Island Condensate	0.869	0.914	18.4	29.6	0.26	0.35	1.37	15.03
Sour Bend Crude	0.836	0.875	24.1	25.8	0.31	0.32	1.56	15.70
Statfjord Crude	0.834	0.895	15.0	23.0	0.23	0.30	1.04	15.09
Sweet Blend Crude	0.825	0.840	16.9	20.2	0.25	0.28	1.04	14.88
Synthetic Crude	0.861	0.916	15.5	29.6	0.23	0.35	1.25	15.56
Tarsiut Crude	0.875	0.902	13.9	18.0	0.22	0.26	0.69	11.98
Terra Nova Crude	0.856	0.871	28.8	29.4	0.34	0.34	1.77	15.29
Transmountain Blend Crude	0.855	0.925	19.3	25.1	0.27	0.31	1.21	14.45
Uviluk P-66 Crude	0.897	0.915	8.8	–	0.17	0.17	0.23	7.87
Uviluk Crude	0.879	0.924	12.2	23.5	0.20	0.30	0.79	13.16

Table 6.1: Oil and oil product properties, mean droplet size, and terminal velocity, based on formula 5.1 with $b_f = 0.36$, and mean dissipation rate parameterized by 6.9, and wind speed of 10 m/s.

and all of the work that has stemmed from these seminal papers, is suspect.

Whether the model we have produced here provides useful estimates must be assessed by experiments in which the wave breaking is the principal turbulence source.

Chapter 7

Model for Three-Dimensional Current Structure

7.1 Introduction

Our objective of developing a predictive system for near-surface currents as an operational tool for risk assessment studies of oil transport requires a method of calculating the effects of Langmuir circulation. *Operational* purposes cannot be served by computation with the complete mathematical formulation for Langmuir circulation in the ocean mixed layer, since the computational effort exceeds available capacity, and this will not change in the foreseeable future. Instead, we need to devise an extremely rapid procedure to extract the information we need for surface transport from the more complete theory. This must allow the repetitive evaluation of many scenarios so that statistical inferences can be drawn concerning risk.

The most important feature of Langmuir circulation for the surface transport of floating material is the water velocity right at the surface. At the surface, oil is swept into convergence lines and then accelerated downwind relative to the horizontally averaged surface current. The oil in collected in surface convergences is subject to being drawn into suspension in the water column as described in Chapter 5. Thus the downwelling component of the current underlying surface convergences is also of special interest.

The goal of this Chapter is to construct a compact description of the surface sweeping motions, surface downwind jets, and the downwelling component that can be rationally related to the surface waves, wind, and mixed layer depth and which is useable for operational purposes.

The description given here is physically based and therefore a reasonable choice to replace the artificial form used for illustrative purposes in Chapter 4. We originally had planned to use the amplitude equation of Cox and Leibovich [13]. After some effort (reported on in interim reports), we came to the conclusion that the amplitude equations required cross-checking against direct numerical simulations to confirm that the large aspect ratio assumption underlying the asymptotic theory of [13] adequately described typical physical realizations for which the aspect ratio is not bery large. At that point, it became clear that the parameterization of a body of synthetic data generated from numerical simulations was a feasible and more direct alternative. This is the approach finally taken and documented in this Chapter.

7.2 Simulation problem

The configuration considered is motion in a layer of water of constant density, overlying a strong thermocline. This is the basic situation contemplated in the section 2.2 of Chapter 2. The motion here is supposed to be two-dimensional. The depth of the layer is d. Empirical observation (see Chapter 1) indicates that the largest scale windrow separation is about three times the depth of the mixed layer. We invoke this informationand require the motion to be periodic in this direction with wavelength fixed L fixed to be $3d$.

We take the (y, z) plane to normal to the wind direction, x - and time. A constant applied wind stress measured by the (water side) friction velocity u_* is assumed at the mean air-sea interface $z = 0$. At the base of the mixed layer, $z = -d$, the stress is prescibed by a parameterization of momentum lost to internal waves below and by entrainment effected by any mixed layer deepening. The parameterized form is given in Chapter 3. With this choice, the velocity vector may be written as

$$\mathbf{v} = u_* \left\{ R_* \left[\frac{z}{d} + 1 + \frac{(1-m)}{\alpha_b} + u \right] \mathbf{e}_x + R_*^{-1} \left[v\mathbf{e}_y + w\mathbf{e}_z \right] \right\}, \qquad (7.1)$$

where $R_* = u_* d/\nu_T$. Here u is the dimensionless perturbation velocity component in the wind direction caused by the presence of vertical motions in the Langmuir circulation system, (v, w) are the dimensionless components of the system in the cross-wind (y), and vertical (z) directions. When $u, v,$ and w are all zero, the current is a linear shear, and this "structureless

equilibrium" is a possible solution to the problem, but is unstable when the Rayleigh number (see below), which measures the relative importance of the wind and wave forcing to viscous resistance, exceeds a threshold that permits Langmuir circulation to grow.

Unless specifically noted to the contrary, in the subsequent discussion it is assumed that all lengths have been made dimensionless with respect to the depth d, even though the coordinate labels are retained, so that now x, y, and z are dimensionless coordinates. The latter two (dimensionless) cross-plane velocity components can be represented by a streamfunction, ψ by

$$v = \frac{\partial \psi}{\partial z} \tag{7.2}$$

$$w = -\frac{\partial \psi}{\partial y}. \tag{7.3}$$

For the purposes of the simulations, the surface wave spectrum is assumed to be narrow band, and the wave field replaced by a monochromatic wave with wavelength equal to that at the spectral peak. The vertical profile of the Stokes drift is taken to be exponential with surface drift speed U_s,

$$\mathbf{u_s} = U_s \mathrm{e}^{\kappa z} \mathbf{e}_x, \tag{7.4}$$

corresponding to a monochromatic wave with wavelength at peak of the Pierson-Moskowitz spectrum, or

$$\kappa = kd = 0.774 \frac{gd}{U^2}.$$

The governing equations for u and ψ are

$$\left(\frac{\partial}{\partial t} - \nabla^2\right) \nabla^2 \psi = Rh(z) \frac{\partial u}{\partial y} + J(\psi, \nabla^2 \psi),$$

$$\left(\frac{\partial}{\partial t} - \nabla^2\right) u = \frac{\partial \psi}{\partial y} + J(\psi, u).$$

Taking the limit of $m \to 1$ in (7.1) and $\alpha_{t,b} \to 0$ in the stress boundary conditions of Chapter 3 implies that

$$\frac{\partial (u, v, w)}{\partial z} = 0 \text{ at } z = -1 \text{ and at z=0.} \tag{7.5}$$

The parameter R is the "Rayleigh number," given by

$$R = R = \frac{d^4 u_*^2}{\nu_T^3} \frac{\partial U}{\partial z} \frac{\partial u_s}{\partial z}(0). \tag{7.6}$$

With the choice of exponential Stokes drift, this becomes

$$R == 2\kappa \frac{U_s}{u_*} R_*^3. \tag{7.7}$$

The dimensionless problem is now determined by two dimensionless numbers, R and κ, with the latter appearing as an independent parameter through its involvement in the Stokes drift profile, $h(z)$.

We note that if we were to take the surface value of the Stokes drift to be given by the Pierson-Moscowitz spectrum, then the ratio U_s/u_* would be a fixed number, giving

$$R = 24\kappa R_*^3.$$

In the limiting process referred to earlier, we set

$$\lambda = \lim_{m \to 1, \alpha_b \to 0} \frac{(1-m)}{\alpha_b}.$$

Then (7.1) providing the dimensional current is

$$\mathbf{v} = u_* \left\{ R_* \left[\frac{z}{d} + 1 + \lambda + u \right] \mathbf{e}_x + R_*^{-1} \left[v\mathbf{e}_y + w\mathbf{e}_z \right] \right\}, \tag{7.8}$$

and λ is chosen to fix the horizontal average surface Lagrangian current to be $0.035U$. This choice, clearly rather arbitrary, allows us to beg the question of a specification of internal wave and entrainment drag, instead fixing the horizontal mean current to be a commonly used value, while not prejuding the *variation* of the current from the mean value caused by the Langmuir circulation.

Langmuir circulation fields were generated by direct numerical simulation for 23 different combinations of κ and R using a pseudospectral code written and provided to us by G. Chini. The code solves the time-dependent problem in a vorticity-streamfunction form, using Fourier series expansions in the cross-wind direction and Chebyshev polynomials in the vertical. In each case, the final asymptotic condition is a steady state. Once a solution was obtained and recorded, it was used as initial condition for a neighboring point in the R, κ parameter space.

To guide to these computations, we utilized the known information on the linear stability characteristics of the structureless equilibrium fo this problem. These were first determined by Lele [58] and are also quoted by Cox and Leibovich [13]. Lele found that the Langmuir circulation instability is operable if $R > R_0(\kappa)$, and that the threshold values $R_0(\kappa)$ are given by

$$R_0 = \frac{32\kappa^5}{1 - \kappa + \kappa^3/3 - e^{-2\kappa}(1 + \kappa - \kappa^3/3)}.$$

These threshold values occur in the limit of infinite windrow spacing, or $L/d \to \infty$. For finite values of L/d, larger values of R are required for instability. From the computations described in the next paragraph, we infer that for the aspect ratio $L/d = 3$ used in this Chapter, the critical value, $R_c(\kappa)$, of R for instability is approximately twice R_0, and we therefore used

$$R_c(\kappa) = \frac{64\kappa^5}{1 - \kappa + \kappa^3/3 - e^{-2\kappa}(1 + \kappa - \kappa^3/3)}, \tag{7.9}$$

in our analysis of the data.

The results of the computations may be anticipated. Increasing R causes the Langmuir system to increase in strength. The effect of varying κ is to increase the asymmetry of the circulation system. When $\kappa = 0$ (occuring as the wavelength of the surface waves becomes extremely large compared to the water depth), the Langmuir system is symmetric about the mid-depth of the layer, and upwelling and downwelling are interchangeable except for direction, and the maximum value of both occur at mid-depth. As κ increases, downwelling is stronger than upwelling, and the depth at which maximum downwelling occurs decreases. This continues as κ increases at fixed R until the system is rendered stable (since $R_c(\kappa)$ will also be increasing) or, if R is simultaneously increased to keep $R > R_c(\kappa)$, the position of maximum upwelling will rise to an asymptotic depth around one-third of the layer depth.

Three series of data sets were acquired, that reflect the anticipated scenario. In the first series, we fixed $\kappa = 1$ and varied R, with computations at $R = 650, 750, 1\times10^3, 5\times10^3$ to 14×10^3 in steps of $10^3, 16\times10^3, 18\times10^3, 2\times10^4$. A computation at $R = 600$ decayed, indicating that the system is stable to Langmuir circulation at that point; the linear stability limit is therefore inferred to be between $R = 600$ and 650 when $\kappa = 1$, and the latter value is the lowest one reported for this series. In the second series, we fixed $R = 10^4$ and varied κ, with computations at $\kappa = 0.5, 1, 2,$ and 4. The system is stable

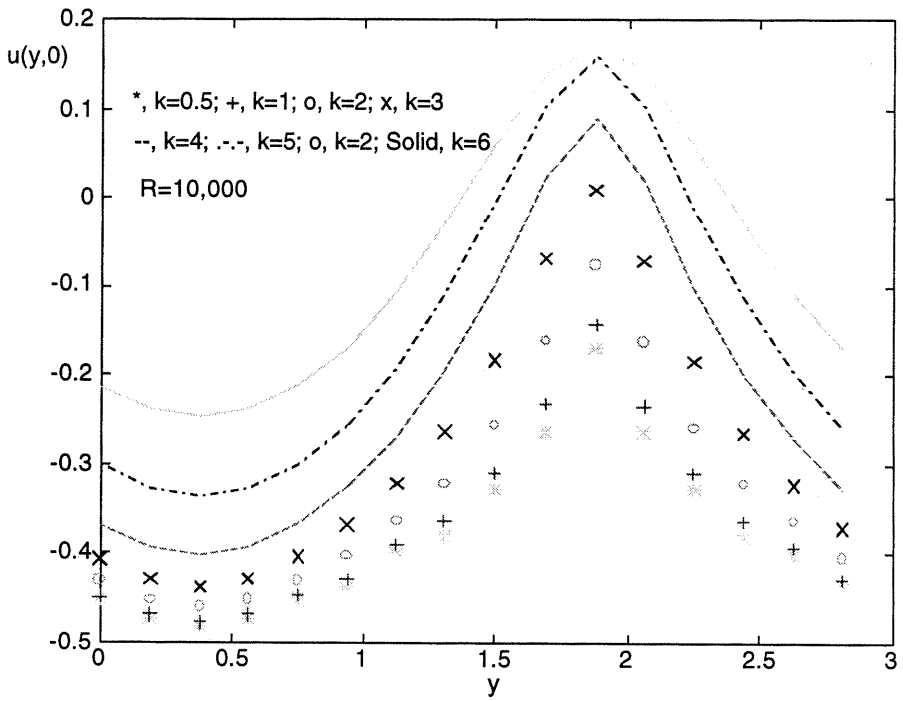

Figure 7.1: Variation of the perturbation windward velocity component profile at the surface with κ for fixed R(=10,000).

for values of κ around 7 and larger. A third series increased R as κ was increased, and the points $(\kappa, R) = (10, 25\times10^3), (15, 5\times10^4)$, and $(20, 8\times10^4)$ were added.

The Eulerian surface velocity component in the direction of the wind is, from (7.1),

$$U_{LC} = u_* R_* \{1 + \lambda + u(y, 0)\} . \tag{7.10}$$

Figure 7.2 is a plot of $u(y, 0)$ for various values of κ at $R = 10^4$. Figure refusurfk1 gives the corresponding plot showing how $u(y, 0)$ varies for a fixed value of κ as R is varied. The figures are similar, and follow the same trend if the convective activity in the system increases as $R/R_c(\kappa)$ increases, as would be expected from stability theory.

The component U_{LC} has jet-like behavior over lines of surface conver-

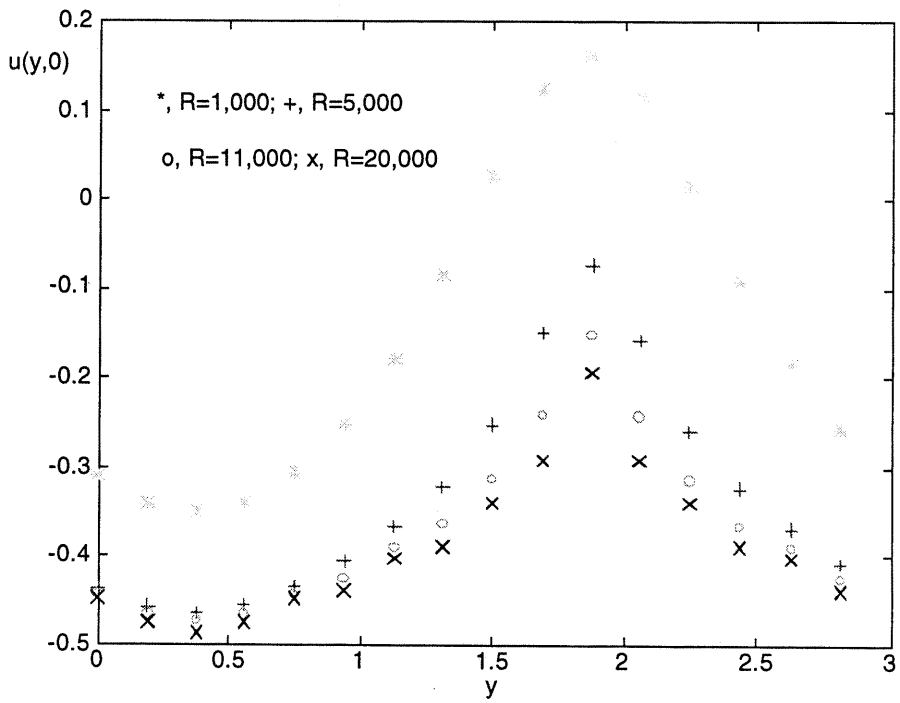

Figure 7.2: Variation of the perturbation windward velocity component profile at the surface with R for fixed κ =(=1).

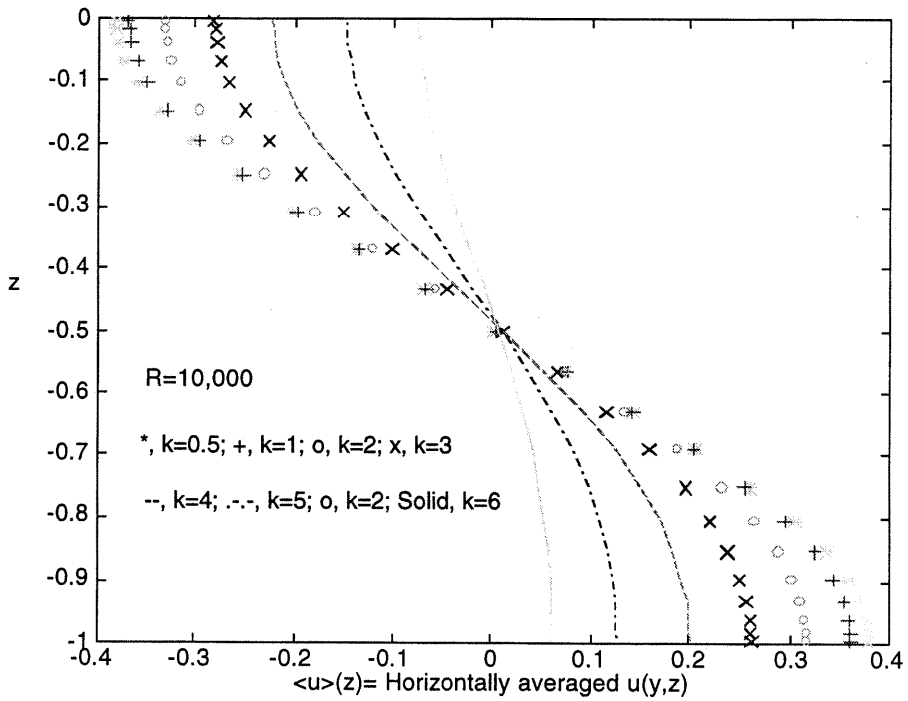

Figure 7.3: Vertical profile of the horizontally averaged perturbation current corresponding to the (κ, R) data in Figure 7.2.

gence. When the parameter $\bar{\Gamma}$ (defined in Chapter 4) is very large, oil is collected in surface convergences and moves with a speed close to the maximum value in the surface jet. Consequently, although we have found a functional form that fits U_{LC}, the principal interest is in the velocity with which the jet exceeds the horizontal average surface current. If the horizontal average is denoted by angle brackets, then

$$\langle U_{LC} \rangle = u_* R_* \{1 + \lambda + \langle u(y,0) \rangle\} .$$

Profiles of the horizontally averaged perturbation current as a function of depth, $\langle u(z) \rangle$, are shown in Figures 7.2 and 7.2 for the data (κ, R) data in Figures 7.2 and 7.2, respectively.

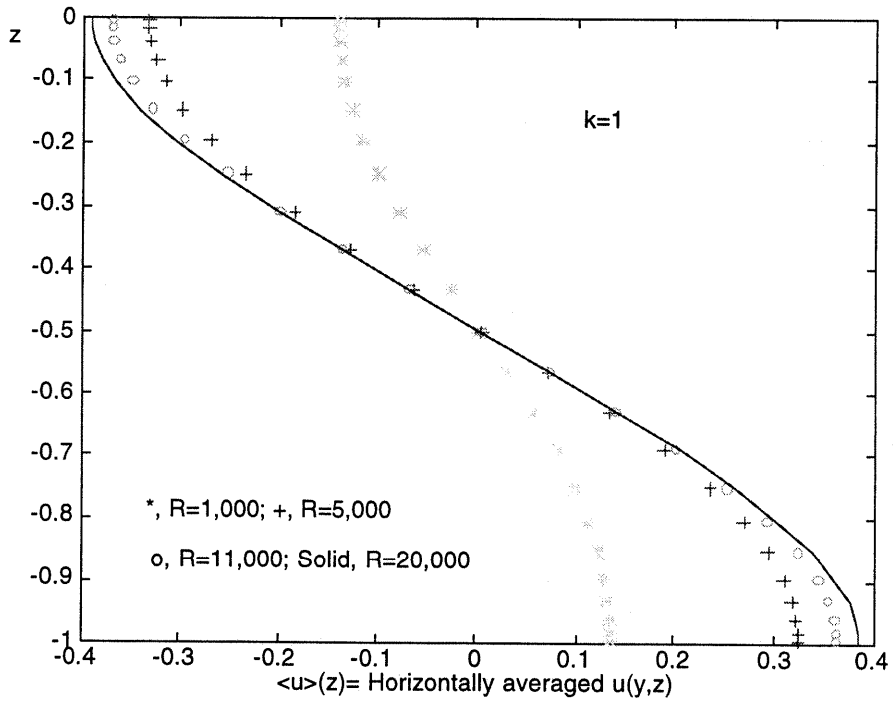

Figure 7.4: Vertical profile of the horizontally averaged perturbation current corresponding to the (κ, R) data in Figure 7.2.

The maximum speed at the surface is then in the jet, and

$$\langle U_{LC} \rangle + u_* R_* u_{jet},$$

where u_{jet} is defined to be

$$u_{jet} = \max_y u(y,0) - \langle u(y,0) \rangle. \tag{7.11}$$

The jet enhancement was found to be fitted by

$$u_{jet} = \sqrt{r}\left[0.4e^{-0.278r} + \frac{1}{0.4595r + 2.3879\sqrt{r} + 0.7515}\right] \tag{7.12}$$

where

$$r = \frac{R - R_c(\kappa)}{R_c(\kappa)}$$

for $R > R_c(\kappa)$ to reasonable accuracy, and is zero for $R < R_c(\kappa)$ (where no Langmuir circulation takes place). The jet enhancement, u_{jet} rises from zero to a maximum of about 0.314 at $r = 1.8$, and then decreases algebraically. A composite of our data for the various numerical experiments is shown in Figure 7.2, which shows that the data is collapsed by the scaling with r, and also shows the curve fit (7.12).

The increase in u_{jet} from zero value at $r = 0$ is understandable, since there is no Langmuir activity for negative values of r. As r increases, the convective activity and associated mixing of momentum increases. When fully mixed, the current in the wind direction would be uniform with depth, and therefore there could be no variation of the windward current in the cross wind direction even in the presence of convection, and therefore $u_{jet} \to 0$ for sufficiently large r. This is reflected also in the horizontally averaged current profiles in Figures 7.2 and 7.2. As r increases, the surface value of $\langle u(z) \rangle$ becomes increasingly negative, while the value at the bottom of the layer becomes increasingly positive. This is added to the uniformly sheared current that exists in the absence of convective motion, and therefore the complete current becomes increasingly uniform with depth. The situation cannot progress beyond the uniform current, which is coincident with $u_{jet} = 0$.

The vertical velocity below lines of surface convergence in the simulations is well fitted to the following form,

$$W(z) = -5.4\frac{u_*}{R_*}\sqrt{\frac{R - R_c(\kappa)}{R_c(\kappa)}}\, z\left(p_1 z^2 + p_2 z + p_3\right) \tag{7.13}$$

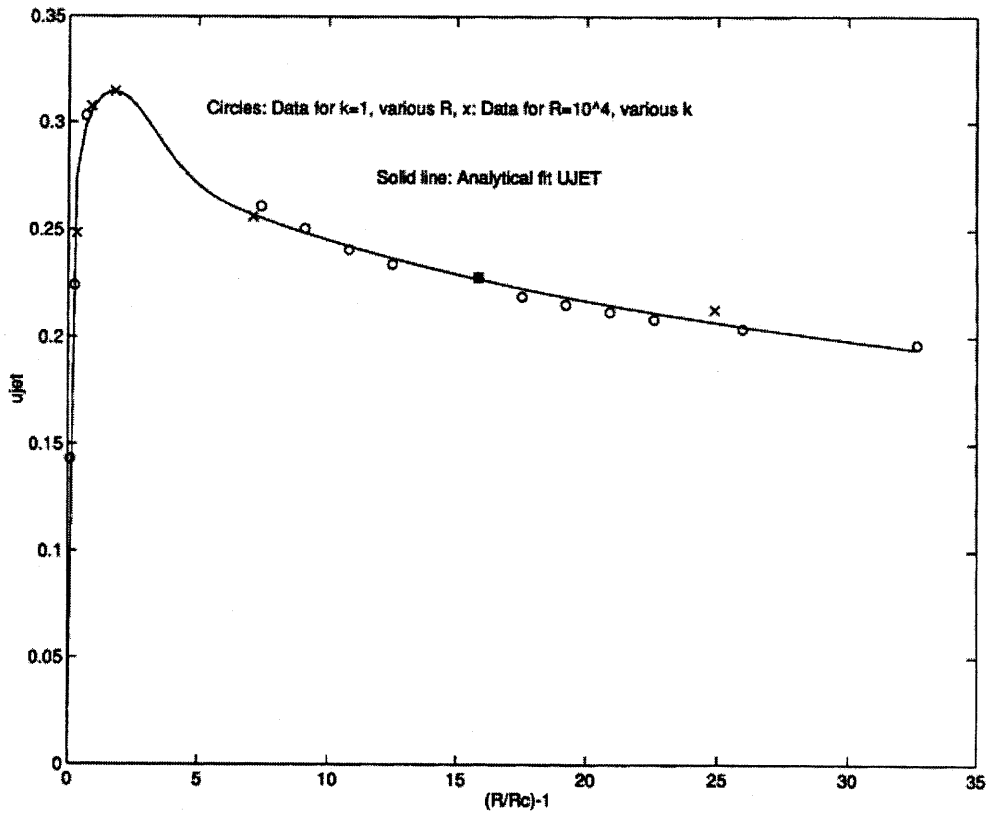

Figure 7.5: Jet enhancement for the simulated data is collapsed by scaling with $r = (R - R_c(\kappa))/R_c(\kappa)$. The symbols are data, the solid line is the function in (7.12).

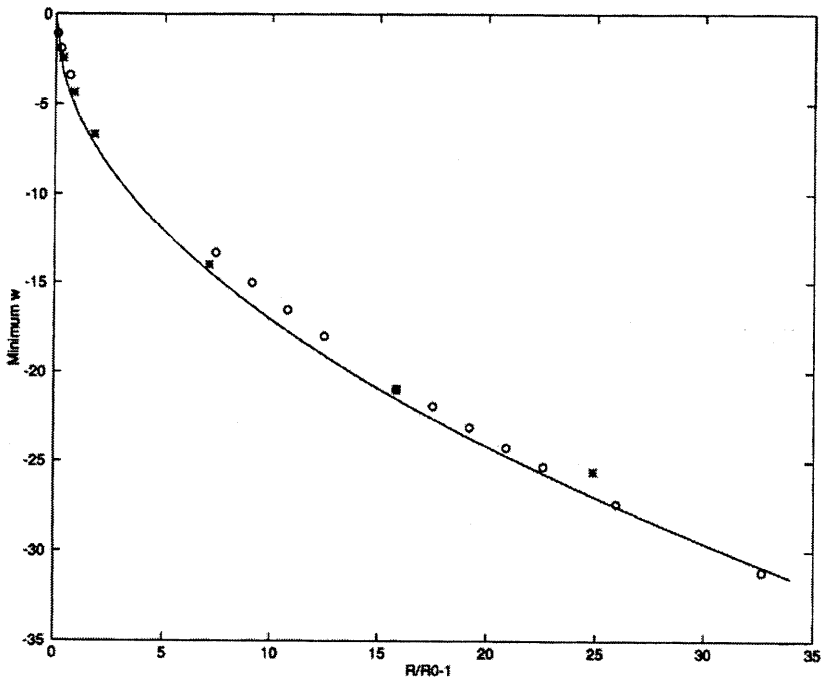

Figure 7.6: Data points from the data set at fixed $k = 1$, various R are shown as circles, and those from the set with $R = 10^4$, various k are shown by x's. The solid line is the fit (7.13).

where $-z$ is the depth normalized by the total mixed layer depth, and $p_{1,2,3}$ are constants that are determined by the normalized depth, $z = z_m$, of the maximum vertical speed. Figure 7.2 shows the data together with the fit provided by (7.13). When the gravity waves are extremely long compared to the depth of the mixed layer, or $\kappa \to 0$, the vertical speed is symmetrical with respect to the mid-depth of the mixed layer under the boundary conditions utilized, so $z_m = -0.5$. It may be expected that z_m depends on κ, and this is borne out by the simulations, which show that the location of the maximum downwelling moves towards the surface as κ increases. This movement has an asymptote, however, at a specific depth. From our simulations, which

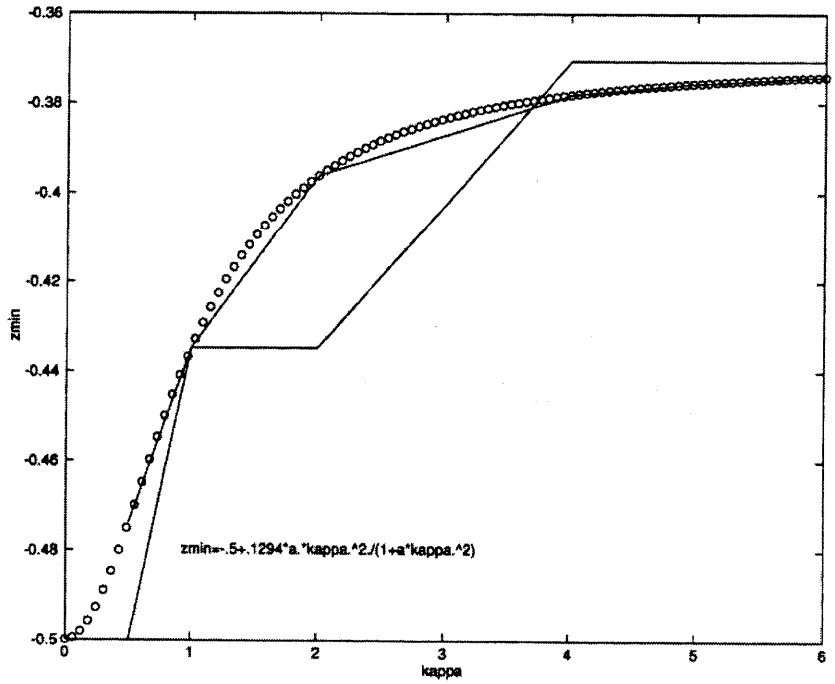

Figure 7.7: The data points correspond to the points $(\kappa, z_m) = (1, -0.4347), (2, -0.4347), (4, -0.3706), (5, -0.3706), (6, -0.3706)$ joined by the step-like solid line. The circles correspond to the fit (7.14).

can only establish this movement of z_m crudely, we estimate

$$z_m = -0.5 + 0.1318\frac{\kappa^2}{(1 + 1.0187\kappa^2)}. \tag{7.14}$$

In terms of z_m, the constants $p_{1,2,3}$ are

$$p_1 = -\frac{2z_m + 1}{z_m^2(1 + z_m)^2}, \quad p_2 = \frac{3z_m^2 - 1}{z_m^2(1 + z_m)^2}, \quad p_3 = \frac{3z_m + 2}{z_m(1 + z_m)^2}.$$

The fit to the steplike data points in shown in figure 7.2.

The surface sweeping velocity component, $V_s(y)$, is approximately sinusoidal, with a maximum value V_m that depends only on $(R - R_c)/R_c$,

$$V_m = 6.07\sqrt{\frac{(R - R_c)}{R_c}}. \tag{7.15}$$

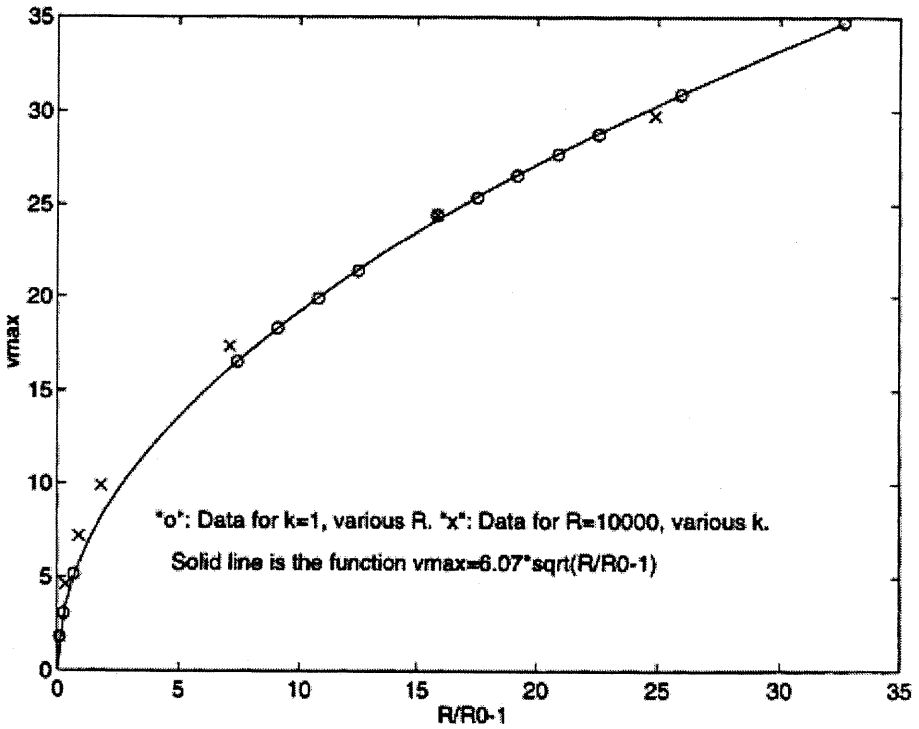

Figure 7.8: Data points from the data set at fixed $k = 1$, various R are shown as circles, and those from the set with $R = 10^4$, various k are shown by x's. The solid line is the fit (7.15).

Figure 7.2 shows the data points from simulation, together with the fit (reffitvee).

The shape of the wavy function $V_s(y)$ depends on κ and $(R - R_c)/R_c$. The maximum amplitude occurs at the cell center for small values of κ for sufficiently large $(R-R_c)/R_c$ and migrates towards the zeros of $V_s(y)$ corresponding to the lines of surface convergence as κ increases. This migration, which can be seen in figure 7.2, will be neglected, and we will take

$$V_s(y) = -V_m \sin\left(\frac{2\pi}{L_s}(y - y_c)\right),$$

where a convergence line is located at y_c.

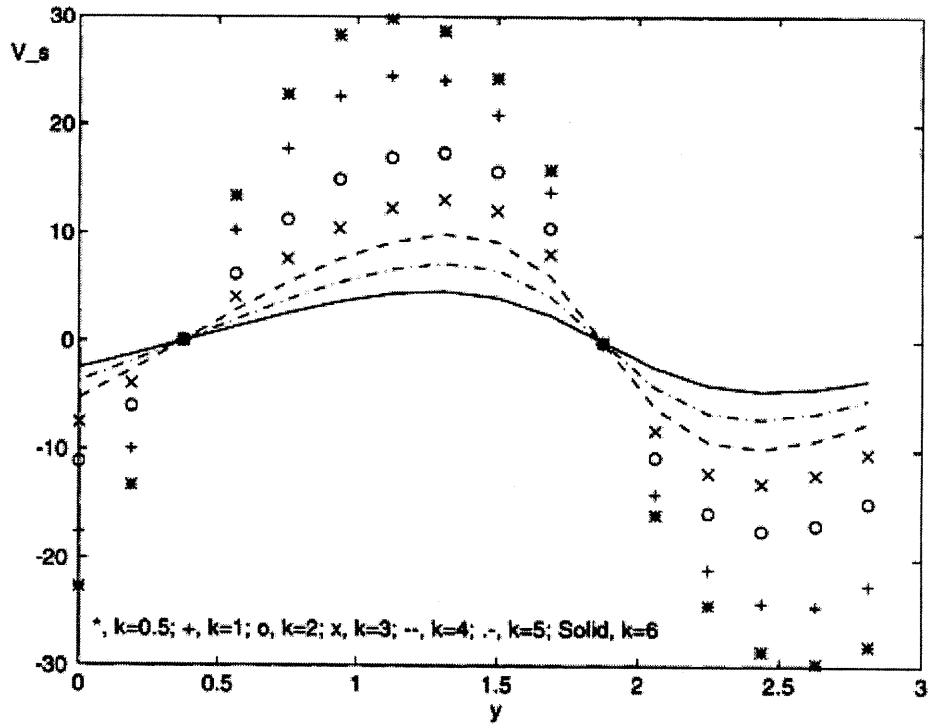

Figure 7.9: Data for the surface value of the sweeping velocity component for seven values of κ at $R = 10^4$. Ordinate is the (dimensionless) value of V_s and the abscissa is the cross wind coordinate. As κ increases, the maximum and minimum values of V_s migrate towards the surface convergence.

Bibliography

[1] A catalogue of crude oil and oil product properties (1990 version). Report EE-125 to the Minerals Management Service and Environmental Emergencies Technology Division of Environment Canada, 1990.

[2] Y.C. Agrawal, E.A. Terray, M.A. Donelan, P.A. Hwang, A.J. Williams III, W.M. Drennan, and S.A. Kahma, K.K.and Kitaigorodsky. Enhanced dissipation of kinetic energy beneath surface waves. *Nature*, 359:219–220, 1992.

[3] D.G. Andrews and M.E. McIntyre. An exact theory of nonlinear waves on a lagrangian–mean flow. *Journal of Fluid Mechanics*, 89:609–646, 1978.

[4] K. Arai, M. Konno, Y. Matunaga, and S. Saito. Effect of dispersed-phase viscosity on the maximum stable drop size for breakup in turbulent flow. *Journal of Chemical Engineering of Jaan*, 10:325–330, 1977.

[5] D.K. Atwood, J.S Benjamin, and J. Farrington. The mission of the september 1979 researcher/pierce ixtoc-i cruise and the physical situation encountered. In D.K. Atwood, editor, *Preliminary Results from the September 1979 RESEARCHER/PIERCE IXTOC-I Cruise*, pages 1–18. U.S. Dept. Commerce, NOAA, 1980.

[6] R. Bainbridge. The size, shape, and density of marine phytoplankton concentrations. *Camb. Phil. Soc. Biol. Rev.*, 32:91–115, 1957.

[7] K.F. Bowden. The effect of eddy viscosity on ocean waves. *Phil. Mag.*, 41:907–917, 1950.

[8] K.F. Bowden. Turbulence. *Oceanogr. Mar. Biol. Ann. Rev.*, 2:11–30, 1964.

[9] K.F. Bowden. *Physical Oceanography of Coastal Waters.* Ellis Horwood, Ltd., Chichester, 1983.

[10] N. E. Busch. Fluxes in the surface boundary layer over the sea. In E.B. Kraus, editor, *Modelling and Prediction of the Upper Layers of the Ocean*, pages 72–91. Pergamon Press, Oxford, 1977.

[11] M. M. Clark. Drop breakup in turbulent flow–i. conceptual and modeling considerations. *Chemical Engineering Science*, 43:671–679, 1988.

[12] M. M. Clark. Drop breakup in turbulent flow–ii. experiments in a small mixing vessel. *Chemical Engineering Science*, 43:681–692, 1988.

[13] S.M. Cox and S. Leibovich. Langmuir circulation in a surface layer bounded by a strong thermocline. *Journal of Physical Oceanography*, 23:1330–1345, 1993.

[14] A. D. D. Craik and S. Leibovich. A rational model for langmuir circulations. *Journal of Fluid Mechanics*, 73:401–426, 1976.

[15] R. H. Cross and D. P. Hoult. Collection of oil slicks. *Journal of Waterways, Harbors, and Coastal Eng. Div. ASCE*, May,1971:312–322, 1971.

[16] A. Davey and K. Stewartson. On the nonlinear evolution of three–dimensional disturbances in plane poiseuille flow. *Journal of Fluid Mechanics*, 73:401–426, 1976.

[17] J. T. Davies. Drop sizes of emulsions related to turbulent energy dissipation rates. *Chemical Engineering Science*, 40:839–842, 1985.

[18] J.W. Deardorff. Stratocumulus–capped mixed layers derived from a three–dimensional model. *Boundary–Layer Meteorology*, 18:495–5270, 1980.

[19] K.L. Denman and T.M. Powell. Effects of physical processes on planktonic ecosystems in the coastal ocean. *Oceanogr. Mar. Biol. Ann. Rev.*, 22:125–168, 1984.

[20] M.J.R. Fasham. The statistical and mathematical analysis of plankton patchiness. *Oceanogr. Mar. Biol. Ann. Rev.*, 16:43–79, 1978.

[21] M.F. Fingas, D.A. Kyle, J.B. Homes, and E.J. Tennyson. The effectiveness of dispersants: Variation with energy. In *Proceedings of the 1993*

International Oil Spill Conference, pages 567–572, Washington, D.C., 1993. American Petroleum Institute.

[22] M.F. Fingas, D.A. Kyle, and E.J. Tennyson. Dispersant effectiveness: Studies into the causes of effectiveness variations. In Peter Lane, editor, *The Use of Chemicals in Oil Spill Response, ASTM STP 1252*, page To appear, Philadelphia, 1994. American Society for Testing and Materials.

[23] M.F. Fingas, D.A. Kyle, Z. Wang, D. Handfield, D. Ianuzzi, and F. Ackerman. Laboratory effectiveness testing of oil spill dispersants. In Peter Lane, editor, *The Use of Chemicals in Oil Spill Response, ASTM STP 1252*, page To appear, Philadelphia, 1994. American Society for Testing and Materials.

[24] J. Galt. Investigations of physical processes. In W. Hess, editor, *The AMOCO CADIZ Oil Spill*, chapter 2. NOAA/EPA Special Report, 1978.

[25] J. Galt. Personal communication. NOAA, Seattle, WA., 1980.

[26] R.E. George, R.and Flick and R.T. Guza. Observations of turbulence in the surf zone. *Journal of Geophysical Research: Oceans*, 99:801–810, 1994.

[27] A.S. Gurvich and A.M. Yaglom. Breakdown of eddies and probability distributions for small-scale turbulence. *Physics of Fluids*, 10:S59–S65, 1967.

[28] P. R. Halmos. Random alms. *Annals of Mathematical Statistics.*, 15:182–189, 1944.

[29] K. Hasselmann, D.B. Ross, P. Müller, and W. Sell. A parametric wave prediction model. *Journal of Physical Oceanography*, 6:200–228, 1976.

[30] W.N. Hess, editor. *The AMOCO CADIZ Oil Spill: A Preliminary Report.* NOAA/EPA Special Report, (2nd Printing), August 1978.

[31] J.O. Hinze. Fundamentals of the hydrodynamic mechanism of splitting in dispersion processes. *A.I.Ch. E. Journal*, 1:289–295, 1955.

[32] C. Hooper. Personal communication. NOAA, Boulder, CO., 1980.

[33] N.E. Huang. Derivation of stokes drift for a deep–water random gravity wave field. *Deep Sea Res.*, 18:255–259, 1971.

[34] N.E. Huang. On the surface drift currents in the ocean. *Journal of Fluid Mechanics*, 91:191–208, 1979.

[35] T. Ichiye. Upper ocean boundary–layer flow determined by dye diffusion. *Physics of Fluids*, Supplement:S270–S277, 1967.

[36] Batelle Memorial Institute. Review of the santa barbara channel oil pollution incident. Report to the Dept. of Interior, FWPCA, and to the Dept. of Transportation, U.S. Coast Guard, 1969.

[37] I.S.F. Jones. Turbulence below wind waves. In Y. Toba and H. Misuyasu, editors, *The Ocean Surface – Wave Breaking, Turbulent Mixing, and Radio Probing*, pages 437–442, Dordrecht, 1985. Reidel.

[38] L.H. Kantha. Note on the role of internal waves in thermocline erosion. In E.B. Kraus, editor, *Modelling and Prediction of the Upper Layers of the Ocean*, pages 173–177. Pergamon Press, Oxford, 1977.

[39] L.H. Kantha and O.M. Phillips. On turbulent entrainment at a stable density interface. *Journal of Fluid Mechanics*, 79:753–768, 1976.

[40] M. L. Khandekar. *Operational Analysis and Prediction of Ocean Wind Waves.* Springer–Verlag, New York, 1989.

[41] A.N. Kolmogorov. The breakup of droplets in a turbulent stream. *Dok. Akad Nauk SSR*, 66:99–101, 1949. Translated from the Russian by E.R. Hope, Directorate of Scientific Information, DRB Canada, June, 1956.

[42] A.N. Kolmogorov. A refinement of previous hypotheses concerning the local structure of turbulence in a viscous incompressible fluid at high reynolds number. *Journal of Fluid Mechanics*, 13:82–85, 1962.

[43] J. S. Lagisetty, P. K. Das, and P. Kumar. Breakage of viscous and non-newtonian drops in stirred dispersions. *Chemical Engineering Science*, 41:65–72, 1986.

[44] I. Langmuir. Surface motion of water induced by wind. *Science*, 87:119–123, 1938.

[45] W. G. Large and S. Pond. Open ocean momentum flux measurements in moderate to strong winds. *Journal of Physical Oceanography*, 11:324–336, 1981.

[46] S. Leibovich. A natural limit to the containment and removal of oil spills at sea. *Ocean Engineering*, 3:715–724, 1975.

[47] S. Leibovich. Oil slick instability and the entrainment failure of oil containment booms. *Journal of Fluids Engineering*, 98:98–105, 1976.

[48] S. Leibovich. Convective instability of stably stratified water in the ocean. *Journal of Fluid Mechanics*, 82:561–581, 1977.

[49] S. Leibovich. Hydrodynamic problems in oil-spill control and removal. *Journal of Petroleum Technology*, March,1977:311–324, 1977.

[50] S. Leibovich. On the evolution of the system of wind drift currents and langmuir circulations in the ocean. part i. theory and the averaged current. *Journal of Fluid Mechanics*, 79:715–743, 1977.

[51] S. Leibovich. On wave–current interaction theories of langmuir circulations. *Journal of Fluid Mechanics*, 99:715–724, 1980.

[52] S. Leibovich. The form and dynamics of langmuir circulations. *Annual Review of Fluid Mechanics*, 15:391–427, 1983.

[53] S. Leibovich and J.L. Lumley. A theoretical appraisal of the joint effects of turbulence and of langmuir circulations on the dispersion of oil spilled at sea. Report CG-D-26-82, U.S. Coast Guard, Washington, DC, 1982.

[54] S. Leibovich and S. Paolucci. The langmuir circulation instability as a mixing mechanism in the upper ocean. *Journal of Physical Oceanography*, 10:186–207, 1980.

[55] S. Leibovich and K. Radhakrishnan. On the evolution of the system of wind drift currents and langmuir circulations in the ocean. part 2. structure of the langmuir vortices. *Journal of Fluid Mechanics*, 80:481–507, 1977.

[56] S. Leibovich and K. Radhakrishnan. On the evolution of the system of wind drift currents and langmuir circulations in the ocean. part 2. structure of the langmuir vortices. *Journal of Fluid Mechanics*, 80:481–507, 1977.

[57] S. Leibovich and Z. Yang. Turbulent flow in natural water bodies driven by wind and surface waves. *jfm, in review.*

[58] S. K. Lele. *Some Problems of Hydrodynamic Stability Arising in Geophysical Fluid Dynamics.* PhD thesis, Cornell University, Ithaca, N.Y., 1985.

[59] V.G. Levich. *Physicochemical Hydrodynamics.* Prentice–Hall, Englewood Cliffs, NJ, 1962.

[60] M. Li and C. Garrett. Is langmuir circulation driven by surface waves or surface cooling? *Journal of Physical Oceanography*, 25:64–76, 1995.

[61] W. T. Lindenmuth, E. R. Miller, and C. C. Hsu. Studies of oil retention boom hydrodynamics. Report 714102/A/008, AD 719294, U.S. Coast Guard, Washington, 1970.

[62] M. S. Longuet-Higgins. On the statistical distribution of the heights of sea waves. *Journal of Marine Research*, 11:245–266, 1952.

[63] M. S. Longuet-Higgins. On wave breaking and the euilibrium spectrum of wind–generated waves. *Proceedings of the Royal Society*, A. 310:151–159, 1969.

[64] J.C McWilliams, P. P. Sullivan, and C-H. Moeng. Langmuir turbulence in the ocean. *jfm, in review.*

[65] W. K. Melville. Energy dissipation by breaking waves. *Journal of Physical Oceanography*, 24:2041–2049, 1994.

[66] P.A.P Moran. *Introduction to Probability Theory.* Oxford University Press, Oxford, 1968.

[67] A. C. Newell, T. Passot, and M. Souli. The phase diffusion and mean drift equations for convection at finite rayleigh numbers in large containers. *Journal of Fluid Mechanics*, 220:187–252, 1990.

[68] P.P. Niiler and E.B. Kraus. One–dimensional models of the upper ocean. In E.B. Kraus, editor, *Modelling and Prediction of the Upper Layers of the Ocean*, pages 143–172. Pergamon Press, Oxford, 1977.

[69] A.M. Obukhov. Some specific features of atmospheric turbulence. *Journal of Fluid Mechanics*, 13:77–81, 1962.

[70] R. W. Owen, Jr. Small scale, horizontal vortices in the surface layer of the sea. *Journal of Marine Research*, 24:56–65, 1966.

[71] O.M. Phillips. *The Dynamics of the Upper Ocean.* Cambridge University Press, second edition, 1977.

[72] W.J. Pierson and L. Moscowitz. A proposed spectral form for fully developed wind seas based on the similarity theory of s.a. kitaigorodskii. *Journal of Geophysical Research*, 69:5181–5190, 1964.

[73] R. T. Pollard. Observations and theories of langmuir circulations and their role in near surface mixing. In M. Angel, editor, *A Voyage of Discovery: G. Deacon 70th Anniversary Volume*, pages 235–251, New York, 1977. Pergamon Press.

[74] R.T. Pollard and Jr. R. C. Millard. Comparison between observed and simulated wind-generated inertial oscillations. *Deep Sea Res.*, 17:813–821, 1970.

[75] S. Pond and G.L. Pickard. *Introductory Dynamic Oceanography.* Pergamon Press, Oxford, 1978.

[76] J. Robinson. Personal communication. NOAA, Boulder, CO., 1980.

[77] R. Shinnar. On the behaviour of liquid dispersions in mixing vessels. *Journal of Fluid Mechanics*, 10:259–275, 1961.

[78] E. D. Skyllingstad and D. W. Denbo. An ocean large eddy simulation of langmuir circulations and convection in the surface mixed layer. *jgr*, 100:8501–8522, 1995.

[79] C.A. Sleicher. Maximum stable drop size in turbulent flow. *A.I.Ch. E. Journal*, 8:471–478, 1962.

[80] J. Smith, R. Pinkel, and R.A. Weller. Velocity structure in the mixed layer during mildex. *Journal of Physical Oceanography*, 17:425–439, 1987.

[81] G. G. Stokes. On the theory of oscillatory waves. *Trans. Camb. Phil. Soc.*, 8:41–71, 1847.

[82] H. Stommel. Trajectories of small bodies sinking slowly through convection cells. *Journal of Marine Research*, 8:24–29, 1948.

[83] A. Tandon and S. Leibovich. Secondary instabilities in langmuir circulation. *Journal of Physical Oceanography*, 25:1206–1217, 1995.

[84] H. Tennekes and J.L. Lumley. *A First Course in Turbulence.* MIT Press, Cambridge, 1972.

[85] E.A. Terray, M.A. Donelan, Y.C. Agrawal, W.M. Drennan, A.J. Williams III, P.A. Kahma, K.K.and Hwang, and S.A. Kitaigorodsky. Estimates of kinetic energy dissipation under breaking waves. Preprint, 1994.

[86] The WAMDI Group. The wam model – a third generation ocean wave prediction model. *Journal of Physical Oceanography*, 18:1775–1810, 1988.

[87] S.A. Thorpe. On the clouds of bubbles formed by breaking wind-waves in deep water,and their role in air-sea gas transfer. *Proceedings of the Royal Society*, A 304:155–210, 1982.

[88] R. A. Weller and J.F. Price. Langmuir circulation within the oceanic mixed layer. *Deep Sea Res.*, 35:711–747, 1988.

[89] R.A. Weller, J. Dean J.P.and Marra, J.F. Price, E.A. Francis, and D.C. Boardman. Three–dimensional flow in the upper ocean. *Science*, 227:1552–1556, 1985.

[90] Frank White. *Viscous Fluid Flow.* McGraw-Hill, 1974.

[91] R. Williams. Personal communication. Exxon Production Research Company, Houston, TX., 1979.

[92] A. H. Woodcock. A theory of surface water motion deduced from the wind–induced motion of the physalia. *Journal of Marine Research*, 5:196–205, 1944.

[93] H. Yamazaki. Breakage models: lognormality and intermittency. *Journal of Fluid Mechanics*, 219:181–193, 1990.

[94] H. Yamazaki and R. Lueck. Why oceanic dissipation rates are not lognormal. *Journal of Physical Oceanography*, 12:1907–1918, 1990.

Surface and Near-Surface Motion of Oil in the Sea Part II: Computer Code

Submitted to Minerals Management Service
Department of the Interior

Prepared by
S. Leibovich
Environmental Sciences of Ithaca
Contract 14–35–0001–30612

March 29, 1997

Contents

1 Introduction **3**

2 Description of OILTRACK **3**
2.1 Input Data and Assumptions 3
2.2 Large scale currents 3
2.3 Surface wind velocity 4
2.4 Sea State 5
2.5 Mixed layer depth 6
2.6 Oil properties 7

3 Output Oil Spill Attributes and Spill Trajectory **7**
3.1 Oil lane separation attribute 7
3.2 Oil sweep time attribute 8
3.3 Current structure attributes 8
3.4 Mass-weighted surface current speed attribute 11
3.5 Surface oil thickness attribute 11
3.6 Clean surface water attribute 12
3.7 Subsurface oil size attribute 12
3.8 Subsurface oil terminal velocity attribute 13
3.9 Subsurface oil submergence zone 14

4 OILTRACK Listing **15–31**

1 Introduction

OILTRACK is a computational model, written in Matlab, for a first generation of operational model for oil spill trajectory simulation incorporating the effects of both wind and waves. It is of the simplest possible structure, with little attention paid to computational efficiency and execution speed. The purpose of OILTRACK is to bring together – in concrete form – the physical models for near surface oil transport that have been developed under MMS Contract 14–35–0001–30612. The program can be integrated into existing oil trajectory codes with modest expenditure of effort.

2 Description of OILTRACK

2.1 Input Data and Assumptions

It is presumed that for applications of risk analyses, the available environmental information will be limited. For this reason, in this effort we assume that direct environmental data is limited to surface wind speed and direction, on the grounds that this is the information most readily available in real time, and the most readily forecasted, that is directly relevant to surface transport estimates. Since this first model makes modest demands on observed information, it makes substantial demands on modelling assumptions to link the wind data to surface motion. These modelled links amount to synthesized data. The surface transport model is expected to be improved if synthetic data is replaced by real data. Furthermore, the transport model should be revised by comparing its performance in tests designed for this purpose.

More sophisticated models can be developed subsequently to account for other relevant physical factors, such as air and sea surface temperatures and consequent heat transfers.

2.2 Large scale currents

"Large scale" here means horizontal scales large compared to the mixed layer depth, or horizontal scales on the order of kilometers. It is assumed that these current patterns, which incorporate the bathymetry of the region, are available from other sources. These currents are assumed to be supplied, in meters/second, at regular time intervals. Intervals on the order of 4 hours are probably adequate. Defining a coordinate system with X

measuring distances from the origin in an eastward direction, and Y in a northward direction, the large scale surface currents are denoted by the vector $\mathbf{U}_c(X, Y, t) = (U_c, V_c)$, where (U_c, V_c) are the eastward and northward components, respectively.

2.3 Surface wind velocity

It is assumed that the surface wind speed, given in meters/second, and direction given by the angle θ measured from the X-axis, is available on a grid, and is updated periodically. The length scales of the relevant velocity variations in Langmuir circulation are on the order of tens of meters, and since the grid is assumed very much larger (kilometers or more), the wind field appears uniform within a grid so far as the dynamics of the circulation are concerned. The time scale for formation of the circulations is typically tens of minutes. Since the time scale of the change of the wind forcing is anticipated to be long compared to the Langmuir circulation time, the wind field in a given grid appears to the Langmuir circulation system to be essentially steady.

The surface wind speed is converted to the friction velocity u_* employed in the model development according to the following formula derived from the bulk aerodynamic drag coefficients of Large and Pond, as cited in Chapter 3. Converting stress to water friction velocity gives the relationship between friction velocity and wind speed U at anemometer height

$$u_* = \sqrt{\rho_a C_D / \rho_w} U.$$

In this relationship, we always take $\rho_a/\rho_w = 1.2 \times 10^{-3}$, which is appropriate for the sea-level value of air density in the standard atmosphere, and a seawater density of 1.02gm/cc. Under neutral atmospheric conditions, Large and Pond correlate their data for C_D with the

$$C_D = \begin{cases} 1.2 \times 10^{-3}, \text{ for } U < 11\text{m/s} \\ (0.49 + 0.065U) \times 10^{-3}, \text{ for } 11\text{m/s} < U < 25\text{m/s}. \end{cases}$$

Available data did not permit extension to wind speeds larger than 25m/s. Such high wind speeds are rare events. In the absence of data, for wind speeds higher than 25m/s, we shall retain the value occuring at the upper end of Large and Pond's correlation, or

$$C_D = 2.1 \times 10^{-3} \text{ for } U > 25\text{m/s}.$$

2.4 Sea State

Sea state data is needed to specify the Stokes drift speed, $u_s(z)$, as a function of depth $|z|$, in the horizontal and vertical transport model. This is done by first fixing the surface value, $u_s(z)$, of the Stokes drift by its value corresponding to a surface wave spectrum of Pierson-Moscowitz (PM) form. According to Chapter 2, this gives

$$u_s(0) = \frac{8}{3\pi^2}\frac{\alpha}{\nu}U\int_0^\infty e^{-\frac{5}{4}\mu^{-4}}\frac{d\mu}{\mu^2}, \tag{1}$$

where

$$\nu = \frac{U\omega_m}{2\pi g},$$

and ω_m is the angular frequency at the peak of the wave spectrum. Both α and ν are dimensionless parameters that Pierson and Moscowitz take to be .0081 and $\nu = 0.14$, but we can extend the model to developing situations, as explained in Chapter 2, by taking $\alpha = 0.032\nu^{2/3}$, and then relating ν to the wind duration and fetch. We can evaluate the integral to obtain

$$u_s(0) = \frac{2}{3\pi^2}\frac{\alpha}{\nu}\left(\frac{4}{5}\right)^{1/4}\Gamma\left(\frac{1}{4}\right)U, \tag{2}$$

where $\Gamma(x)$ is the Gamma function, and $\Gamma\left(\frac{1}{4}\right) = 3.6256$.

Therefore we take the surface Stokes drift speed to be

$$u_s(0) = 0.232\frac{\alpha}{\nu}U = \begin{cases} 0.013U, \text{ for fully-developed seas,} \\ 0.0074\,\nu^{-1/3}U, \text{ for developing seas, ,} \end{cases}$$

where the development is prescribed by prescription of ν, according to Chapter 2. In the model, we suppose unlimited fetch, so the development of the sea is limited by the wind duration, and then

$$\nu = \left(\frac{743\,U}{gt}\right)^{3/7}.$$

In the prototype model, however, no account is taken of wind duration, and a fully-developed sea is the program default.

The depth variation of the Stokes drift is taken to be a simple exponential, as in a monochromatic spectrum, with the frequency taken to be that

at the peak of the PM spectrum. Invoking the deep water wave dispersion relation, this leads to a wavenumber

$$k_m = \frac{0.774g}{U^2}$$

at the spectral peak, and the Stokes drift is therefore taken to be

$$u_s(z) = u_s(z) \exp\left(\frac{0.774\, gz}{U^2}\right).$$

2.5 Mixed layer depth

The surface current estimates are based on a two-layer model in which the upper layer thickness is assumed known, and supplied in units of 1 meter. It is assumed that this data is provided from another source, such as a predictive model for the "large scales" or from observation. In any event, the depth of the first significant density gradient (or the depth to the bottom if this is the "first significant density gradient") is assumed to be the local mixed layer depth.

If no estimate of the water temperature variation with depth is known, then we replace the mixed layer arising in our model by twice the depth of the Ekman layer. This, in turn, is estimated by supplying the latitude, λ, of the location. In particular, the scaling depth is taken to be

$$d = 2d_E = 0.5\frac{u_*}{f}$$

where $f = 2\Omega \sin\lambda = 1.4544 \times 10^{-4} \sin\lambda$ radians/s is the Coriolis parameter, and u_* is the water friction velocity. The length d_E represents the e-folding depth of the turbulent Ekman layer computations of Coleman et al. (1990). Estimating $d \sim 2d_E$, with d_E taken to be from the Coleman et al. computations is consistent with the eddy viscosity estimates of Chapter 3, where the eddy viscosity was taken to be ku_*d, where d is the order of magnitude of the surface layer depth. Our LES computations reported in Milestone 7 gave $k \approx 1/18$. If d were set at $2d_E$ for the purposes of setting the eddy viscosity, then the e-folding depth of the classical quasi-laminar Ekman layer would agree with turbulent Ekman layer computations of Coleman et al. for $k = 1/16$. The argument for substituting an Ekman layer depth for the mixed layer depth is simply that this layer contains the active wind generated shear, and Langmuir circulation takes place in such a layer. The argument is admittedly not overly compelling, and points to the desirability of obtaining density data.

2.6 Oil properties

The oil properties used in our analyses consist of oil density and oil-seawater interfacial tension only. These can be adjusted for ambient water temperature, but this will not be done in the prototype. The water density is that of sea water at a specified water temperature and salinity, but this adjustment also will be omitted in the prototype, which fixes the default water density to be 1.02 gm/cc.

3 Output Oil Spill Attributes and Spill Trajectory

The model assumes that oil on the surface moves with the velocity vector

$$\begin{aligned} \mathbf{U}_{oil}(X,Y,t) &= \mathbf{U}_c(X,Y,t) + \{\bar{U}_{LC}(X,Y,t) + 0.013U(X,Y,t)\} \\ &\quad \times \{\cos\theta(X,Y,t)\mathbf{e}_X + \sin\theta(X,Y,t)\mathbf{e}_Y\}\,. \end{aligned} \tag{3}$$

In this relation, the terms refer to the following factors.

- $\mathbf{U}_c(X,Y,t)$ is the surface velocity vector of the prescribed background current field.
- $\bar{U}_{LC}(X,Y,t)$ is a *mass-weighted* average of the surface current speed, parallel to the wind, in the Langmuir circulation field. This attribute will be explained further.
- $U(X,Y,t)$ is the wind speed, and $0.013U(X,Y,t)$ is the surface Stokes drift with the assumptions already made on the surface wave spectrum. The sum $\bar{U}_{LC}(X,Y,t) + 0.013U(X,Y,t)$ is the wind-generated Lagrangian speed of a oil floating on the surface (and assumed parallel to the local wind direction), relative to the background surface current.

This transport model is characterized by the attributes $\bar{U}_{LC}(X,Y,t)$, and by the modifying attributes L_s, the oil lane separation, and by t_{sweep}, the characteristic time for oil collection into oil lanes. Each of these now will be specified more fully.

3.1 Oil lane separation attribute

The transport model assumes that oil is collected into oil lanes coinciding with the dominant Langmuir circulation windrow, and that the time required for this collection to take place is negligible compared to the time

scale of interest in a simulation. The oil lane separation,

$$L_s = 3 \times d, \tag{4}$$

where d is the prescribed depth of the mixed layer.

3.2 Oil sweep time attribute

This time measure is taken to be equation (20) of Milestone 9, on noting that the symbol L appearing there is $L_s/2$, the width of one dominant Langmuir circulation cell, which is half the distance between dominant windrows,

$$t_{sweep} = 86 \frac{d}{U} \frac{\sqrt{gd}}{U}. \tag{5}$$

This attribute is found as a check that it is small compared to the simulation time.

3.3 Current structure attributes

Three speed profiles in the Langmuir circulation convective field are of particular interest for transport computations. These are $U_{LC}(y)$ and $V_s(y)$, the surface values of the Eulerian speeds in the wind direction and in the crosswind direction, respectively, as functions of crosswind coordinate, y, and $W(z)$, the vertical velocity below windrows as a function of depth.

These current features are abstracted from data obtained by direct simulation of the two-dimensional Langmuir circulation problem. In the simulations, the Stokes drift is assumed to be an exponential function of depth corresponding to a monochromatic surface wave field. The wavenumber of the surface waves is assumed to be determined by the peak of the Pierson-Moskowitz spectrum. Once the Stokes drift is specified, the simulation depends on a single dimensionless parameter,

$$R = \frac{\partial u_s}{\partial z}(0)\, U_c \frac{d^3}{\nu_T^2}$$

where U_c is a charateristic surface current speed determined by boundary conditions, ν_T is the eddy viscosity, and u_s is the Stokes drift. The boundary conditions determining the simulations are described in Part I. They result in

$$R = 23.6 \kappa R_*^3,$$

where

$$\kappa = 0.774\frac{gd}{U^2}$$

is the dimensionless gravity wave wavenumber at the spectral peak of the Pierson-Moskowitz spectrum, and

$$R_* = \frac{u_* d}{\nu_T}$$

is a Reynolds number based on the friction velocity imparted to the water by the wind stress. Thus, the result of the simulations are that the velocity structure of the Langmuir circulation system is determined by the two dimensionless parameters, κ and R or, alternatively, κ and R_*.

The three velocity profiles found from simulations at 16 values of R ranging from $R = 650$ (just above the value for which Langmuir circulation cannot be sustained) to $R = 20,000$ for $\kappa = 1$ and for 9 values of κ ranging from $\kappa = 0.5$ to $\kappa = 20$ for values of R ranging from 10000 to 80000 were fitted to simple functional forms of R and κ. In particular, the critical value of $R = R_c$ below which Langmuir circulation with aspect ratio $L_s/d = 3$ decays was found to be approximately

$$R_c = 2R_0(\kappa).$$

Here $R_0(\kappa)$ is the theoretical value found by Lele (1985) for $L/d = \infty$, and this produces

$$R_c = \frac{64\kappa^5}{1 - \kappa + \kappa^3/3 - e^{-2\kappa}(1 + \kappa - \kappa^3/3)}.$$

The component U_{LC} has jet-like behavior over lines of surface convergence. When the parameter $\bar{\Gamma}$ (defined below) is very large, oil is collected in surface convergences and moves with a speed close to the maximum value in the surface jet. Consequently, although we have found a functional form that fits U_{LC}, the principal interest is in the excess velocity in the jet. We have set the horizontal average of U_{LC} to be

$$\langle U_{LC} \rangle = 0.022U,$$

and the maximum speed in the jet is then

$$\langle U_{LC} \rangle + u_* R_* u_{jet}.$$

The jet enhancement was found to be fitted by

$$u_{jet} = \sqrt{r}\left[0.4e^{-0.278r} + \frac{1}{0.4595r + 2.3879\sqrt{r} + 0.7515}\right]$$

where

$$r = \frac{R - R_c(\kappa)}{R_c(\kappa)}$$

for $R > R_c(\kappa)$ to reasonable accuracy, and is zero for $R < R_c(\kappa)$ (where no Langmuir circulation takes place). The jet enhancement, u_{jet} rises from zero to a maximum of about 0.314 at $r = 1.8$, and then decreases algebraically.

The vertical velocity below lines of surface convergence in the simulations is well fitted to the following form,

$$W(z) = -5.4\frac{u_*}{R_*}\sqrt{\frac{R - R_c(\kappa)}{R_c(\kappa)}}z\left(p_1 z^2 + p_2 z + p_3\right)$$

where $-z$ is the depth normalized by the total mixed layer depth, and $p_{1,2,3}$ are constants that are determined by the normalized depth, $z = z_m$, of the maximum vertical speed. When the gravity waves are extremely long compared to the depth of the mixed layer, or $\kappa \to 0$, the vertical speed is symmetrical with respect to the mid-depth of the mixed layer under the boundary conditions utilized, so $z_m = -0.5$. It may be expected that z_m depends on κ, and this is borne out by the simulations, which show that the location of the maximum downwelling moves towards the surface as κ increases. This movement has an asymptote, however, at a specific depth. From our simulations, which can only establish this movement of z_m crudely, we estimate

$$z_m = -0.5 + 0.1318\frac{\kappa^2}{(1 + 1.0187\kappa^2)}.$$

In terms of z_m, the constants $p_{1,2,3}$ are

$$p_1 = -\frac{2z_m + 1}{z_m^2(1 + z_m)^2}, \quad p_2 = \frac{3z_m^2 - 1}{z_m^2(1 + z_m)^2}, \quad p_3 = \frac{3z_m + 2}{z_m(1 + z_m)^2}.$$

The surface sweeping velocity component, $V_s(y)$, is approximately sinusoidal, with a maximum value $V_m$that depends only on $(R - R_c)/R_c$,

$$V_m = 6.07\sqrt{\frac{(R - R_c)}{R_c}}.$$

The shape of the wavy function $V_s(y)$ depends on κ and $(R - R_c)/R_c$. The maximum amplitude occurs at the cell center for small values of κ for sufficiently large $(R - R_c)/R_c$ and migrates towards the zeros of $V_s(y)$ corresponding to the lines of surface convergence as κ increases. This migration will be neglected, and we will take

$$V_s(y) = V_m \sin\left(\frac{2\pi}{L_s}(y - y_c)\right),$$

where a convergence line is located at y_c.

3.4 Mass-weighted surface current speed attribute

The speed $\bar{U}_{LC}$ called for in (3) for the computation of surface oil mass transport is

$$\bar{U}_{LC} = \frac{1}{L_s h_0}\int_0^{L_s} h(y) U_{LC}(y) dy, \tag{6}$$

where h_0 would be the thickness of the oil film if it were spread uniformly over the surface, and $U_{LC}(y)$ is the surface value of the downwind Eulerian speed. A method for calculating the cross-wind variation of the oil film thickness, $h(y)$ from the surface sweeping speed, $V_s(y)$ is provided in Part I. When the parameter $\hat{\Gamma}$ (see below) is large, as it is expected to be, $\bar{U}_{LC} \approx \langle U_{LC} \rangle + u_* R_* u_{jet}$, or the maximum speed surface in the direction of the wind. This form is used for the model implemented in Oiltrack.

3.5 Surface oil thickness attribute

This is the oil thickness $h(y)$ used in defining $\bar{U}_{LC}$. In Part I, this is found from the surface sweeping speed, $v_s(y)$ by balancing the stress imposed on the oil layer by the sweeping component and the gravity spreading force. The surface stresses sweep oil towards the convergences, piling it into windrows. Surface tension spreading is ignored, so monomolecular layers of oil may remain in water that has been nominally swept clean of oil.

In this description, we have defined $y = 0$ at lines of surface divergence, so that in the notation of the previous section $y_c = 0$ there, and $|y| = L_s/2$ at a adjacent lines of surface convergence. Considering the region between a surface divergence and the convergence at $y = L_s/2$, the water surface is "clean" from $y = 0$ to $y = y_0$, so $h(y) = 0$ for $0 \le y \le y_0$, and is given by

$$\frac{h(y)}{h_0} = \sqrt{\frac{2C_w}{g\chi}\frac{\rho_w}{\rho_0}\int_{y_0}^{y} V_s^2(y)\, dy}, \text{ for } y_0 \le y \le \frac{L_s}{2}. \tag{7}$$

Substituting for $V_s(y)$ from the previous section, and defining

$$\hat{\Gamma} = \frac{V_m^2}{gL_s}\frac{C_w}{\chi}\frac{\rho_w}{\rho_o}\left(\frac{L_s}{h_0}\right)^2,$$

we have

$$\frac{h}{h_0} = \sqrt{\hat{\Gamma}}\left\{\eta - \eta_0 - \frac{1}{\pi}\cos\pi(\eta+\eta_0)\sin\pi(\eta-\eta_0)\right\},$$

where

$$\begin{aligned}\eta &= \frac{2y}{L_s}\\ \eta_0 &= \frac{2y_0}{L_s}.\end{aligned}$$

3.6 Clean surface water attribute

This is defined here as the fraction of the surface for which $h(y) = 0$. It is therefore given by η_0, which is found by imposing oil mass conservation,

$$\frac{2}{L_s}\int_{y_0}^{L_s/2}\frac{h}{h_0}dy = 1, \text{ or } \int_{\eta_0}^{1}\frac{h}{h_0}d\eta = 1,$$

as explained in Part I. It is expected that $\hat{\Gamma}$ is a large number. When this is the case, $1-\eta_0$ will be small, and the integral needed to find η_0 can be approximated. In particular, when $1-\eta_0$ is small, so is $\eta-\eta_0$, and so expanding h/h_0 when these variables are small leads to

$$\pi\sqrt{\hat{\Gamma}}(1-\eta_0)^{5/2}\int_0^1\sqrt{\frac{1}{3}p^3 - p^2 + p}dp = 1, \tag{8}$$

so the large $\hat{\Gamma}$ approximation leads to

$$\eta_0 = 1 - 0.7352\hat{\Gamma}^{-1/5}. \tag{9}$$

3.7 Subsurface oil size attribute

The model presented in Part I gives the mean oil droplet radius to be

$$\bar{a} = 0.235a_\epsilon = 0.085\left(3\frac{\sigma}{\rho}\right)^{3/5}(2\epsilon)^{-2/5},$$

where the near-surface mean turbulent dissipation rate ϵ is taken to be

$$\bar{\epsilon} = 4.7 \times 10^{-6} gU.$$

The interfacial tension, σ, and ρ is the seawater density, both of which are input data without need for processing.

3.8 Subsurface oil terminal velocity attribute

This is found from the force balance given in Part I, using the drag coefficient

$$C_D = \frac{24}{Re} + \frac{6}{1+\sqrt{Re}} + 0.4,$$

where Re is the Reynolds number

$$Re = \frac{2V_T a}{\nu}.$$

The force balance can be expressed as

$$Re\sqrt{C_D(Re)} = 4\frac{a}{\nu}\sqrt{\frac{2ga}{3}\frac{\Delta\rho}{\rho}}.$$

Here ν is the molecular viscosity of seawater, and V_T is the terminal velocity. The left-hand side of this equation is approximately linear. Over the range of $100 < Re < 1000$, it may be approximated by

$$0.74Re + 46.11$$

to within about 10%. For the data in Table 6.1 of Part I, the results are therefore reasonably well fitted by the rule

$$V_T = 1.35\left\{\sqrt{\frac{2\Delta\rho}{3\rho}ga} - \frac{11.53\nu}{a}\right\}. \tag{10}$$

Thus, the terminal velocity at any wind speed, U, can be calculated by first calculating the average drop radius, and then calculating the terminal velocity using (10).

3.9 Subsurface oil submergence zone

This is taken to be the depth of the Stommel retention zone, as given in Chapter 5 of Part II. Specifically, given the terminal velocity V_T (previous section), this depth is found from the vertical speed $W(z)$ of subsection 3.3 as the root of

$$W(z) + V_T = 0 \tag{11}$$

having the largest absolute value.

4 OILTRACK Listing

```
clear
global hx hy U Theta U_c Theta_c ustar fric Rstar Kp D Kp r k


% Set up grid.  Each grid point, (I,J) represents
% the southwest corner of a cell in which wind and current
% are assumed constant.
NE =10;% input('Number of surface grid points to the East = ');
NN =10;%input('Number of surface grid points to the North = ');
IMAX=NE+1;
JMAX=NN+1;
hx=5;%input('x- Mesh point separation (in km)= ');
hy=5;%input('y- Mesh point separation (in km)= ');
XMAX=hx*NE;
YMAX=hy*NN;
%%%%%%%%%%%%%%%%%%%%%%%%%%%%%%%%%%%%%%%%%%%%%%%%%%%%%%%%%%%%%%%%%%%%%%%%%%%%%%%
%                    %%%%%%%%% Time Intervals %%%%%%%%%
%
% Nt = number of time instants for which wind and current data is provided.
Ttotal=144; %input('Total tracking time=');
Nt =Ttotal;%input('Number of time instants for  wind/current data  = ');
tstep=Ttotal/Nt;         %time-step increment
deltXcross=tstep;
deltYcross=tstep;
%%%%%%%%%%%%%%%%%%%%%%%%%%%%%%%%%%%%%%%%%%%%%%%%%%%%%%%%%%%%%%%%%%%%%%%%%%%%%%%
%                    %%%%%%%%%     Parameters     %%%%%%%%%
lat=40;      % Latitude in degrees
Rstar=10;  % Reynolds number Rstar=ustar*D/(eddy viscosity)
rhow=1.02;   % Water density
rhoo=0.99;   % Oil density
chi=1-rhoo/rhow;
g=9.81;      % Acceleration of gravity
Cw=0.004;    % Oil-water friction coefficient
ho=0.001;    % Average thickness of oil, in meters.
gamma=(Cw/chi)*(rhow/rhoo)/(g*ho^2);
sigma=20;    % Interfacial tension, dynes/cm
visc=0.01;   % Kinematic viscosity of water in cm^2/s.
%%%%%%%%%%%%%%%%%%%%%%%%%%%%%%%%%%%%%%%%%%%%%%%%%%%%%%%%%%%%%%%%%%%%%%%%%%%%%%%
%         Initialize  Problem
x0=input('Initial x position=');
y0=input('Initial y position=');
XP=[x0 y0];
if (x0*(XMAX-x0) < 0) | (y0*(YMAX-y0) < 0)
       error('Initial point is outside domain boundary')
end
X= XP;       % X-Matrix will contain particle location history.
%                        % Rows are  time levels
%                        % Columns are(east,north) particle coordinates
XNEW=[0 0];
attributes=[];
%              ************************************************
```

```
%                                   Begin time loop

clf
tracker=plot(X(1,1),X(1,2),'.','MarkerSize',12);
axis([0 hx*NE 0 hy*NN])
axis('square')
grid
hax=gca;
xtickmarks=[0:hx:hx*NE];
ytickmarks=[0:hy:hy*NN];
set(hax,'XTick',xtickmarks,'YTick',ytickmarks);
hold on
    for itime=1:Nt
            XP=X(itime,:);      % Position at start of time step
            I=ceil(XP(1)/hx);   % Locate grid cell containing particle
            J=ceil(XP(2)/hy);
            wind; seastate;     % Update wind and seastate over simulation region
            frictionvel; depth; % Stress and effective depth of layer
            current;            % Background current
            [Vel,r,k,E]=V(I,J);
            XNEW=XP+tstep*Vel;  % Step time and spill position

            %If a domain boundary was crossed, stop.


            if (XNEW(1)*(XMAX-XNEW(1)) < 0) | (XNEW(2)*(YMAX-XNEW(2)) < 0)
                'Hit! Domain boundary was crossed'
                    if XNEW(1) <0
                        P=[0 XP(2)];
                    elseif XNEW(1)>XMAX
                        P=[XMAX XP(2)];
                    elseif XNEW(2) <0
                        P=[XP(1) 0];
                    elseif XNEW(2)>YMAX
                        P=[XP(1) YMAX];
                    end
                plot(P(1),P(2),'r*','MarkerSize',18)
                break
            end


            II=ceil(XNEW(1)/hx); %Locate the cell containing the new spill
            JJ=ceil(XNEW(2)/hy); %position.

            % Find out if a grid cell boundary was crossed in this time step.
            %If so, backtrack, and correct for the fraction of the time step
            % taken in each of the cells.

            [VelNext,r,k,E]=V(II,JJ);
            if (II~=I)
                % Here a cell boundary was crossed in the x-direction
```

```
            % Therefore Vel(1,1)~=0
                XB=(II-1)*hx; % This is the cell boundary crossed
                deltXcross=(XB-XP(1))/Vel(1,1);
                % This is the time travelled after crossing the cell bndry
        end
        if (JJ~=J)
            % Here a cell boundary was crossed in the y-direction
            % Therefore Vel(1,2)~=0
                YB=(JJ-1)*hy; % This is the cell boundary crossed
                deltYcross=(YB-XP(2))/Vel(1,2);
        end

        if (II~=I | JJ~=J)
            XP=XNEW; % Saves the uncorrected position
            deltCross=min(deltXcross,deltYcross);
            XNEW=XP+(tstep-deltCross)*(VelNext-Vel); %Corrects position
        end
        % This corrects the position to account for the interval within
        % time step that the particle moves with a new velocity due to
        % crossing into another cell.
                    %If a domain boundary was crossed, stop.


        if (XNEW(1)*(XMAX-XNEW(1)) < 0) | (XNEW(2)*(YMAX-XNEW(2)) < 0)
            'Hit! Domain boundary was crossed'
                if XNEW(1) <0
                    P=[0 XP(2)];
                elseif XNEW(1)>XMAX
                    P=[XMAX XP(2)];
                elseif XNEW(2) <0
                    P=[XP(1) 0];
                elseif XNEW(2)>YMAX
                    P=[XP(1) YMAX];
                end
            plot(P(1),P(2),'g*','MarkerSize',18)
            break
        end

    X=[X;XNEW]; % Append the position at current time level to trajectory array.
    fric=ustar(II,JJ);
    tempr=sqrt(r);
    d=D(II,JJ);
    wd=5.4*tempr*fric/Rstar;     % Peak vertical speed
    vm=6.07*tempr*fric/Rstar;    % Peak sweep  speed
    sweeptime=(1.5*d/vm)/3600;  % Characteristic time (in hrs) for surface sweeping
    Gamma=vm^2*3*d*gamma;        % Parameter fixing clean water fraction
    CleanWater=1-.7352/Gamma^(.2);
    drop;
    attributes=[attributes; E Hs(II,JJ) vm wd  sweeptime CleanWater V_T];%  SubmerDepth
%plot(XNEW(1),XNEW(2),'.','MarkerSize',12); drawnow
end
```

```
plot(X(:,1),X(:,2),'.','MarkerSize',12);
plot(X(:,1),X(:,2))  % Connect the dots
hold off
```

```
% Reads in background surface and direction (or computes it, given the
% wind velocity)

% 'U_c' = current speed matrix of dimension NE,NN. This is updated for each
% of the Nt time instants for which the tracer trajectory is to be computed.
%
% 'Theta_c' is the current direction measured counterclockwise in degrees from East.
% The organization of this data imitates that for U_c.

% The data given here is artificial, produced by a random fluctuation of
% speed and direction about a mean current of 10cm/sec=.1m/sec and a mean direction
% of due North.

%U_c = .1*ones(NE,NN) + .03*rand(NE,NN);
U_c = zeros(NE,NN) ;
Theta_c= 90*ones(NE,NN) + 6*rand(NE,NN);
```

```
% Read depth files.
% Set initial arrays for the 3 possible layer depths to minimum)
dml=20.*ones(NE,NN);          % Depth of observed mixed layer array

dbottom=100.*ones(NE,NN);% Depth to bottom topography array, assumes no layer
% of interest will be more than 100 meters, in which case this serves as
% an upper bound.
coriolisparam=2*7.2722*10^(-5)*sin(pi*lat/180);
dekman=0.5.*ustar./coriolisparam;
% Compare each depth, and select the smallest for each grid point

d1=min(dml,dbottom);
D=min(d1,dekman);          % d has the smallest elements of the 3 possibilities.
```

```
function y=downwelling(r)
% Functional fit to the minimum value of w as as function of r= R/R_c-1
% Here R_c=2*R_0(kappa), or twice the minimum Rc that occurs at L=infinity.
y=5.4.*sqrt(r)
```

```
ep=2*4.24*g*10^(-2)*U(II,JJ); %in cm^2/s^3
a=0.085*(3*sigma/rhow)^(0.6)*(ep)^(-.4); % a is drop radius in cm.
V_T=0.38*(visc/a)*(chi*981*a^3/visc^2)^(.7); % Terminal velocity in cm/s
```

```
% Water friction velocity matrix
% 'ustar' computed from Large & Pond bulk aerodynamic drag coefficient.
% 'U' is the wind speed matrix in m/s.

ustar=.001*sqrt(1.2*(.49+.065.*U)).*U;
if min(min(U))<11
    [itest,jtest]=find(U<11);replace=[itest jtest];
    ustar(replace(:,1),replace(:,2))=.0012*U(replace(:,1),replace(:,2));
end;
if max(max(U))>25
    [ktest,ltest]=find(U>25); Replace=[ktest ltest];
    ustar(Replace(:,1),Replace(:,2))=0.0015931*U(Replace(:,1),Replace(:,2));
end;
```

```
function y=R_c(kappa)
% Critial Rayleigh # for constant stress layer of aspect ratio 3
% This is twice the value for aspect ratio infinity.
% kappa=gravity wave wavenumber
den=(1-kappa+kappa.^3./3)-exp(-2.*kappa).*(1+kappa-kappa.^3./3);
y=64.*kappa.^5./den;
```

```
% 'U' is the wind speed in m/s.
% 'Us'=surface Stokes drift, assuming either fully-developed seas (P-M),
%  where 'P-M' means "Pierson-Moskowitz spectrum", or developing seas.
% 'Kp'=wavenumber (in m^{-1}) at the peak of the P-M spectrum,
% 'Lp' = length of the waves at the spectral peak, in meters,
% 'Hs' = significant wave height according to Longuet-Higgins.

global Us Kp
g=9.8; % acceleration of gravity
nut=.14;% nu(time,U); % The PM spectral parameter according to Milestone 2
%
Us=(0.013).*U; %This is appropriate for the P-M fully developed sea.
%
%Us=0.0074.*U./nut.^(1/3); %This is appropriate for the developing sea of Mile2.
Kp=(2*pi.*nut).^2*g./U.^2;
Lp=(2*pi)./Kp;
Hs=2.83*sqrt(.0081/5)./Kp; % See (4) of Mile 16 (with 4 replaced by 2.83)
%
```

```
function v=sweep(r)
% Fit to the maximum of the surface sweeping component. Here r=(R-Rc)/Rc,
% where Rc=2*R_0(kappa)
v=6.07.*sqrt(r);
```

```
function y=ujet(r)
% functional fit to combined ujet data
rm=1.7983;um=.3143;sigma=2*rm;
x=r;
%u1=.1966;x1=18.1672;
xh=x.^(.5); x2=r./sigma;
ebl=.04.*exp(-x2);
y=xh./(.7515+2.3879.*xh+.4595.*xh.^2)+xh.*ebl;
```

```
function [vel,r,k]=V(IX,JY)
% Computes the velocity at the current particle location, in km/hr.
% Input z=[t x], where x is the vector-valued location.
% Located x within the grid defined by the input data.
global U Theta U_c Theta_c ustar Rstar Kp D
theta=pi*Theta(IX,JY)/180;          %Wind direction, in radians
theta_c=pi*Theta_c(IX,JY)/180;      %Current direction, in radians
k=Kp(IX,JY)*D(IX,JY);
r=23.6*Rstar^3*k/R_c(k)-1;
U_LC(IX,JY)=0.035*U(IX,JY)+ustar(IX,JY)*Rstar*ujet(r);
% U_LC= Stokes drift + horizontal average Eulerian speed
vel=U_c(IX,JY)*[cos(theta_c) sin(theta_c)];                                  % Background cu
vel=vel+U_LC(IX,JY)*[cos(theta) sin(theta)];    % Adds wind forced speed.
vel=3.6*vel;                                    % Converts m/s to km/hr. (3600 sec/hr)*(10^
```

```
function w=W(z)
% Vertical velocity on plane of surface convergence. z is the vertical
% coordinate, measured from the surface, so -z is the depth below the air-sea
% interface.
global r k fric Rstar
zm=-0.5+.1318*k^2/(1+1.0187*k^2);
den=zm^2*(1+zm)^2;
p1=-(2*zm+1)/den;
p2=(3*zm^2-1)/den;
p3=(3*zm+2)*zm/den;
downspeed=5.4.*sqrt(r)*fric/Rstar;
w=-downspeed.*z.*(p1*z.^2+p2*z+p3);
```

```
%%%%%%%%%%%%%%%%%%%%%%%%%%%%%%%%%%%%%%%%%%%%%%%%%%%%%%%%%%%%%%%%%%%%%%%%%%%%
% Reads in wind speed data from external files or internally
% generated randomized wind field.
% Produces friction velocity array.

% 'U' = current speed matrix of dimension NE,NN. This
% is updated for each of the Nt time instants
% for which the tracer trajectory is to be computed.
%
% 'Theta' is the wind direction measured counterclockwise
% in degrees from East.
% Its organization imitates that for U.

% The data given here is artificial, produced by a random fluctuation of
% speed and direction about a mean wind  and a mean direction.
%

U = 10*ones(NE,NN) + 10*rand(NE,NN)- 10*rand(NE,NN);
Theta= 45*ones(NE,NN)+ 180*rand(NE,NN)-180*rand(NE,NN);
```